Development of nanotechnology-based therapeutic approaches to treat HIV

Cleo Dodgen

A thesis submitted in fulfilment of the requirements for the degree of Masters in Science in the Department of Biotechnology, Faculty of Science, University of the Western Cape.

Supervisor: Dr Mervin Meyer

Abstract

C.G. Dodgen

MSc thesis, Department of Biotechnology, Faculty of Natural Sciences, University of the Western Cape

The rapidly expanding field of nanotechnology has been the focus of many biologists with regard to drug delivery. The ability of nanoparticles to enter cellular compartments makes it possible to explore specific treatment strategies for life-threatening diseases such as AIDS. Since HIV primarily infects CD4+ cells, we aim to use CD4 as a selectable marker to deliver pro-apoptotic nano-devices to HIV infected cells. The objective is to selectively induce cell death or apoptosis in CD4+ HIV infected cells. Apoptosis is activated through a number of biochemical pathways. The apoptosis promoting protease, caspase-3 is central to the induction of apoptosis. Caspase-3 is produced as an inactive zymogen and is activated by other proteases through proteolytic cleavage. We take advantage of the fact that HIV-infected cells produce HIV-1 protease, which is responsible for the production of infectious virions through proteolytic cleavage of the HIV proteins, Gag and Pol. Our strategy was to generate a mutant form of the caspase-3 protease that is only cleavable by HIV-1 protease.

Gold nanoparticles were used to selectively deliver mutant caspase-3 to CD4$^+$ cells that mimic HIV infection through the use of a CD4-targeting peptide that specifically recognizes CD4$^+$ cells.

Gold nanoparticles were synthesised and functionalised with nitriloacetic acid (NTA). Dose response cell culture experiments indicate that NTA-functionalised gold nanoparticles did not induce apoptosis or cytotoxicity on their own. NTA-functionalised particles were conjugated to a histidine-tagged CD4-targeting peptide, as well as histidine-tagged mutant caspase-3. Upon treatment of mammalian cells representing HIV-infection, NTA-CD4-targeting peptide-mutant caspase-3 gold nanoparticles showed a decline in cell viability at all concentrations tested. Apoptosis was not detected at high levels in treated cells after 24 hours, but based on the data, it is likely that early apoptosis occurred shortly after treatment, thus not allowing the detection of apoptosis at the 24 hour timepoint.

Our results suggest that gold nanoparticles could serve as an effective drug delivery tool due to their size and chemical properties. Moreover, mutant caspase-3 targeted to cells expressing HIV-1 protease and CD4 seemed to exhibit changes in cellular morphology, reminiscent of a process termed autophagy. Additional experimental data would confirm the nature of this process, and determine whether this process occurs as a protective mechanism until the cellular environment resumes back to normal, or if the changes eventually result in death of these cells. This data serves as the basis for further investigation of functionalised gold nanoparticles for the eradication of diseased cells.

Development of nanotechnology-based therapeutic approaches to treat HIV

Cleo Grace Dodgen

June 2012

KEYWORDS:

HIV-1 (Human Immunodeficiency Virus Type 1)

Apoptosis

Nanotechnology

Caspase-3

HIV-1 protease

CD4 (Cluster of differentiation 4)

CHOs

Drug delivery

Targeting peptide

Site-directed mutagenesis

Declaration

I declare that "**Development of nanotechnology-based therapeutic approaches to treat HIV**" is my own work, that it has not been submitted for any degree or examination in any other university, and that all the sources I have used or quoted have been indicated or acknowledged by complete references.

Cleo Grace Dodgen   June 2012

Signed: ....

Abbreviations

AIDS	Acquired Immunodeficiency Syndrome
Caspases	Cysteinyl Aspartate Proteinases
CCR5	C-C chemokine receptor 5
CD4	Cluster of differentiation 4
cDNA	complementary DNA
CHO	Chinese Hamster Ovary
CPPs	Cell-Penetrating Peptide
CXCR4	C-X-C chemokine receptor 4
DISC	Death-Inducing Signaling Complex
EDX	Energy Dispersive X-ray spectroscopy
EGFR	Epidermal Growth Factor Receptor
env	Envelope
FACS	Fluorescence Activated Cell Sorter
FDA	Food and Drug Administration
FSC	Forward SCatter
Gag	Group-specific Antigen
GFP	Green Fluorescent Protein
gp120	Envelope glycoprotein GP120
HIV	Human Immunodeficiency Virus
HTLV	Human T-cell Leukemia Virus
IPTG	Isopropylthio-ß-galactoside
LTR	Long Terminal Repeat
NRTIs	Nucleoside Reverse Transcriptase Inhibitors

NNRTIs	Non-Nucleoside Reverse Transcription Inhibitors
NTA	Nitriloacetic acid
PCR	Polymerase Chain Reaction
PGL	Persistent Generalised Lymphadenopathy
PHCA	Polyhexylcyanoacrylate
PIs	Protease Inhibitors
PIC	Pre-Integration Complex
Pol	Polymerase
rev	regulator of viral protein expression
RMA	repulsive membrane acidolysis
SSC	Side SCatter
SPR	Surface Plasmon Resonance
SWCNT	Single-Walled Carbon Nanotubes
tat	transactivator of transcription
TEM	Transmission Electron Microscopy
tRNA	transfer RNA
VEGF	Vascular Endothelial Growth Factor
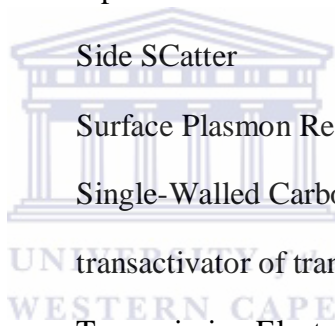
Acknowledgements

It is with sincere gratitude that I wish to thank the individuals who have made this an unforgettable journey of discovery. I would like to express my thanks to my supervisor and mentor, Dr Mervin Meyer. Thank you for the years of encouragement and support. I have learned so much from you, and those learnings will stay with me always. I would like to thank Professor Jasper Rees, who dreamed big and gave this project life, and who motivated me to keep going even when the odds were stacked against me. To Dr Abram Madiehe, thank you for your constant support and your belief in me. You are truly valued. I wish to thank Mr Francois Taute, my colleague, sounding board and friend, who has supported me in every way and has been a true inspiration. Thank you for always pushing me to reach new heights. To all my colleagues at the University of the Western Cape, especially the NIC Biolabels and Apoptosis groups, thank you so much for the support and for being my family over the years.

To my close friends, and fellow researchers, Alexis Neumann and Nelusha Gounden, thank you for being the positivity in my life when I felt ready to throw in the towel. I will treasure your friendship forever. To my partner, Heinrich Groenewald, thank you so much for supporting me and standing by me. You've been my rock, and I am truly grateful for the role you've played in my success.

To my family, thank you so much for your love and understanding, and for supporting me in everything I do. Finally, I wish to thank the Department of Science and Technology (DST), the National Research Foundation (NRF) and Mintek for funding me during the course of my research.

Table of Contents

CHAPTER 1: INTRODUCTION

CHAPTER 2: MATERIALS AND METHODS

CHAPTER 3: CONSTRUCTION OF A "HIV-INFECTED" CELL MODEL SYSTEM

CHAPTER 4. GENERATION OF MUTANT CASPASE-3 IN A BACTERIAL EXPRESSION SYSTEM FOR TARGETING TO "HIV-INFECTED" CELLS

CHAPTER 5. DESTRUCTION OF "HIV-INFECTED" CELLS USING CD4-TARGETING Ni-NTA MUTANT CASPASE-3 GOLD NANOPARTICLES

CHAPTER 6. DISCUSSION AND CONCLUSION

List of Figures and Tables

Figures

Tables

1. The Human Immunodeficiency Virus Type I (HIV-1)

The Human Immunodeficiency Virus, more commonly referred to as HIV, is the cause of HIV infection. HIV infection places the infected individual at risk for the occurrence of opportunistic infections, resulting in Acquired Immunodeficiency Syndrome (AIDS) (Broder, 2010). This disease is known to be life-threatening and the cause of millions of deaths across the globe every year (Girard *et al*, 2011). It is not known where exactly HIV originated from, but the very first cases of HIV were reported to the National Institute of Health (NIH) in the USA in 1981 (Gallo and Montagnier, 2003). During the late 1970s, it was thought that epidemic diseases, caused by either bacteria or viruses, no longer threatened developed nations (Gallo and Montagnier, 2003). It was during this period that HIV/AIDS started to make its appearance. In the early 1980s, AIDS was already identified as a disease, the cause of which was unknown at the time. A range of possible causes was investigated, including fungi and exposure to chemical agents (Gallo and Montagnier, 2003). In the year 1983, research scientists at the Pasteur Institute in France discovered a retrovirus, made clear by the presence of the enzyme reverse transcriptase. This virus was recovered from a man with persistent generalised lymphadenopathy (PGL), a condition that was suspected to be associated with AIDS (Levy, 2006). The virus was found to be similar to the Human T-cell Leukemia Virus (HTLV), in that it characteristically depleted CD4 T-cells. However, the symptoms of the unknown virus were found to be different from those associated with HTLV.

This, together with the elimination of the idea that a microorganism (other than a virus) could be responsible for the disease, led researchers to start the search for a virus similar to HTLV. In 1984, researchers at the Pasteur Institute in France, as well as those in Bethesda, Maryland (United States of America) isolated a viral strain that infected all growing T-cell lines. Upon the discovery of HIV in 1984, a link was made between HIV and AIDS. The reason for this was that HIV was repeatedly found in the bloodstream of AIDS patients and the blood test used for this purpose was highly reproducible (Gallo and Montagnier, 2003). It was at this time, late in 1984, that HIV was acknowledged in the medical community as being the causative agent for the disease known as AIDS and the name HIV was given in 1986 by the International Committee on Taxonomy of Viruses (Levy, 2006). According to the United Nations Acquired Immunodeficiency Syndrome (UNAIDS) 2010 Report on the Global AIDS Epidemic, an estimated 33.3 million people globally are infected with HIV (United Nations Acquired Immunodeficiency Syndrome (UNAIDS) Report on the Global AIDS Epidemic, 2010).
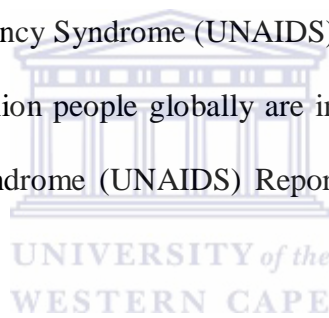
1.1 HIV biology

In order for HIV to effectively infect human cells, it is important that its structure is suited to function. The structure of HIV has been determined as a 120 nm spherical particle, comprised of various structural and functional proteins. The production of these proteins, essential for the survival of the virus, is made possible by a well-organised genome (Girard *et al.*, 2011), as shown in Figure 1.1.
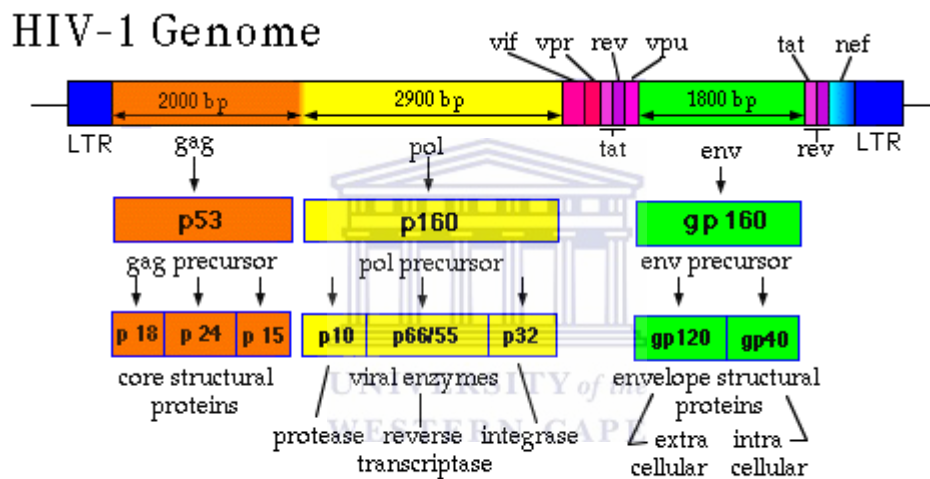
Figure 1.1. Structure of the HIV-1 genome
(Adapted from www.yale.edu/bio243/HIV/genome.htm).

The genome is comprised of the gag (group-specific antigen), pol (polymerase) and env (envelope) genes, which encode the viral nucleocapsid, polymerase and envelope proteins. A long terminal repeat (LTR) region flanks these genes, and all of them, together with tat (transactivator of transcription) and rev (regulator of viral protein expression), make up the genome of the human immunodeficiency virus (Costin, 2007). Free virus, concentrated in the blood plasma, begins the process of infection by binding to the immuno-specific CD4 T-helper cell (Girard *et al.*, 2011). CD4 is a 58 kDA protein that is found on approximately 60% of T-lymphocyte cells (Hoffmann *et al*., 2007). Research has shown that HIV is capable of infecting other cells in the body (including monocytes, macrophages and dendritic cells) but that the virus has the strongest affinity for CD4. However, it has been established that CD4$^+$ cells promote viral replication, whereas CD4$^-$ cells do not (Douek *et al.*, 2002).
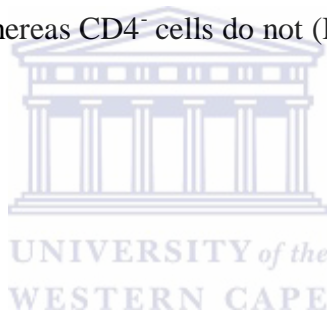
1.1.1 Viral entry

The first step in the infection of these CD4$^+$ cells is the binding of the HIV membrane protein gp120 to the CD4 cell surface. This protein, which binds to the CD4 receptor, is a structural protein synthesised from the *env* gene (Figure 1). Though it is necessary, the CD4 receptor is not the only receptor required for HIV infection and entry into the cell

(Hernandez *et al.*, 1996; Edo-Matas *et al.*, 2011). CD4 acts as a primary receptor, but co-receptors, such as CCR5 and CXCR4, are also needed and act as secondary receptors for the entry and infection of cells with HIV (Edo-Matas *et al.*, 2011) .

Although other co-receptors have been identified, these two chemokines have been implicated as being the most active co-receptors during the process of viral entry. Experiments done with recombinant human CD4 provided evidence that viral fusion and entry was made possible by an Env-mediated reaction, but that a co-receptor was needed to facilitate this process (Berger *et al.*, 1999). Although these co-receptors have been positively pinpointed as being the active coreceptors during HIV infection, it has also been determined that the active coreceptor (either CCR5 or CXCR4), is specific for the HIV-1 variant (Hoffmann *et al.*, 2007). Experimental analysis has shown that CXCR4 is the specific coreceptor for viral entry in T-cell lines and these variants are therefore called TCL-tropic variants (Berger *et al.*, 1999). In the case of primary T cells, both CXCR4 and CCR5 are active in viral entry, making these variants of HIV-1 dual-tropic. Finally, in macrophage cells, CCR5 has been identified as the coreceptor active in HIV-1 viral entry, and these variants are aptly named M-tropic lines (Berger *et al.*, 1999). The fact that these receptors are present in specific cells has led to the idea that certain individuals could be resistant to specific variants of HIV-1. This was proven when it was found that persons who were homozygous for a 32bp deletion in the CCR5 gene, were resistant to infection with that particular variant of HIV-1 (Navenot *et al.*, 2001). These important discoveries have also made the co-receptors of HIV-1 prime targets for HIV-1 treatment strategies (Tsibris and Kuritzkes, 2007). Upon binding to the cellular surface, the gp120 viral membrane protein interacts with CD4 on the membrane surface of the target cell. This triggers the activation of, amongst others, the CXCR4 and CCR5 cellular receptors, which indirectly allow for the engulfment and uptake of the virus into the cell (Tsibris and Kuritzkes, 2007).

1.1.2 Reverse transcription and integration

In order for viral replication to take place, the virus must insert its genome into that of its host (Bushman and Craigie, 1991). Upon cellular entry, the HIV-1 virion undergoes an uncoating process during which its outer "shell" is removed, exposing the core of the virus. This is then followed by a series of events, starting with the binding of tRNA primers (Hoffmann *et al.*, 2007). Subsequent to tRNA primer binding, the proviral strand of DNA is synthesised, and viral RNA is degraded by RNAse H. A template switch from haplogroup R to haplogroup U5 DNA is followed by full-length polymerisation of the proviral DNA (Hoffmann *et al.*, 2007). This polymerisation process is followed by host cellular activation of the viral integrase enzyme. Integrase then binds to attachment sites at the end of each viral long terminal repeat (LTR). Once the cDNA synthesis from RNA is complete, a cutting process, in which two nucleotides are cut from each of the viral LTRs, can occur (Vandegraaff and Engelman, 2007). The aforementioned process is key during the formation of the pre-integration complex (PIC). The viral PIC, as demonstrated in Figure 1.2, is comprised of a number of factors, including the viral DNA (transcribed by reverse transcriptase), the matrix protein, integrase as well as Vpr. In order for integrase to facilitate DNA-strand transfer, the PIC needs to come into close contact with chromatin DNA.

Integrase is then able to cleave specific viral DNA sequences during 3´ processing (Vandegraaff and Engelman, 2007) and the entire PIC is then transported from the host membrane to the nucleus, where it is integrated into the host genome (Sherman and Greene, 2002).
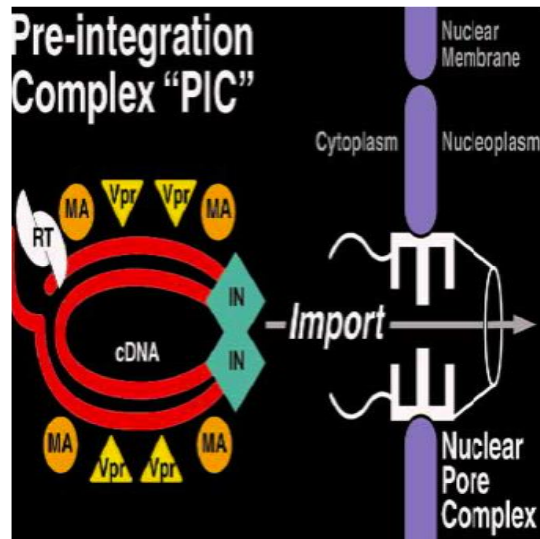
Figure 1.2 Pre-integration and nuclear import of HIV.

(Adapted from Sherman and Greene, 2002).

1.1.3 Post-integration

Subsequent to viral integration, the synthesised viral DNA undergoes transcription by the host organism. This process is facilitated by various elements, but particularly by the nuclear transcription factor NF-κB, which initiates transcription by binding to the long terminal repeat (LTR) of the virus (Trkola, 2004). The regulatory viral proteins, tat and rev, are also synthesised at this point. These proteins play a key role in the promotion of transcription of viral DNA and the formation of mature viral particles (Hoffmann *et al.*, 2007). Another important protein that is synthesised at this point is the HIV-1 protease. The protease is needed for the cleavage of the gag-pol polyprotein in order to produce mature, infectious viral particles (Simon *et al.*, 2006). Upon completion of transcription, viral transcripts are efficiently packaged and the release of mature virus is facilitated by the budding process, an almost equal, but opposite process to membrane fusion during HIV entry (Trkola, 2004).

1.1.4 HIV-1 protease: structure and function

HIV-1 protease functions in a critical role to cleave the viral gag-pol polyproteins, as seen in Figure 1.3, towards the production of both structural as well as functional viral proteins. The importance of the protease has been demonstrated by mutation studies that revealed that in the absence of active protease, the virus cannot be formed as an infectious structure (Kohl *et al.*, 1988).
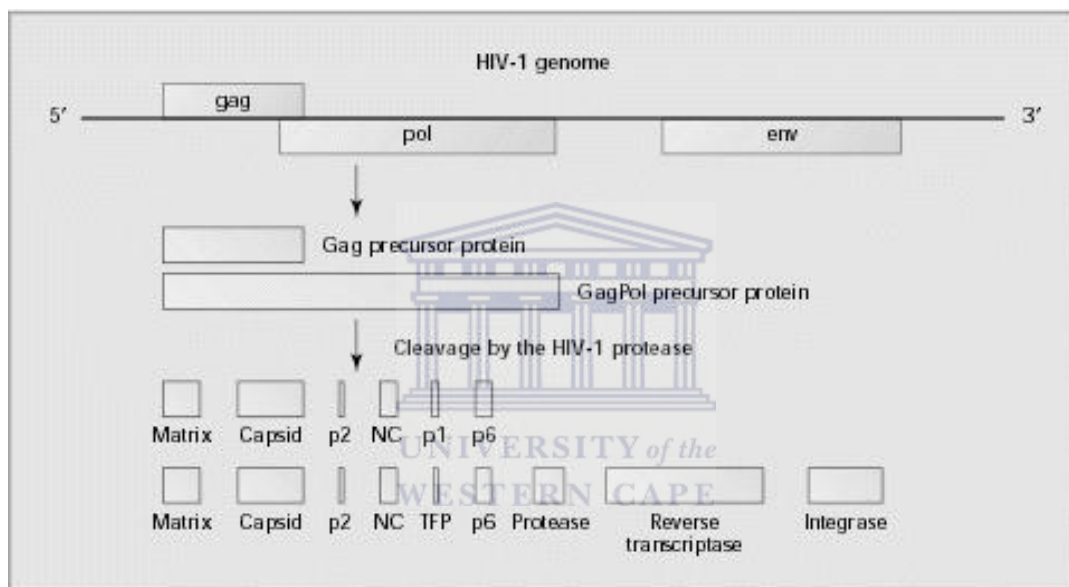
Figure 1.3 Cleavage of the Gag-Pol polyprotein by HIV-1 protease (Nijhuis *et al.*, 2007).

The very first crystal structure of HIV-1 protease was obtained by Merck laboratories, which was followed by a more detailed structure in 1989 (Brik and Wong, 2003). HIV-1 protease is an aspartic acid protease, comprised of two non-covalently bonded identical monomers, 99 residues long.

HIV-1 protease has a binding cleft that allows for the cleavage of various viral precursors for the production of active protein, as can be seen in Figure 1.4 (Ghosh *et al.*, 2009).

Each of the monomers has a glycine-rich loop which partially serves as the substrate-binding region. It also houses the essential Asp-25 aspartyl residue, labelled in Figure 1.4, which is essential for protease function. Since HIV-1 protease is classified as an aspartic protease, it contains the conserved Asp-Thr-Gly domain.

Mutational analysis, as well as three-dimensional structure of the HIV-1 protease confirms that it is similar in both structure and mechanism to the aspartic proteases (Brik and Wong, 2003). The viral protease is, therefore, similar to other aspartic proteases, including caspases, which also play a role in cell death.
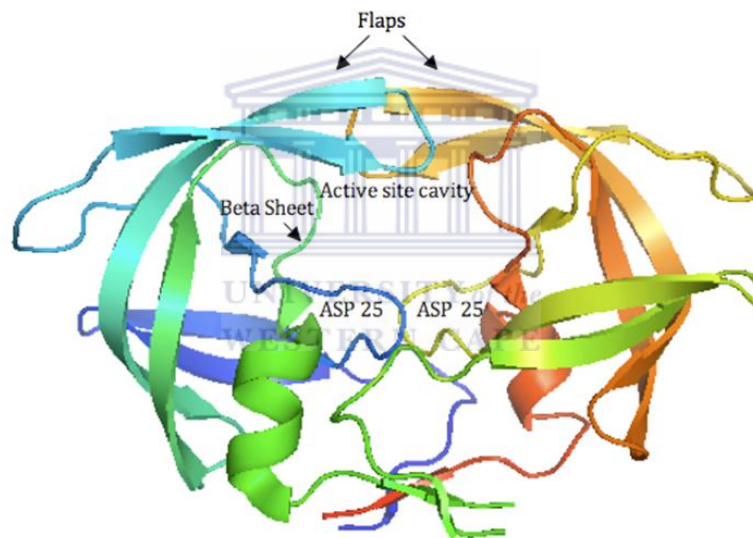
Figure 1.4 Crystal structure of HIV-1 protease demonstrating active sites and domains (Adapted from Ghosh *et al.*, 2009).

1.2 Infection and pathogenesis

The most common route for infection by HIV-1 is by sexual transmission. It can also enter the body via other means, including intravenous drug use, contact with infected blood, maternofetal transmission and, in rare cases, during blood transfusion (Hoffmann *et al.*, 2007). The virus replicates and spreads throughout the body at such a fast pace that it can be detected in the blood only 5 days after infection (Kahn and Walker, 1998). This earliest stage of HIV infection is known as acute HIV infection. At this stage, approximately 0.1% of the body's total CD4 lymphocytes are infected with HIV (Richman, 2001). During this phase of the infection, the virus is replicating at an alarming rate and the individual will present with symptoms similar to a viral infection. It is this similarity to common viral infections, such as influenza, that makes it difficult to diagnose the patient during this phase (Hoffmann *et al.*, 2007). Unfortunately, it is also during this phase that correct diagnosis could result in the patient receiving the best antiretroviral treatment. This, however, does not occur very often, since the symptoms are commonly mistaken for a simple viral infection (Kahn and Walker, 1998). During this phase, viraemia is at its highest, causing the risk of transmission to be highest here. This phase is also concurrent with the rapid decline of $CD4^+$ T cells. The most common symptoms associated with acute HIV-1 infection are listed in Table 1.

Table 1. Most common symptoms experienced by HIV-1 infected patients (Adapted from Kahn and Walker, 1998).

SYMPTOMS	PERCENTAGE PATIENTS
Fever	>80-90
Fatigue	>70-90
Rash	>40-80
Headache	32-70
Lymphadenopathy	40-70
Pharyngitis	50-70
Myalgia	50-70
Nausea, vomiting, diarrhea	30-60
Night sweats	50
Aseptic meningitis	24
Oral ulcers	10-20
Genital ulcers	5-15
Thrombocytopenia	45
Leukopenia	40
Elevated hepatic enzyme levels	21
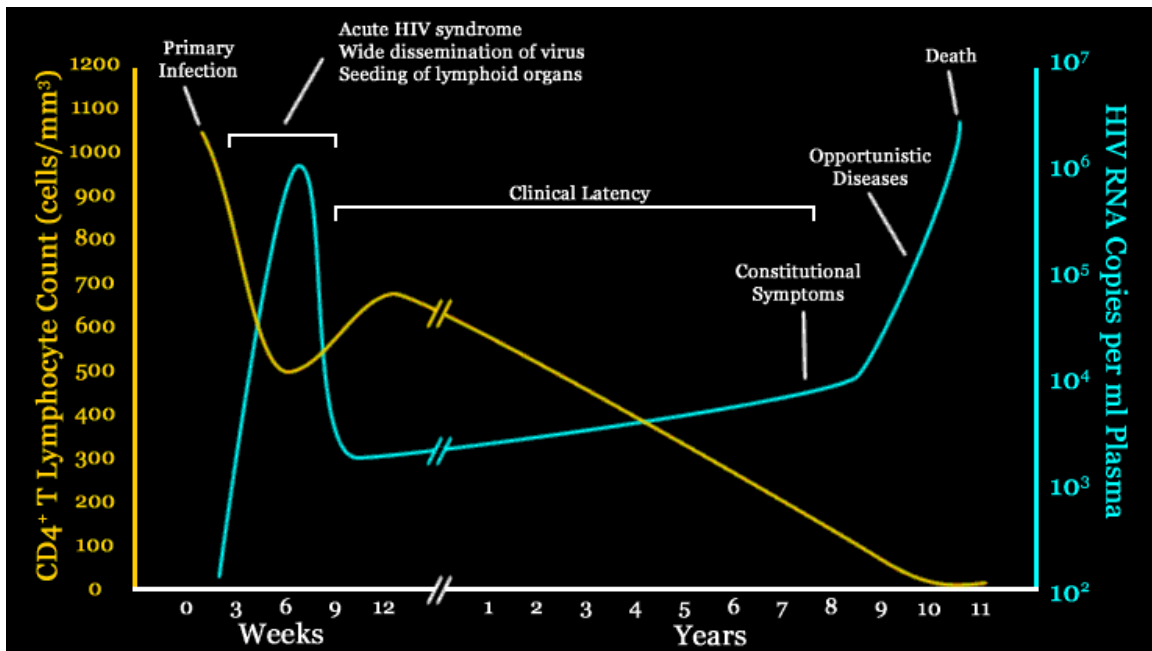
Figure 1.5. Clinical stages of HIV infection (adapted from Pantaleo *et al.*, 1993).

The phase that follows the acute phase is fairly asymptomatic, but disease progression is still dramatic, as can be seen in Figure 1.5. The final stage of disease is the development of AIDS. It is during this stage that the individual will experience high levels of viraemia, complemented by CD4$^+$ depletion (Simon *et al.*, 2006).

These combined features of the disease result in compromised immunity and the patient becomes susceptible to opportunistic infections. Since the immune system cannot fight off these infections, death is more than likely to ensue (Hoffmann *et al.*, 2007).

1.3 Current antiretroviral treatments

Antiretrovirals have been the topic of much controversy in the pharmaceutical and economic world. Their ability to slow down the rate at which cells are infected, and thereby prolong life, is countered by a number of setbacks (Adamson and Freed, 2008). The pill-burden of antiretrovirals and various side-effects associated with them have prompted research for alternative treatment strategies (Godnick, 2007). Since HIV was discovered, a number of antiretroviral agents have been developed and are available for use. These drugs are discussed in the next section in further detail.

1.3.1 Nucleoside and Nucleotide Reverse Transcriptase Inhibitors (NRTIs)

Nucleoside residues can be described as nucleobases attached to either a ribose or deoxyribose sugar (Matthews *et al.*, 2000). Analogues of nucleosides, as well as nucleotides, are used to inhibit the action of the reverse transcriptase enzyme required for HIV replication (Hoffmann *et al.*, 2007). These drug types were the very first anti-HIV drug to be developed and were thought to be the solution the world was after (Squires, 2001). These bases are rather similar to the naturally occurring nucleosides and nucleotides, with a slight difference in, e.g., one base. This difference causes an alteration in the building blocks of DNA, thereby interfering with DNA synthesis of HIV (Hoffmann *et al.*, 2007).

Nucleoside Reverse Transcriptase Inhibitors (NRTIs) are still a large component of the combination therapy for HIV, and the level of tolerance in patients has proven to be bearable, save for the gastrointestinal side-effects and mild headaches (Hoffmann *et al.*, 2007).

However, it has been determined that the long-term effects of this type of drug are not so minor (de la Rosa *et al*., 2004). Aside from the well-known mitochondrial toxicity associated with these NRTIs (Brinkman *et al*., 1999), patients also suffer from pancreatitis, lactate acidosis and myelotoxicity (Hoffmann *et al.*, 2007). Not only does one have to consider the physiological effects of this drug, but the virus has now developed resistance to many of the existing nucleoside analogues (Menendez-Arias and Tozser, 2008).

1.3.2 Non-nucleoside Reverse Transcriptase Inhibitors (NNRTIs)

This group of antiretrovirals are similar to the above-mentioned ones, in that it also targets the enzyme reverse transcriptase. Where they do differ, however, is that NNRTIs bind specifically to reverse transcriptase to form an enzyme-substrate complex that causes the deceleration of reverse transcription action (Hoffmann *et al.*, 2007). Another difference between these two inhibitors is that NRTIs require phosphorylation to become active, whereas NNRTIs do not (Temesgen *et al*., 2006). Between the years of 1996 and 1998, three NNRTIs were accepted for clinical use. These included efavirenz, nevirapine and delavirdine (Hoffmann *et al.*, 2007). Delavirdine, however, is not used very often in the clinical environment due to the high dosage required (pill burden) and its low efficacy (Temesgen *et al*., 2006). Amongst the most common effects of delavirdine is the range of central nervous system effects. These could range from sleeplessness to mania and occur in as many as 40% of patients (Carr and Cooper, 2000).

1.3.3 Protease Inhibitors (PIs)

HIV-1 Protease cleaves the gag-pol polyprotein into its active subunits, generating viral protein needed for maturation. If these proteases are inhibited, the virus is unable to produce infectious, mature virion (Hoffmann *et al.*, 2007). Protease inhibitors function by inhibiting HIV-1 protease, thereby preventing the production of the proteins required for viral maturation. These inhibitors are used in combination with other ARVs for the inhibition of viral replication (Flexner, 1998). A number of protease inhibitors have been licensed in the US and have been made available for use (listed below). Although these inhibitory drugs have been used successfully in combination with other ARVs, there remains a range of adverse effects associated with PIs (Carr and Cooper, 2000). Aside from the high dose required for the drug to function effectively, PIs have also been known to cause gastrointestinal disturbances, lipodystrophy, dyslipidemia, sexual dysfunction as well as cardiovascular disease (Flexner, 1998). It is for this reason that different approaches are being researched for the improvement of HIV drug treatment (Adamson and Freed, 2008).

Table 2. Side-effects observed in some individuals after administration of protease inhibitors (Adapted from Carr and Cooper, 2000).

	INDINAVIR	NELFINAVIR	RITONAVIR	SAQUINAVIR	AMPRENAVIR
TOXIC EFFECT	Renal calculi	Diarrhoea	Perioral paraesthesiae	Nausea	Hypersensitivity
	Hyperbilirubinaemia	Nausea	Nausea	Diarrhoea	Perioral paraesthesiae
	Reflux oesophagitis	Cytochrome P450 interaction of drug metabolism	Diarrhoea and Flushing	Cytochrome P450 interaction of drug metabolism	Cytochrome P450 interaction of drug metabolism
	Retinoid effects	Spontaneous bleeding in haemophiliacs	Cytochrome P450 interaction of drug metabolism	Spontaneous bleeding in haemophiliacs	Spontaneous bleeding in haemophiliacs
	Haemolytic anaemia		Spontaneous bleeding in haemophiliacs		
	Cytochrome P450 interaction of drug metabolism				
	Spontaneous bleeding in haemophiliacs				

1.3.4 Other anti-HIV drug developments

Other than the antiretrovirals that have been developed for reverse transcriptase and protease inhibition, research has also focused on a number of entry inhibitors as well as integrase and maturation inhibitors (Adamson and Freed, 2008). Entry inhibitors, as the name suggests, inhibits the binding of the viral gp120 to the CD4 receptor, or the co-receptors, CCR5 and CXCR4 (Briz *et al.*, 2006), thereby blocking entry of HIV into host cells. Since viral entry occurs via three phases, there are also three different types of entry inhibitors. These include attachment, co-receptor as well as fusion inhibitors. Of these drugs, a number are currently on the market, and include the fusion inhibitor enfuvirtide (Briz *et al.*, 2006), a CCR5 receptor inhibitor, maraviroc (Dorr *et al.*, 2005), as well as the integrase inhibitor, raltegravir

1.4 Alternative strategies for HIV-1 eradication

Due to the increasing occurrence of resistance to antiretrovirals via genetic mutation, researchers have been focusing their attention on more effective treatment strategies (Fauci, 2003). Aside from the increase in the number of antiretroviral developments, there has also been a trend toward the eradication of HIV-infected cells by inducing cell death.

Vocero-Akbani *et al* demonstrated one such strategy in 1999 when they suggested a Trojan horse strategy that specifically targets and kills HIV-infected cells through the initiation of apoptosis. HIV-1 protease is necessary for the production of new viral particles (Haseltine, 1991). This strategy exploits the fact that HIV-1 protease is an aspartic acid protease similar to caspases.

Instead of inhibiting the protease, as with previous strategies, the protease was exploited by inserting residues for HIV-1 protease into caspase-3, a cell death-inducing protein (Vocero-

17

Akbani *et al.*, 1999). This would allow HIV-infected cells to be killed specifically and without the destruction of neighbouring, uninfected cells. This strategy, and others like these, could very well be a more permanent answer to the problems we have been faced with for more than 20 years (Fauci, 2003).

1.5 Apoptosis

1.5.1 What is apoptosis?

Apoptosis can be defined as a process during which cells in the body are programmed to undergo a sequence of biochemical events leading to their death. This process is a neat, highly controlled one and is often referred to as cellular suicide. This phenomenon was first discovered by Kerr *et al* in 1972, when they referred to this targeted cell death as 'apoptosis'. The term was chosen since it directly translates to 'falling off' of leaves from trees in Greek. At the time, necrosis, a different type of cell death, was already known (Santini *et al.*, 2000).

Necrosis was, however, much less controlled when compared to apoptosis. During necrotic cell death, cells experience mitochondrial swelling, membrane disintegration as well as leaking of cell contents into the surrounding tissues. This results in the activation of the inflammatory response, and leads to the eventual death of surrounding, healthy cells. This type of cell death, since it is uncontrolled and causes harm to adjacent cells, is more commonly referred to as pathological cell death (Kanduc *et al.*, 2002).

Upon comparison of apoptosis and necrosis, distinct differences have been detected. These differences are listed in table 3.

Table 3. Necrotic versus Apoptotic Cell Death (Adapted from Zador *et al.*, 2003)

NECROSIS	APOPTOSIS
Morphological differences	
Membrane integrity lost	Membrane blebbing, Membrane integrity maintained
Mitochondrial and organelle swelling	Shrinkage and condensation of cytoplasm
Cell lysis and leakage	Cell fragmentation, Vesicle formation
Biochemical differences	
No energy-dependence	Energy-dependent process
Loss of ion homeostasis	Highly controlled enzymatic process
Randomized DNA digestion	Specific, DNA fragmentation
Physiological differences	
More than one cell affected at a given time	One cell targeted and affected
Pathogical death	Death induced by physiological stimuli
Induction of inflammatory response	No inflammatory response

During the apoptotic process, cells are individually targeted for elimination. This occurs via a number of stages that include cell shrinkage, organelle shrinkage, chromatin condensation and the formation of vesicles that are phagocytosed by surrounding macrophages (Matute-Bello and Martin, 2003). Apoptotic cells are also easily identified by the externalisation of phosphatidylserine at their cell surface (Earnshaw *et al.*, 1999).

Apoptosis does not occur in a large number of cells at a given time, and this type of death is therefore not seen in large groups of cells. Cells are usually induced to undergo apoptosis in response to an imbalance in tissue homeostasis and apoptosis is characteristically seen during embryonic development. In response to disease, apoptosis also acts to eliminate cells affected by cancerous growth as well as viral infections like HIV (Kam and Ferch, 2000). Wherever it is involved, the main function of apoptosis remains to induce physiological death in cells that pose a threat to the body (Elmore, 2007).
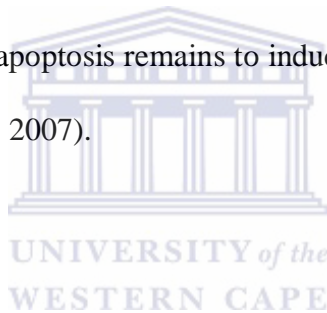
1.5.2. Caspase structure and activation

The apoptosis pathways, whether intrinsic or extrinsic, are largely dependent on the cleavage of a family of proteases termed caspases (Chowdhury *et al.*, 2008). The first caspase known to result in apoptosis, however, was identified in *C. elegans* as the cell death gene and called ced-3 (Kumar, 2007). Since then, the number of mammalian caspases that have been identified has risen to 15 of which 11 have been identified as human (Nicholson, 1999).

Caspases are **c**ysteinyl **asp**artate protein**ases** and cleave substrates after the Asp residue (Kumar, 2007). The first member of this family to be identified was the protease required for the maturation of pro-IL-1β, at the time called **i**nterleukin-1β-**c**onverting **e**nzyme (ICE). It was subsequently cloned and called caspase-1 (Chowdhury *et al.*, 2008).

Caspases are synthesised as catalytically inactive zymogens known as pro-caspases, before being cleaved by other caspases to become active, mature caspases, as demonstrated by Figure 1.7. The small and large subunits of active caspases are derived from the inactive pro-domain. The large subunit contains the proteolytic region, including the cysteine and histidine residues of the active site. Residues S4-S1 from both subunits make up the substrate-binding cleft (Nicholson, 1996), similar in structure to the HIV-1 protease mentioned earlier.
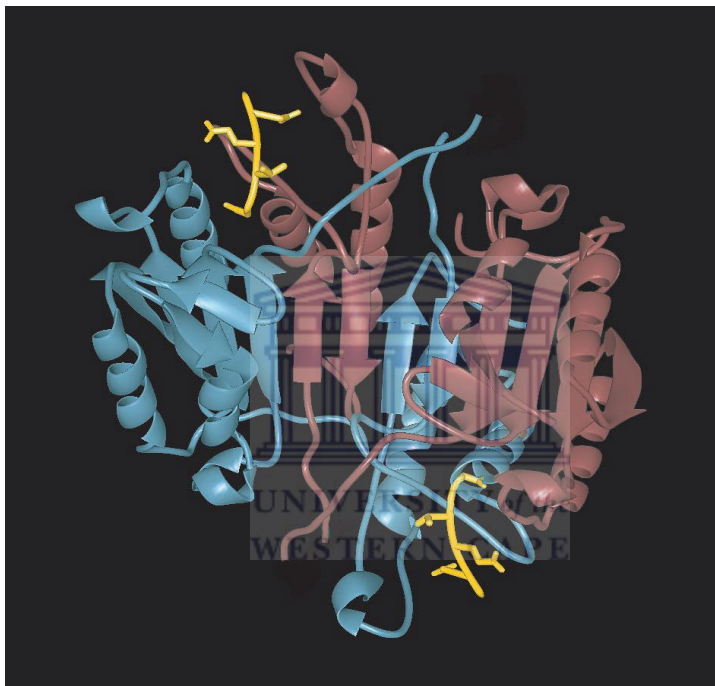
Figure 1.6. X-Ray crystal structure of caspase-3 in complex with a substrate-based inhibitor (Adapted from Nicholson, D.W., 1999).

Caspases are divided into two groups, namely initiator caspases and effector caspases. Initiator caspases function to activate effector caspases, which make apoptosis possible (Boatright and Salvesen, 2003).
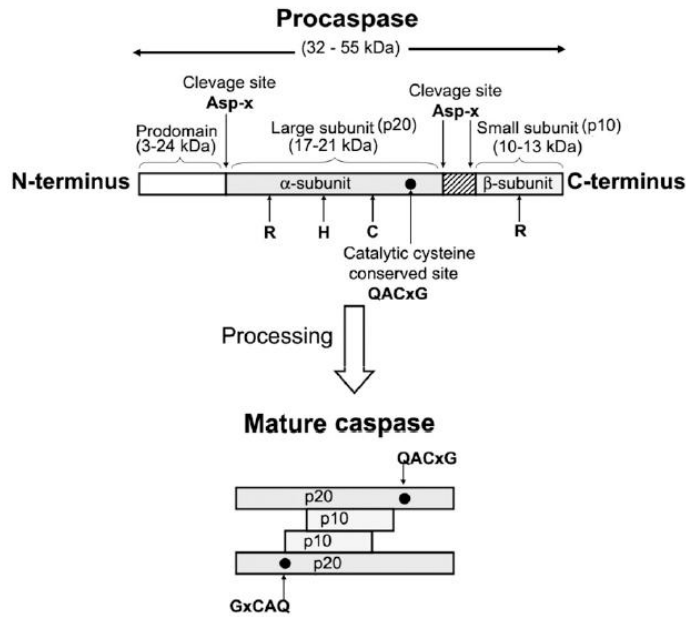
Figure 1.7. Activation of a pro-caspase into a mature, active caspase (Chowdhury *et al.*, 2008).

Mammalian, apoptotic caspases, apart from having differences in function, also differ in their prodomain structure. Initiator caspases have long pro-domain structures at the N-terminus, comprised of a death effector domain (DED) or a caspase recruitment domain (CARD) (Chen and Wang, 2002). These include caspases 1, 2, 4, 5, 8, 9, 10, 11, 12 and 13. Effector caspases, however, caspases 3, 6, 7 and 14 possess short pro-domains (Nunez *et al.*, 1998). Caspase active sites are, however, highly conserved among both effector and initiator caspases, as demonstrated in Figure 1.8.

```
caspase-5   VDEKNLTARD MESVLRAFAA RPEHKSSDST FLVLMSHG.. .....ILEGI CGTAHKKKKP DVLLYDTIFQ IFNNRNCLSL KDKPKVIIVQ ACRGEKHGEL
caspase-4   DVEENLTARD MESALRAFAT RPEHKSSDST FLVLMSHG.. .....ILEGI CGTVHDEKKP DVLLYDTIFQ IFNNRNCLSL KDKPKVIIVQ ACRGANRGEL
caspase-1   DVKKNLTASD MTTELEAFAH RPEHKTSDST FLVFMSHG.. .....IREGI CGKKHSEQVP DILQLNAIFN MLNTKNCPSL KDKPKVIIIQ ACRGDSPGVV
caspase-7   IVYNDCS.CA KMQDLLKKAS EEDHTNAACF ACILLSHGEE .......NVI YGK.....DG V.TPIKDLTA HFRGDRCKTL LEKPKLFFIQ ACRGTELDDG
caspase-3   RNKNDLT.RE EIVELMRDVS KEDHSKRSSF VCVLLSHGEE .......GII FGT.....NG P.VDLKKITN FFRGDRCRSL TGKPKLFIIQ ACRGTELDCG
caspase-6   KCFNDLK.AE ELLLKIHEVS TVSHADADCF VCVFLSHGEG .......NHI YAY.....DA K.IEIQTLTG LFKGDKCHSL VGKPKIFIIQ ACRGNQHDVP
caspase-8   KPHDDCT.VE QIYEILKIYQ LMDHSNMDCF ICCILSHGDK .......GII YGT.....DG QEPPIYELTS QFTGLKCPSL AGKPKVFFIQ ACQGDNYQKG
caspase-10  HIHNNVTKVE MEMVLQKQKC NPAHADGDCF VFCILTHGRF .......GAV YSS.....DE ALIPIREIMS HFTALQCPRL AEKPKLFFIQ ACQGEEIQPS
caspase-9   EVKGDLTAKK MVLALLELAR .QDHGALDCC VVVILSHGCQ ASHLQFPGAV YGT.....DG CPVSVEKIVN IFNGTSCPSL GGKPKLFFIQ ACGGEQKDHG
caspase-2   HVLCDQTAQE MQEKLQNFAQ LPAHRVTDSC IVALLSHGVE .......GAI YGV.....DG KLLQLQEVFQ LFDNANCPSL QNKPKMFFIQ ACRGDETDRG
```

Figure 1.8 Amino acid sequence alignment of caspases, showing active site conservation (Adapted from Cohen, 1997).

1.5.3 Caspase-3 and its role in apoptosis

Caspase-3, also termed CED-3 or CPP32, was the first identified effector caspase found to be involved in apoptosis of mammalian cells (Kang *et al.*, 2008). Caspase-3 is known to be one of the most frequently activated caspases involved in apoptosis and has therefore been known to play a critical role in the process as a whole (Porter and Jänicke, 1999). The activation of this effector caspase occurs via two pathways, namely the extrinsic and the intrinsic pathways. In the extrinsic pathway, death receptors result in the formation of a death-inducing signaling complex (DISC), which results in the accumulation of active caspase-8. Caspase-8 then results in the activation of the effector caspase-3, thereby resulting in apoptosis. In the intrinsic pathway, which is mediated by the mitochondria, cytochrome *c* is released. Upon release of cytochrome *c*, a cytoplasmic complex, the apoptosome, is formed, which is responsible for the activation of procaspase-9. Once again, the effector caspase, caspase-3, is activated and this results in apoptotic cell death (Chowdhury *et al.*, 2008).

1.5.4 Caspase-3 as a death-inducing protein for HIV-1 infection

As mentioned in section 1.5, a strategy that employed caspase-3 as a death-inducing protein for HIV-infected cells was demonstrated by Vocero-Akbani *et al* in 1999. They suggested a strategy that makes use of the function that HIV-1 protease has in cleaving the gag-pol protein to produce new viral proteins (Haseltine, 1991). The current treatment regime for HIV-1 infection includes, amongst others, inhibitors of HIV-1 protease to combat viral replication. In the strategy by Vocero-Akbani and colleagues, however, the protease was used to trigger apoptosis in cells representing HIV infection. This was achieved by site-directed mutagenesis of caspase-3 by replacing caspase-3 cleavage sites with HIV-1 protease cleavage sites. Caspase-3 and HIV-1 protease are both aspartic proteases, and are similar in both structure and mechanism of function. This strategy therefore resulted in the cleavage of caspase-3 into its active form in the presence of HIV-1 protease, which subsequently resulted in the activation of apoptosis in cells containing HIV-1 protease. It can therefore be concluded that this strategy successfully demonstrated the destruction of cells containing HIV-1 protease by apoptotic cell death (Vocero-Akbani *et al.*, 1999).

The study is not, however, without limitations. One such limitation is that, due to the use of the transactivator of transcription (TAT) protein transduction domain, the mutant caspase-3 was not targeted to cells, and as a result, was non-specific.

Protein transduction domains, also called protein derived cell penetrating peptides (CPPs), promote cellular internalization, but are not specific (Zorko and Langel, 2005). Non-specific delivery of a therapeutic is not ideal, since it reduces the efficacy thereof. One way of combating the aforementioned limitation is by targeted delivery of the mutant caspase-3.

Many strategies for delivery exist, but in this study, nanotechnology was used as a means of targeted delivery of the therapeutic. Nanotechnology offers an exciting new solution to the problems associated with drug delivery, and is explored further in the next section.

1.6 Nanotechnology

Nanotechnology can be described as the study, design, synthesis, creation, utilisation or manipulation of structures in the nano size range (1×10^{-9} of a meter) to produce desired effects (Salamanca-Buentello *et al.* 2005; Maynard, 2007). Aside from setting the research world abuzz, nanotechnology has also been hailed in popular press as the latest major technological breakthrough. Working in the nano size range allows scientists to explore a world that has, until recently, remained unknown.

The nanotechnology hype started in the 1990's, when Eigler and Schweizer had the letters IBM printed on a nickel substrate using only 35 xenon atoms (Eigler and Schweizer, 1990). This was the first work done in the nano size range. However, the concept of working at an atomic scale was first unveiled in a Nobel laureate's lecture in the year 1959. When the reknowned physicist, Richard Feynman, talked in his lecture about manipulating atoms at the nano level, he postulated that it was indeed possible to work at an atomic scale. He also stated that at the time, science had not been able to put it in practice, but that in the future, it would become possible (Feynman, 1959). Since then, nearly 50 years into the future, the technology is being utilised in a wide range of applications. This ranges from enhanced energy production and agricultural activities to improved food processing, biomedical applications (Salamanca-Buentello *et al.*, 2005).

The nanostructure era started with the development of liposome technology by Bangham *et al* in 1965. The development of semiconductor quantum dots by Eskimov *et al* in 1982 soon followed and later, in 1985, the discovery of fullerenes by Smalley *et al*. The discovery of starburst polymers (later identified as dendrimers) came in that same year (Tomalia *et al*., 2007). The identification of single-walled carbon nanotubes (SWCNT) came in 1991 (Ferrari, 2005) and very soon, structures in the nano size range were the order of the day. Among these nanostructures also emerged the development of colloidal gold nanoshells or nanoparticles. The first known synthesis of pure colloidal gold was performed by Michael Faraday in 1857, which was prepared by reducing gold chloride with phosphorus (Edwards and Thomas, 2007).

According to the National Nanotechnology Initiative (NNI) in the US, the ability to develop and manipulate materials and devices at the nanoscale will contribute roughly $1 trillion dollars to the US economy by 2015 (Hood, 2004). This is a large figure when one considers how "new" the field really is. Although the field is still in its infancy, a number of nanotechnology-based strategies have been developed. The following table demonstrates nanotechnologies that have been approved or are under review by the Food and Drug Administration (FDA) of the United States of America.

Table 4. Some nanoparticle-based pharmaceuticals approved or under review by the FDA (Adapted from Bawa, R., 2008).

Product name	Active ingredient	Company	Approved indication	Approval date
Doxil Caelyx	Pegylated doxorubicin liposomes	Orthobiotech Schering-Plough	Metastatic ovarian cancer	November 1995
Abraxane	Paclitaxel nanoparticles	Abraxis BioScience AstraZeneca	Metastatic breast cancer	January 2005
DaunoXome	Daunorubicin citrate liposomes	Gilead Sciences	Kaposi's sarcoma related to HIV infection	April 1996
VivaGel	Dendrimer gel	StarPharma Holdings	Vaginal microbicide for HIV prevention	IN TRIALS
Aurimmune	Gold particles coupled to TNF	CytImmune Sciences	Solid tumours	IN TRIALS

1.6.1 Nanotech to biotech: biological applications of nanotechnology

Biologically speaking, although nanotechnology has applications in numerous fields and industries, its application in medicine, termed nanomedicine, is undoubtedly amongst the most important (Park *et al.*, 2007). Research prospects and advances in nanotech in the medical field include targeted drug delivery, disease detection, cellular imaging as well as sensor technology (Kubik *et al.*, 2005). Since biological processes operate under the control of nanoscale processes, it only makes sense that nanotechnology and biology should form a convergence of sorts (Hood, 2004). Most biological components range between 1 and 100 nm in size, the exact size range that defines nanotechnological processes (Roco, 2003), providing an ideal arena for nanotechnology to be applied. Nanostructures that are currently being researched in the field include dendrimers, SWCNT, liposomes, micelles, semi-conductor quantum dots and colloidal nanoparticles. The following sections will demonstrate the application of these structures as well as their advantages and pitfalls.

1.6.1.1 Dendrimers

Dendrimers, or dendritic polymers, were first synthesised in 1985 by Tomalia *et al*. In this paper, they describe dendrimers to be starburst, hyperbranched macromolecules that emerge from a central core. They are generally made up of both carbohydrates and amino acids (Cloninger, 2002). The dendritic branches were seen as an ideal opportunity for the additions of various functional groups, as demonstrated by Figure 1.9. Due to their size, the high level of branching and its globular nature, dendrimers soon became of great interest as a scaffold in the field of drug delivery (Gillies and Frechet, 2005). In the cancer research arena, dendrimers carrying anti-cancer nucleotides were successfully delivered to various cancer cell lines (Ferrari, 2005). Since its synthesis, a vast amount of research has been conducted for various applications of dendrimers.
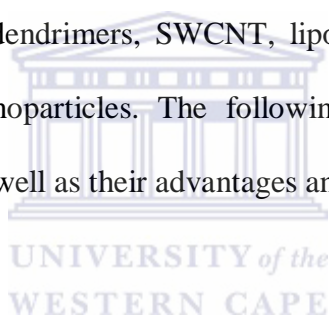
Aside from their application to drug delivery, they have also been applied as magnetic resonance contrast agents to improve MRI, *in vitro* diagnostics for determining heart muscle damage as well for the treatment of burns (Klajnert and Bryszewska, 2001).

There are, however, a number of challenges related to dendrimers. Firstly, dendrimers that are currently synthesised do not remain in circulation long enough to be effective as drug delivery vehicles. Another problem, that initially seemed to be an advantage, is that dendrimers have a globular structure, making steric hindrance a problem for the attachment of different proteins or peptides (Gillies and Frechet, 2005). Finally, dendrimers, like most other nanoparticles, still present a huge barrier with regard to toxicity. Since they have not been used in long term studies, the long term effects and toxicology of these particles are not well documented (Yiyun and Tongwen, 2005).
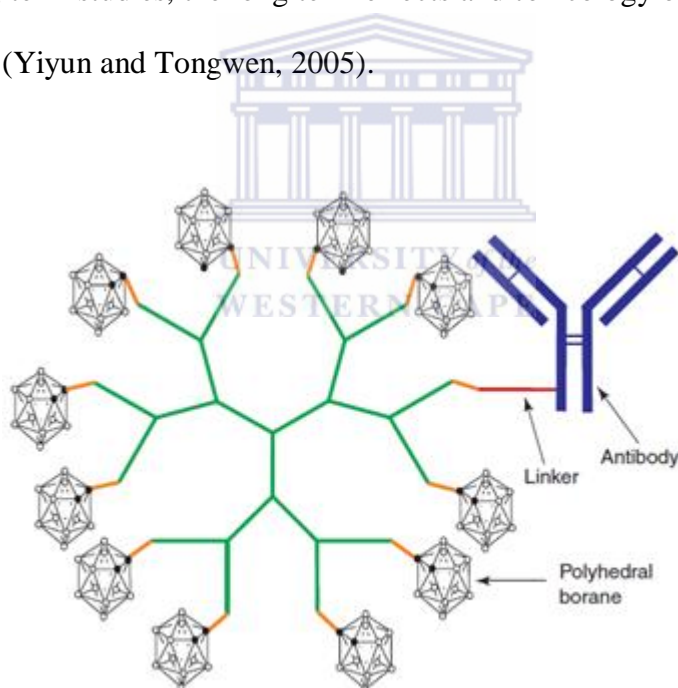
Figure 1.9 Example of dendrimer acting as drug targeting molecule (Adapted from Gillies and Frechet, 2005).

1.6.1.2 Carbon nanotubes

Single or multi-walled carbon nanotubes can be defined as tubular structures, seen in Figure 1.10, in the nano size range (Yih and Al-Fandi, 2006). These structures are usually grown on glass or quartz substrates, in the presence of a nickel catalyst. Nanotubes can vary in size between 30 and 150 nm in diameter and are surprisingly strong for their size. They have a tensile strength 100 times that of steel, indicating that these tiny structures are very strong (Kubik *et al*., 2005).

Due to the rigid nature of these tubes, they have been exploited in various aerospace and bone surgery applications. Though these structures, given their small size and electrical properties (Kubik *et al*., 2005), would seem highly applicable to biological systems, research has suggested otherwise. According to a study done by Shvedova *et al*. in 2004, single wall carbon nanotubes have adverse effects in rodents. A suspension of carbon nanotubes administered to mice and rats resulted in pulmonary inflammation, granuloma formation as well as mortality. During *in vitro* studies, the result was not much different. Carbon nanotubes caused oxidative stress in cell, indicated by free radical formation and the depletion of antioxidants. Even though a separate study, during which radiolabeled carbon nanotubes were administered to rodents, showed intact renal excretion, the safety and toxicity of carbon nanotubes is a major challenge for use in biomedical applications.
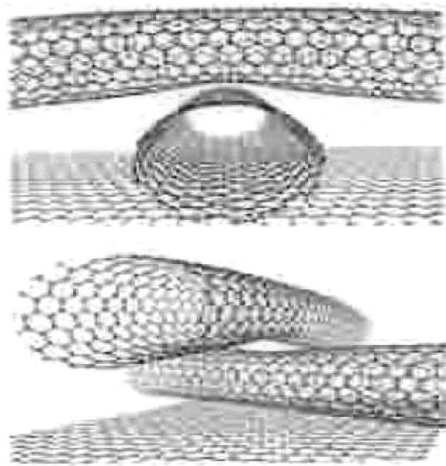
Figure 1.10 Single wall carbon nanotube structures (Adapted from Mamalis, A.G., 2007).

1.6.1.3 Liposomes

Liposomes were one of the first nanostructures to be applied in industry, having been around for nearly 35 years (Ferrari, 2005). Comprised of phospholipids and cholesterol, lipid-based vesicles such as liposomes and micelles have the potential to become the superstars of drug and gene delivery. In the past, liposomal development was hindered by the inability to understand how the body processes them. Lipoidal vesicles can accommodate a variety of substrates in their spaces, are capable of targeted delivery, facilitate slow release and also prevent degradation by enzymes (Sofou and Sgouros, 2008). A number of liposome formulations have been developed for various drug delivery applications, as can be seen in Figure 1.11. Due to these capabilities, drugs such as doxorubicin have been successfully encapsulated in a liposomal vesicle for the treatment of Kaposi's sarcoma (Ferrari, 2005). Lipid-based nanovectors such as liposomes and micelles have the advantage of being very small, allowing them to accumulate in areas with leaky vasculature, such as tumour tissue (Torchilin and Lukyanov, 2003). To facilitate targeted drug delivery, antibodies could easily be attached to the liposome surface (Sofou and Sgouros, 2008).

Other useful applications of liposomes in recent years have also included cosmetic applications such as wrinkle reduction and acne treatment. The micelle, another lipid-based structure, is very similar to liposomes, but have the disadvantage of having lower encapsulation ability in comparison to liposomes (Samad *et al*., 2007). Even though liposomes have so many advantages, a number of challenges do exist. Since polar drugs and drugs without charge are not encapsulated, the ability to deliver material to cells is rather low. When one considers the requirements for pharmaceutical use, liposomes do not have a long shelf life, something that would be considered crucial in the pharmaceutical industry. The long-term effects of these liposomal vesicles are also unknown (Soloman and Gabizon, 2008), leaving the door wide open for toxicity.
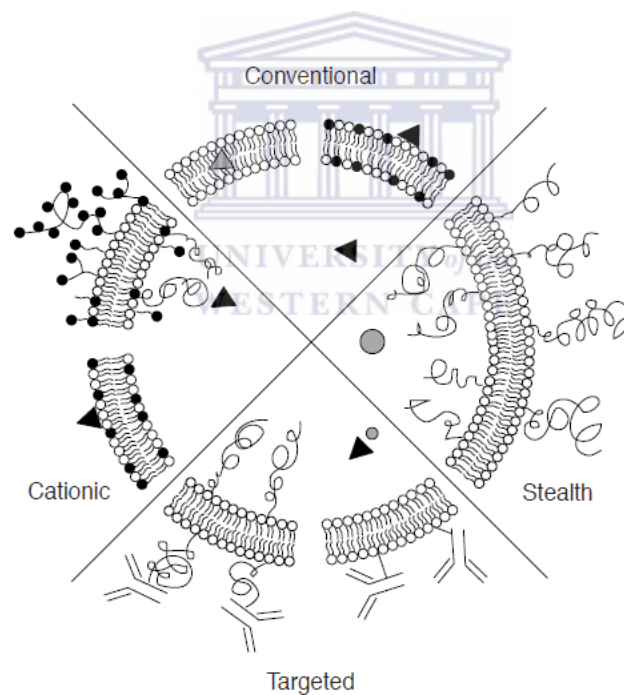
Figure 1.11 Primary types of liposomes used in various drug delivery applications (Adapted from Storm and Crommelin, 1998). Conventional liposomes remain either neutral or anionic in charge. Stealth liposomes refer to polymer-coated liposomes that exhibit increased circulation times. Targeted liposomes or immunoliposomes have antibodies which target them to antigens. Cationic liposomes refer to positively charged liposomes.

1.6.1.4 Semi-conductor quantum dots

In the ever-growing field of nanotechnology, semi-conductor nanocrystals have gained popularity for their inimitable optical and electronic capabilities (Jaiswal *et al*., 2003). In comparison to existing nanostructures, these particles seem to possess properties that the others do not, standing them in good stead for application in industry. Theoretically, semi-conductor quantum dots can be described as nanocrystals that have been synthesised and dispersed in a solvent (Alivisatos *et al*., 2005). Their synthesis is usually facilitated using precursor materials such as cadmium oxide (CdO) and in order to control the size thereof, nanocrystals are grown by means of the Ostwald process. This entails a ripening process during which small nanocrystals are broken up into tiny atoms and these atoms then form the basis for the synthesis of larger crystals (Chan *et al*., 2002).

Semiconductor nanocrystals in the 10-15 nm range seem to be of more interest to researchers in the field of biology as a result of their size and optical properties. At these sizes, there are hardly any limitations with regard to kinetics and binding. Steric hindrance also seems to be avoided in this range (Gao *et al*., 2007). Their unique optical properties are made possible by a process called 'quantum confinement'. This phenomenon results in the increase in spacing between atomic energy levels as the nanocrystal size is decreased. The most significant properties of these nanocrystals are their increased levels of fluorescence and increased resistance to photobleaching (Jaiswal and Simon, 2004).

Another feature of semiconductor quantum dots over other organic fluorophores is the ability to apply them to multiplexing experiments for coding entire libraries, whereas organic dyes can detect only one gene, protein or peptide at a time (Gao *et al*., 2004).

Up until the advent of quantum dots, the only available probes were organic dyes. These, although effective, are much more susceptible to photobleaching and also undergo a process where fluorescence is switched on and off, called blinking (Jaiswal and Simon, 2004). This makes quantum dots particularly useful in the field of cellular and molecular imaging and recent experiments show that quantum dots can be effectively employed in the tracking and detection of organs, cells, organelles, proteins and mRNA (Alivisatos *et al.*, 2005; Jaiswal and Simon, 2004; Gao *et al.*, 2004).

Figure 1.12 Colour variation of CdSe/ZnS semiconductor quantum dots after being excited with a near UV source (Adapted from Chan *et al.*, 2002). The emission spectrum increases from left to right, demonstrating various colours. The extreme left (dark blue) vial has an emission maximum value of 443 nm, while the vial on the extreme right has an emission maximum value of 655 nm.

Although quantum dots have proven to be a useful tool in the field of nanotechnology, there are a number of concerns regarding their toxicity in humans as well as their eradication from the body. Most of the semiconductor quantum dots used in biological applications are synthesised from cadmium and selenium (Gao *et al.*, 2004). Both of these are known to be toxic to humans in ionic form. Experiments by Derfus *et al.* in 2004 show that upon UV irradiation, cadmium is oxidised to Cd^{2+} ions and results in cell death via apoptosis. If one were to apply quantum dots to biological platforms such as drug delivery and imaging, they would need to be compatible with a biological environment.

To this end, researchers have looked towards adding certain functional groups. Chemical groups such as polyethylene glycol (PEG) and mercapto-undecanoic acid have been added to cadmium-based quantum dots to make them soluble in aqueous biological environments (Shiohara *et al.*, 2004; Alivisatos *et al.*, 2005; Yu *et al.*, 2006).

Figure 1.13 Structure of a quantum dot comprised of a Cadmium Selenide core and a Zinc Sulphide shell, which improves quantum yield and photostability (Adapted from Jaiswal and Simon, 2004).

One other way to protect the cadmium cores of CdSe quantum dots from oxidation is by the addition of a ZnS shell, as can be seen in Figure 1.13. This method also protects the quantum dots from interaction with biological media. Additionally, the coating of nanocrystals with ligands is also employed as a means of solubilising them, as well as creating a platform for the conjugation of biomolecules (Medintz *et al.*, 2005). In experiments performed by Gao *et al.*, quantum dots were conjugated with amphipathic triblock polymers to protect the inner core from the environment and PEG was used to aid with biocompatibility. This allowed successful tracking and mapping of lymph nodes in live animals (Gao *et al.*, 2004).

Even though these extra functionalities do protect the cadmium cores from being exposed, very little is known about the fate of quantum dots. Preliminary work suggests that they are eradicated from the body via kidney excretion and slow filtration (Gao *et al.*, 2004).

These have not yet been supported by scientific evidence and a great deal more research is needed to determine the endpoint of these nanostructures before they can be used in humans. However, a number of advances have been made with the use of quantum dots. Due to their increased fluorescence and size, colloidal nanocrystals have successfully been used in cellular tracking, cell motility, imaging and detection experiments (Alivisatos *et al.*, 2005).

1.6.2 Gold nanoparticles

From ancient Egypt to the California Gold Rush, there is no doubt that the discovery and production of gold has a colourful history. Through the years, gold has been developed as a form of currency and also made into jewellery, as an indication of wealth. Gold has long since provided us with a currency for trade and is currently one of the most valuable commodities in South Africa. The first appearance of gold nanoparticles, however, dates back to ancient times when they were used to produce stained glass (Sperling *et al*., 2008). Aside from its economic value, gold has also been known to have certain medical applications. In the late 1930's, for example, gold salts were found to dramatically improve the condition of patients suffering from rheumatoid arthritis. Back then, however, no precautionary measures were taken to prevent gold from causing a toxic response in patients. Due to this toxic response, mortality resulted in a small number of these patients (Sashin *et al.*, 1939). This initial interest in gold has led to the development and use of gold in small, colloidal clusters in the form of nanoparticles.

1.6.2.1 Preparation of biocompatible gold nanoparticles

The first method for synthesising colloidal gold was introduced by Faraday in 1857 and reworked by Turkevitch and colleagues in 1951 (Turkevitch *et al.*, 1951). The method employed was the citrate reduction of tetrachloroauric acid ($HAuCl_4$) in water, which lead to the synthesis of 20 nm particles (Daniel and Astruc, 2004).

Another method, the two-phase system, was first described by Wilcoxon *et al* in 1993 (Wilcoxon *et al.*, 1993) and then adjusted by Brust *et al* in 1994. This system employs the transfer of gold chloride from an aqueous solution to toluene by means of tetraoctylammonium bromide. The second phase, the reduction, is facilitated by sodium borohydride with dodecainethiol as the supplementary agent (Brust *et al.*, 1994). More recently, however, researchers have developed a method for the large-scale synthesis of nanoparticles at room temperature. These particles can be synthesised in a simple way so that they are of nearly equal molar mass, and the size is controllable by the amounts of tetrachloroauric acid added (Polavarapu and Xu, 2009). These size and structure of these particles is shown in Figure 1.14.
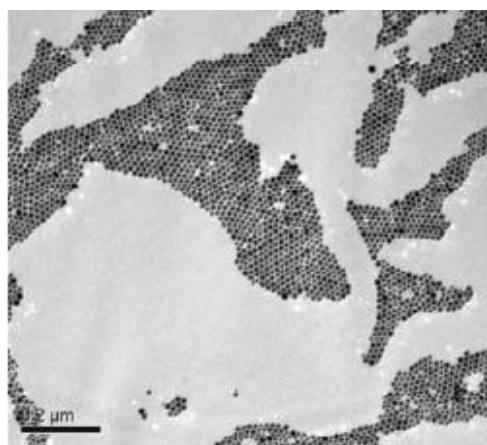
Figure 1.14 Transmission Electron Microscopy (TEM) image of biocompatible gold nanoparticles prepared by citrate reduction of gold chloride at room temperature (Polavarapu and Xu, 2009).

There are a number of characteristics of gold nanoparticles, as mentioned before, that make them an attractive choice for use in biological applications. One in particular is the ability to make these particles biocompatible by the addition of certain functional groups or biomolecules. This was demonstrated in a study by Tshikhudo and colleagues in 2004. In this study, thioalkylated polyethylene glycol ligands were designed and synthesised to generate gold nanoparticles that are soluble in aqueous environments (Tshikhudo, 2004). In a separate study by Shukla and colleagues in 2005, lysine and poly-L-lysine were used as capping agents to generate biocompatible gold nanoparticles (Shukla *et al.*, 2005). Upon adding these ligands, the metal core of the particle is shielded from the external environment and assists in protecting the cellular environment from undergoing a toxic response. Apart from ligands, the number and type of moieties added are naturally dependent on the application for which the particle is needed. The ability to functionalise these gold nanoparticles with organic molecules therefore allows nanoparticles to interact with the biological environment so it can carry out its intended function.
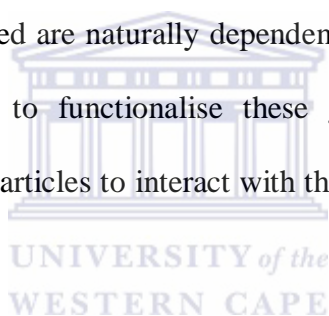
1.6.2.2 Applications of colloidal gold nanoparticles

In recent years, the use of colloidal gold nanoparticles has become very popular indeed. By nature, gold is biologically inert, less toxic than other materials and generally easy to synthesise (Sperling *et al.*, 2008). Colloidal gold nanoparticles have great promise in the development of nanoelectronic devices, biolabeling and biosensing. These are currently among the common applications of gold nanoparticles (Huo, 2007). A particularly useful characteristic of gold nanoparticles is the ability to conjugate and modify them by the addition of biomolecules and functional groups (Mishra *et al.*, 2009).

As demonstrated in Figure 1.15, a protein containing a poly-histidine tag can be functionalised to a nickel-activated nitriloacetic acid (NTA) gold nanoparticle. As a result of this functional ability, gold nanoparticles have been employed in a variety of fields, particularly in the biological sciences. Applications for gold nanoparticles include their use in drug and gene delivery (Moghimi *et al*., 2001). The ability of gold nanoparticles to interact with thiol groups also makes them a good choice for controlled release within the cellular environment and various examples of this can be observed in literature (Ghosh *et al*., 2008).
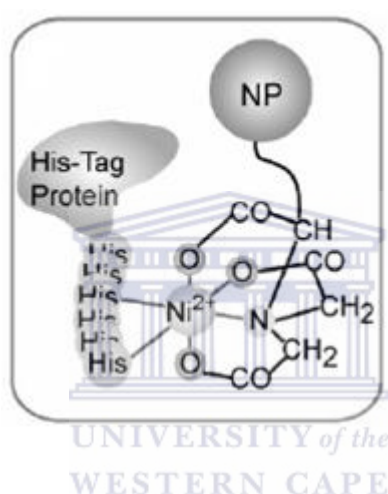
Figure 1.15 Schematic diagram of a gold nanoparticle functionalised with Ni-NTA for conjugation to a poly-histidine tagged protein (Adapted from De *et al.*, 2008).

In a study by Mukherjee and colleagues in 2005, unfunctionalised gold nanoparticles demonstrated anti-angiogenic properties *in vitro* and *in vivo* when they were found to bind heparin-binding proteins. Heparin-binding proteins, such as vascular endothelial growth factor (VEGF), play a key role in the induction of angiogenesis. Since angiogenesis is critical for tumour development and progression, it stands to reason that anti-angiogenic compounds could be utilised to inhibit the growth of tumours (Mukherjee *et al.*, 2005). In 2005, a study by El-Sayed and colleagues demonstrated the imaging capabilities of gold nanoparticles.

In this study, dark-field microscopy was used to differentiate cancerous cells from non-cancerous cells using gold nanoparticles functionalised with an epithelial cancer cell antibody, EGFR (El-Sayed *et al.*, 2005). With regard to drug delivery, a study performed by Choi and colleagues in 2010 demonstrated that gold nanoparticles functionalised with human transferrin were able to enhance the intracellular delivery of therapeutic agents (Choi *et al.*, 2010).

1.6.2.3 Nanotechnology-based treatment strategies for HIV infection

Nanotechnology had received much attention in the area of disease. It has been extensively used to target cancer, with a number of therapeutics already on the market. One of the most challenging diseases with regard to developing therapeutics, however, remains HIV/AIDS. Although humanity has been battling with this disease for 30 years, treatment strategies have not changed dramatically. With this in mind, and owing largely to its novelty, researchers have looked to the field of nanotechnology for a solution (Nie *et al.*, 2007).

The HIV virus measures approximately 150 nm in size and is therefore, in itself, a nanostructure. Due to the size, biocompatibility, toxicity profiles and the possibility of targeted payload delivery, nanotechnology has offered an attractive solution to the treatment of HIV/AIDS (das Neves *et al.*, 2010). A study by Bender and colleagues in 1996 demonstrated that polyhexylcyanoacrylate-based (PHCA) nanoparticles increased the efficacy of antiretroviral drugs such as saquinavir and zalatabine (Bender *et al.*, 1996). Another study, performed by Shah and Amiji in 2006 demonstrated a ten-fold increase in the cellular uptake of saquinavir when conjugated to a nanoparticle (Shah and Amiji, 2006).

Though most of the studies that have been done rely on the use of antiretrovirals conjugated to nanomaterials, a study performed by Elechiguerra and colleagues in 2005 demonstrated that silver nanoparticles with various surface chemistries were able to inhibit the binding of HIV to host cells (Elechiguerra *et al.*, 2005). Figure 1.16 demonstrates these silver nanoparticles bound to HIV-1. A similar study was done in 2008, utilising multivalent gold nanoparticles this time, demonstrating inhibition of HIV fusion to host cells (Bowman *et al.*, 2008).
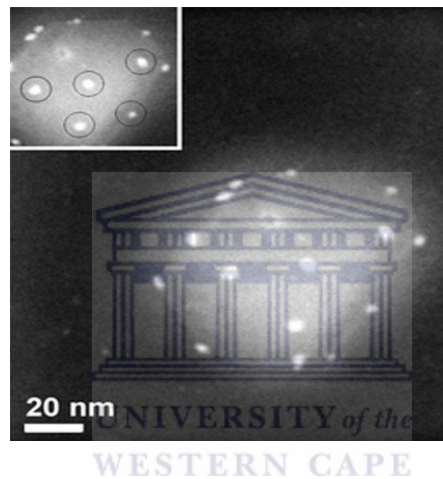
Figure 1.16 High angle annular dark field (HAADF) image of silver nanoparticles bound to an HIV-1 virus (Adapted from Elechiguerra *et al.*, 2005).

The aforementioned research suggests that there exists a definite opportunity for the application of nanotechnology in developing treatment strategies for HIV infection. With the use of nanotechnology and the strategy employed by Vocero-Akbani and colleagues, we aim to demonstrate the targeted destruction of HIV-infected cells towards a therapeutic treatment of this devastating disease.

1.7 Objectives of the project

HIV/AIDS and other incurable diseases have been devastating the quality of life of millions the world over for many years. Since the advent of nanotechnology, many developments have been made in the food, information technology and pharmaceutical industries. The aim of this study is to develop a nanotechnology-based death-inducing delivery system for the destruction of HIV-infected cells.

An *in vitro* cell model system representing an HIV infected cell will be generated by co-transfecting CHO (Chinese Hamster Ovary) cells with two DNA plasmids, which contain the human CD4 gene as well as the HIV-1 protease gene. As a result these mutant CHO cells will resemble HIV-infected cells in two ways: the cells will express human CD4 receptor on their surface and HIV-1 protease in the cytosol. This study will develop a death-inducing system similar to the strategy developed by Vocero-Akbani *et al*. (Vocero-Akbani *et al.*, 1999), with the added advantage of being a targeted delivery system.

The HIV-infected cell model system described above will be used to demonstrate that gold nanoparticles bi-conjugated with a CD4 targeting peptide (Slepushkin *et al.*, 1996) and a mutant form of caspase-3 (that is only cleavable by HIV-1 protease) can be specifically delivered to CD4 expressing cells and induce cell death in these cells through the activation of apoptosis.

Using genetic engineering tools, the apoptosis-inducing protein, caspase-3, will be modified as described by Vocero-Akbani *et al*., and will therefore only be cleavable by HIV-1 protease. This protein will be recombinantly expressed in and purified from *E.coli*. The purified protein will be conjugated to gold nanoparticles and delivered to mammalian cells. These cells will express CD4 on their surface, since HIV primarily infects CD4 expressing cells. The CD4-expressing cells will also be transfected with HIV-1 protease. The conjugated nanostructure will then be targeted to these cells by the addition of a CD4 targeting peptide that specifically recognises $CD4^+$ cells. Upon uptake of the nanostructure by the "HIV-infected" cell, the mutant caspase-3 will be activated by HIV-1 protease, which will cleave it from its inactive form into active caspase-3. This will result in apoptosis of that particular cell, without causing damage to surrounding cells, much like destroying HIV-infected CD4 cells and leaving uninfected CD4 cells unharmed in a clinical scenario. This strategy should result in a decrease in the number of HIV-infected cells, and thereby reduce viral load.
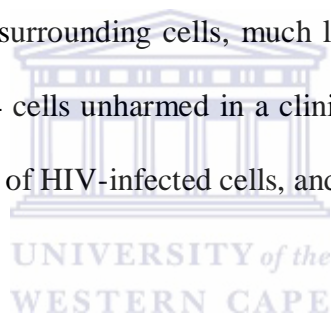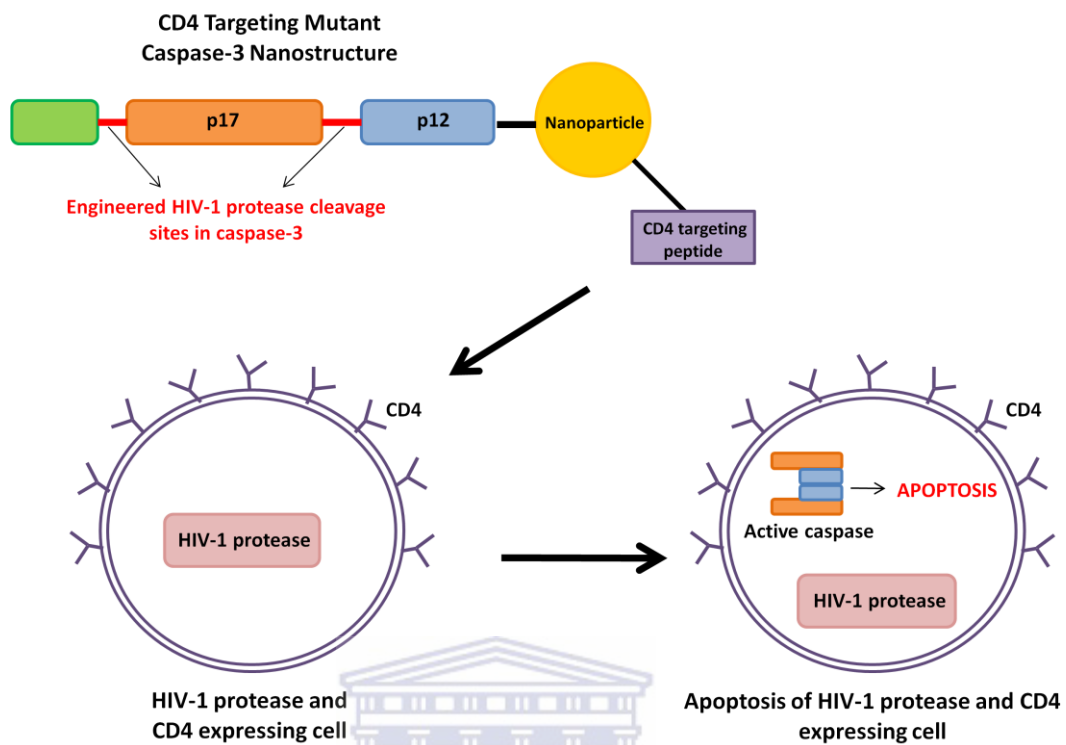
Figure 1.17 Schematic illustration of the targeted destruction of HIV-1 protease and CD4 expressing cells.

The application of nanotechnology to biological systems is an area of scientific research that is still in its infancy and will require much more research. This study intends to answer some of the questions surrounding nanotechnology in biology, and possibly move towards the use of nanotechnology in the treatment of disease.

CHAPTER 2. MATERIALS AND METHODS

2.1 General Chemicals and Reagents

40 % 37.5:1 Acrylamide:bis-acrylamide	Bio-Rad
7-Amino-Actinomycin D (7-AAD)	BD Biosciences
Agarose	Promega
Ammonium persulphate (APS)	Merck
Ampicillin	Roche
APOPercentage™ dye	Biocolor
Bacteriological agar	Merck
Boric acid	Merck
Bovine serum albumin (BSA)	Roche
Bromophenol blue	Sigma
Buffer saturated phenol	Invitrogen
BugBuster® Ni-NTA His•Bind® Purification Kit	Novagen
Caspase-3 antibody	Cell signaling technology
Cesium Chloride (CsCl)	Roche
Cytobuster™ Protein Extraction Reagent	Novagen
Chloroform	BDH
Coomassie Brilliant Blue R-250	Sigma

Dimethyl sulphoxide (DMSO)	Sigma
Dithiothreitol (DTT)	Roche
Ethylene diamine tetra acetic acid (EDTA)	Merck
Ethanol	BDH
Ethidium bromide (EtBr)	Promega
Fluoroshield™ with DAPI (4',6-diamidino-2-phenylindole)	Sigma
G-418 Solution	Roche
Glacial acetic acid	Merck
Glucose	BDH
Glutathione	Sigma
Glycine	BDH
Hydrochloric acid	Merck
Imidazole	Sigma
Isopropyl β-D-thiogalactopyranoside (IPTG)	Promega
Isopropanol	Merck
MES [2-(N-morpholino)ethanesulfonic acid]	Sigma
Methanol	Merck
Metafectene™ Pro Transfection Reagent	Biontex
Mowiol	Sigma

Ni Sepharose™ 6 Fast Flow	GE Healthcare
Nickel sulphate (NiSO$_4$)	Sigma
Paraformaldehyde	Sigma
Phenylmethylsulphonyl fluoride (PMSF)	Roche
Ponceau S	Sigma
Sodium azide	Roche
Sodium borohydride	Sigma
Sodium chloride (NaCl)	Merck
Sodium dodecyl sulphate (SDS)	Promega
Sodium hydroxide	Merck
SuperSignal West Pico Chemiluminescent Substrate	Thermo Scientific
Sybr Safe DNA Gel Stain	Invitrogen
N, N, N', N'-Tetra methylethylene-diamine (TEMED)	Promega
Tetrachloroaurate (gold chloride)	Sigma
Tris [hydroxymethyl] aminoethane (Tris)	BDH
Triton X-100 (iso-octylphenoxypoly-ethoxyethanol)	Roche
Tryptone	Merck

Tween-20 (Polyoxyethylene [20] sorbitan)   Merck

WST-1   Roche

Xylene cyanol   BDH

Yeast extract   Merck

Restriction endonucleases were supplied by New England Biolabs, Fermentas or Roche Diagnostics. T4 DNA ligase was obtained from Promega. ExSel Taq DNA polymerase was obtained from Jain Biologicals. DreamTaq™ Green PCR Master Mix (2 X) and Pfu DNA Polymerase were supplied by Fermentas. Unstained and prestained DNA and Protein Molecular Weight Markers were supplied by Fermentas.
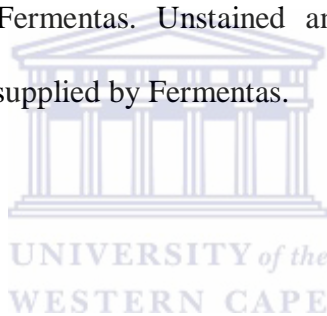
2.2 Buffers and solutions

10 X TBE

0.9 M Tris, 0.89 M boric acid, 0.032 M EDTA; stored at room temperature.

6 X Glycerol DNA Gel-loading Buffer

30 % glycerol, 0.25 % Bromophenol blue and 0.25 % Xylene cyanol.

10 X Tris EDTA (TE)

10 mM Tris-HCl, 1 mM EDTA, pH 7.5.

DNA Loading buffer

0.25 % Bromo-phenol-blue, 0.25 % xylene cyanol, 30 % glycerol.

Diethyl pyrocarbonate (DEPC) water

2 ml diethyl pyrocarbonate in 2 l distilled water; incubated at 22 °C overnight and autoclaved.

GTE

500 mM Glucose, 50 mM Tris-HCl and 10 mM EDTA, pH 8.0.

Lysis solution

200 mM NaOH and 1% SDS

Neutralisation solution

3 M KAc, pH 5.0.

RNAse (DNase free)

A 20 mg/ml stock solution was prepared in a buffer containing 0.1 M sodium acetate and 0.3 mM EDTA (pH 4.8, with acetic acid). This solution was boiled for 15 minutes and cooled quickly by placing it in ice water.

Ampicillin

100 mg/ml ampicillin in distilled water; filter sterilized.

Ammonium persulphate (APS)

A 10 % stock solution was prepared in deionised water.

Cell lysis buffer

PBS, pH 7.4, containing 1 mM DTT, 1 mM PMSF and 100 µg/ml Lysozyme.
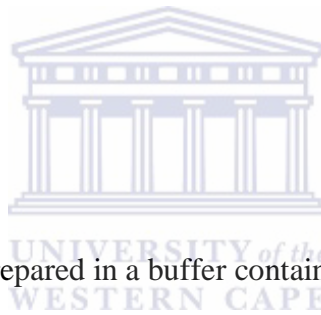
Chloramphenicol

100 mg/ml in absolute ethanol.

Coomassie Staining Solution

0.25 g Coomassie Brilliant Blue R 250, 45 % methanol and 5 % acetic acid.

Destaining solution

30 % methanol and 10 % acetic acid.

Dithiothreitol (DTT)

A 1 M stock solution was prepared in 0.01 M Sodium acetate, pH 5.2. This solution

was sterilised by filtration.
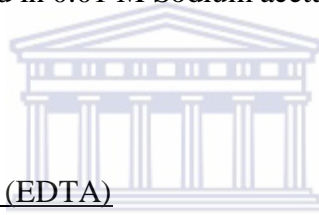
Ethylene diamine tetra acetic acid (EDTA)

A stock solution was prepared at a concentration of 0.5 M in deionised water, pH 8.0.

10 % Sodium dodecyl sulphate (SDS)

10 % SDS in distilled water.

Isopropyl β-D-thiogalactopyranoside (IPTG)

A 1 M stock solution was prepared in deionised water. The solution was sterilised by

filtration.

Kanamycin sulfate

50 mg/ml Kanamycin in distilled water.

Luria Agar

14 g/l Bacteriological agar, 10 g/l Tryptone, 5 g/l Yeast Extract and 5 g/l NaCl.

Luria Broth

10 g/l Bacto-tryptone, 5 g/l Bacto-Yeast Extract and 5 g/l NaCl.

TYM Broth

20 g/l bacto-tryptone, 5 g/l yeast extract, 3.5 g/l NaCl, 2 g/l $MgCl_2$.

Lysozyme

A stock solution was prepared at a concentration of 50 mg/ml in deionised water.

MES Buffer

30 mM MES prepared in deionised water. pH 6.0.

1X Ni-NTA Bind Buffer (used for lysis and binding)

50 mM NaH_2PO_4, pH 8.0; 300 mM NaCl; 10 mM imidazole.

1X Ni-NTA Wash Buffer

50 mM NaH_2PO_4, pH 8.0; 300 mM NaCl; 40 mM imidazole.

1X Ni-NTA Elute Buffer

50 mM NaH_2PO_4, pH 8.0; 300 mM NaCl; 500 mM imidazole.

10 X Phosphate-buffered saline (PBS)

137 mM NaCl, 27 mM KCl, 80 mM Na_2HPO_4, 1.5 mM KH_2PO_4, pH 7.4.

Phenylmethylsulphonyl fluoride (PMSF)

A 10 mM stock solution was prepared in isopropanol.

Ponceau S staining solution

0.1% Ponceau S in 5% acetic acid.

Separating buffer

1.5 M Tris- HCl pH 8.8, stored at 4 °C.

Stacking buffer

0.5 M Tris- HCl pH 6.8, stored at 4 °C.

TBS (Tris-buffered saline)

20 mM Tris-HCl and 150 mM NaCl, pH 7.5.

TBS-T

TBS containing 0.1 % Tween-20.

TBS-MT

TBS containing 5 % low fat dried milk powder and 0.1 % Tween-20.

Tfb1 Buffer

30 mM Potassium acetate, 50 mM $MnCl_2$, 0.1 M KCl, 6.7 mM $CaCl_2$ and 15 %

glycerol (v/v).

Tfb2 Buffer

9 mM MOPS, 50 mM CaCl, 10 mM KCl and 15 % glycerol (v/v).

Transfer Buffer

25 mM Tris, 192 mM glycine and 20 % methanol.

Cell culture media and reagents

The following tissue culture media and supplements were supplied by Invitrogen: nutrient mixture Ham's F12, RPMI, 100 X penicillin-streptomycin, trypsin, PBS without Ca^{2+}/Mg^{2+} and Foetal calf serum (FCS). Metafectene™ Pro was used as transfection reagent and was supplied by Biontex. APOPercentage™ apoptosis assay kit was supplied by Biocolor and 7-AAD was supplied by BD Biosciences. G-418 solution was used as selection antibiotic and was supplied by Roche.

Fluorescence microscopy mounting medium (Mowiol)

A stock solution of Mowiol was prepared by adding 6 g of glycerol to 2.4 g Mowiol (Sigma). While stirring, 6 ml distilled water was added and the solution was left to stir a further 2 hours at room temperature. After 2 hours, 12 ml of 0.2 M Tris (pH 8.5) was added. The solution was incubated at 50 – 60 ºC for 10 minutes to dissolve the Mowiol. Once dissolved, the solution was centrifuged at 5000 x *g* for 15 minutes to remove any undissolved solids. 1 ml aliquots were stored at - 20 ºC.

Paraformaldehyde Fixative

16 g paraformaldehyde was dissolved in 80 ml deionised water by stirring at 70 °C (in fume cupboard). One drop of 2 M NaOH was added. The solution was cooled to room temperature and the volume adjusted to 100 ml with deionised water. This solution was filter sterilised through a 0.45 micron filter and a 100 ml 2 X PBS was added.

2.3. Gel electrophoresis of DNA

2.3.1 Gel preparation and electrophoresis

Gels were prepared by adding the required volume of 1 X TBE to the appropriate mass of electrophoresis grade agarose. The agarose was then boiled and cooled to 55 °C. Ethidium bromide was added to the agarose solution to a final concentration of 0.5 μg/ml. This was then set in the appropriate gel caster, using 10-well combs to make wells. All gels were electrophoresed in 1 X TBE at 8 V/cm. Sybr Safe DNA Gel Stain from Invitrogen™ was added at a 1 X concentration from a 10 000 X stock solution.

2.3.2 Sample preparation

Approximately 1 μl (0.5 vol) of DNA loading buffer was mixed with DNA in 5-20 µl and loaded into the wells of the gel.

2.3.3 Detection of DNA

Gels contained ethidium bromide or Sybr Safe DNA Gel Stain, thus DNA was visualized by illuminating the gel with wavelength UV light on a trans-illuminator. Gels used for the recovery of DNA were exposed to a 360 nm wavelength lamp to avoid damage to the DNA.

2.3.4 Gel purification of DNA

The appropriate sized DNA fragment was removed using a sterile scalpel blade and placed in

a 1.5 ml microcentrifuge tube. DNA was isolated from the gel slice using the QIAquick® Gel Extraction Kit from Qiagen or the Nucleospin Extract II® gel purification kit from Macherey-Nagel, according to manufacturer's instructions. In brief, the excised gel slice was incubated at 50 °C in binding buffer.

Once the gel liquefied, it was passed over a silica membrane. After two wash steps, the DNA was collected in elution buffer and stored at – 20 °C.

2.4 SDS-polyacrylamide gel electrophoresis (SDS-PAGE)

Proteins were separated on SDS-PAGE gels. Gels were made from a 40 % of pre-mix acrylamide: bisacrylamide (37.5:1) (Bio-Rad). The separating gel consisted of 12 to 16 % acrylamide: bisacrylamide (37.5:1), 0.375 M Tris-HCl, pH 8.8, 0.1 % SDS, 0.5 %, ammonium persulphate and 0.1 % TEMED. The stacking gel consisted of 4 % acrylamide: bisacrylamide (37.5:1), 0.125 M Tris-HCl, pH 6.8, 0.1 % SDS, 0.5 % ammonium persulphate and 0.1 % TEMED. The samples were mixed with an equal volume of 2 X Sample Buffer, boiled for 5 min, centrifuged for 10 minutes at 10 000 x g, and electrophoresed in 1 X SDS Electrophoresis Buffer at 100 V/cm (constant voltage) for about 25 minutes using the Mini Protean II electrophoresis system (Bio-Rad). The voltage was increased to 150 V/cm (constant voltage) when the bromophenol blue dye front reached the separating gel. Electrophoresis was stopped when the bromophenol blue dye front reached the bottom of the gel. The gel was incubated in Coomassie Staining Solution for 30 minutes and then incubated in De-staining solution, until suitably de-stained.

2.5 DNA quantification

DNA was quantified using a 2 µl sample of DNA on the NanoDrop® ND 1000. Software version 3.1.2 was used to determine the concentration of nucleic acids at a wavelength of 260 nm.

2.6 Small-scale preparation of plasmid DNA

Plasmid DNA was prepared using the Wizard® Plus SV Minipreps Kit from Promega according to manufacturer's instructions. In brief, 30 ml cultures containing the appropriate antibiotic and the plasmid DNA of interest, were grown overnight at 37 °C with shaking. Bacterial cells were then collected by centrifugation for 20 minutes at 3000 x g. The pelleted bacterial cells were resuspended in resuspension buffer before cell lysis. The cells were centrifuged at 11 000 x g for 10 minutes to produce a cleared lysate. The lysate was then passed over a column to capture the DNA. The column was washed twice in a wash solution containing 95% ethanol and the DNA was eluted with 1 X TE.

2.7 Large-scale preparation of plasmid DNA using CsCl/EtBr fractionation

Part I: Nucleic acid purification

Bacterial cultures (500 ml each) containing the appropriate antibiotic and the plasmid DNA of interest were grown in sterile polypropylene tubes overnight at 37 °C with shaking. Bacterial cells were collected by centrifugation at 4 500 x g for 10 minutes at 4 °C, using a Beckman centrifuge with a JA-14 rotor. The bacterial pellet was resuspended in 4 ml of GTE buffer and incubated on ice for 10 minutes. Cell lysis was facilitated by the addition of 8 ml of lysis solution and the solution was gently swirled while being incubated on ice for 10 minutes. Neutralisation solution at a volume of 6 ml was added and mixed gently to neutralise the alkali, and the mixture was incubated on ice for 10 minutes. The precipitate, containing choromosomal DNA and cell debris, was removed by centrifugation at 4 500 x g for 15 minutes at 4 °C. The supernatant was filtered through glass wool and the nucleic acids were precipitated by the addition of 0.8 volumes of isopropanol, followed by incubation at -20 °C for 20 minutes. The precipitate was pelleted by centrifugation at 10 000 x g for 10 minutes at 4°C. Plasmid DNA was separated from RNA by double CsCl/ethidium bromide fractionation.

Part II: CsCl/EtBr fractionation

The ispropanol pellet from the end of Part I was resuspended in 5 ml of 1 X TE. The solution was mixed with 4 mg/500µl EtBr and 5.75 g CsCl to give a final density of 1.61 g/ml. The density was checked by zeroing a 15ml tube containing 5ml of the sample in a beaker on a scale. 1ml of sample was removed from the tube and the density checked.

The 1ml was replaced and if the density was greater than 1.61 g/ml, 1 X TE was added to bring it down. If the density was below 1.61 g/ml, CsCl-saturated TE was added to take it up. The mixture was then centrifuged at 10 000 x *g*. The supernatant, containing the DNA, was made up to 5 ml with CsCl-saturated TE to give a final density of 1.61 g/ml. The supernatant was transferred to Quick-Seal™ ultracentrifugation tubes from Beckman and centrifuged at 55 000 x *g* for 18 hours at 20 ºC in a Beckman Optima™ L-80 XP Ultracentrifuge, using the NVT 65.2 rotor. The plasmid DNA was visualised with a 360 nm UV illumination. After removing the caps from the centrifuge tubes, DNA was recovered using a 0.5 x 16 mm needle and 5 ml syringe. Plasmid DNA was recovered by adding an equal volume of NaCl-saturated isopropanol to remove the ethidium bromide. This extraction was repeated several times, until the pink colour from the ethidium bromide disappeared. Two volumes of water and one volume of isopropanol were added to precipitate the DNA. This was mixed well and incubated on ice for 10 min. The DNA was recovered by centrifugation at 10 000 x *g* for 15 minutes. The pellet was resuspended in 1 X TE and stored -20 ºC until used.
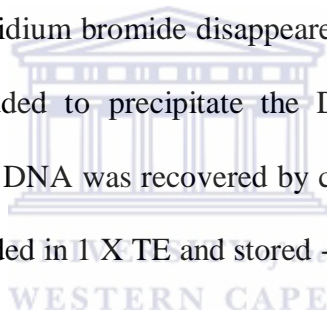
2.8 DNA Sequencing Using the ABI 310 Genetic Analyzer

Sequencing reactions were performed using the DNA Sequencing Kit, BigDye™ Terminator v 3.0 Cycle Sequencing Ready Reaction (Applied Biosystems). The PCR sequencing reactions were performed in a 20 µl final volume containing 3.2 pmol of the sequencing primer, 4 µl Terminator Ready Reaction mix (Applied Biosystems) and 4 µl 2.5 X Sequencing Buffer. For plasmid DNA templates, 500 ng of DNA was added, while the DNA concentration for PCR fragments was dependent on the size of the PCR fragment. For each of the reaction the reagents were added as follows:

Table 2.1. Reagent quantities for use in sequencing reaction

Reagent	Quantity
Terminator Ready Reaction Mix	4.0 µl
2.5 X Sequencing Buffer	4.0 µl
Template:	
DsDNA	200-500 ng
Primer	3.2pmol
De-ionized water	to final volume of 20 µl
Total Volume	**20 µl**

Reactions were carried out according to the manufacturer's protocol. The contents of the tubes were centrifuged briefly. For the extension precipitation of samples in micro-centrifuge tubes the following was done: The entire contents of each extension reaction were aspirated and transferred into a 1.5 ml micro-centrifuge tube, 16 µl of de-ionized water and 64 µl of 95 % ethanol were added to the 1.5 ml tube to precipitate the DNA. The samples were briefly mixed by vortexing.

Samples were left at room temperature for 30 minutes to precipitate the extension products. Thereafter the tubes were placed into a micro-centrifuge and centrifuged for 20- 30 minutes at 10 000 x *g*. The supernatant was discarded. The pellet was washed twice with 250 µl of 70 % ethanol, as follows: ethanol was added and the samples were briefly mixed by vortexing. The tubes were placed into the micro-centrifuge and centrifuged for 10 minutes at 10 000 x *g*.

The supernatant was carefully aspirated. After the second wash the pellet was dried at 37 °C for 10- 15 min. The pellet was stored at –20 °C until sequence analysis was performed on the ABI 310 PRISM® Genetic Analyzer from Applied Biosystems.

The pellet was dissolved in 25 µl of Template Suppressor Buffer (TSR) [Applied Biosystems]. The sample was then heat denatured at 95 °C for 2 min. After denaturing the samples were then transferred immediately to ice for 5 minutes and sequencing using the ABI 310 PRISM™ Genetic Analyzer (Applied Biosystems) followed. Data was collected using the ABI 310 PRISM® Collection Software (Applied Biosystems) and the analysis was done using Sequence Analysis 3.3 Software (Applied Biosystems). Sequencing was also outsourced to Inqaba Biotechnical Industries (Pty) Ltd.
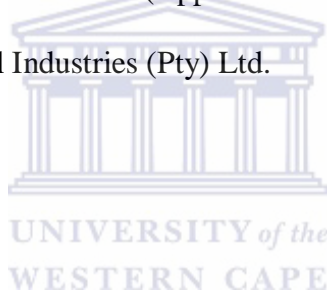
2.9 Oligonucleotides

The following oligonucleotides were synthesised by Inqaba Biotechnical Industries (Pty) Ltd:

Table 2.2. Synthesised primer sequences

Gene	Primer sequence
CD4 Forward Primer	5´-CGTAGAATTCTATGAACCGGGGAGTCCCTTA-3´
CD4 Reverse Primer A	5´-CGTACCCGGGAATGGGGCTACATGTCTTCTG-3´
CD4 Reverse Primer B	5´-CGTACTCGAGTCAAATGGGGCTACATGTCTTC-3´
p12 Forward Primer	5´-GGCGGCTCCCAGGTGTCACAGAACTATCCAATCGTG CAGAACCTGCAGGGCGGTGTTGATGATGACATGGCG-3´
p12 Reverse Primer	5´-CGAGCTACGCCTCGAG'TTAGTGATAAAAATAGAGTTC-3´
p17 Forward Primer	5´-CGCCATATGGGCGGCTGCACCGAACGCCAGGCTAACTTCCT GGGCAAAATCTGGCCAGGCGGAATATCCCTGGACAACAGTTAT AAAATG-3´
p17 Reverse Primer	5´-CCGCCCTGCAGGTTCTGCACGATTGGATAGTTCTGTGACACC TGGGAGCCGCCTGTCTCAATGCCACAGTCCAG-3´
HIV-1 protease TOPO Forward Primer	5´-CACCGATATGCCGCAGATTACCCTGTGG-3´
HIV-1 protease TOPO Reverse Primer	5´-AAAGTTCAGCGTGCAGCC-3´
HIV-1 protease pET Forward Primer	5´-CCGCCATATGCCGCAGATTACCCTGTGG-3´
HIV-1 protease pET R	5´-CCGCCTCGAGAAAGTTCAGCGTGCAGCC-3´

2.10 Cloning vectors

2.10.1 pGEM®-T Easy

The pGEM®-T Easy Vector System (Promega) is used for direct cloning of PCR fragments. This cloning strategy utilises terminal extendase activity of *Taq* polymerase which adds an extra base (usually an adenosine) on the 3' end of PCR products (Clark, 1988).

The pGEM®-T Easy Vector, as supplied for cloning by the manufacturer, contains single 3'-T overhangs at the insertion site, and is able to accommodate the ligation of PCR fragments, as indicated in Figure 2.1.
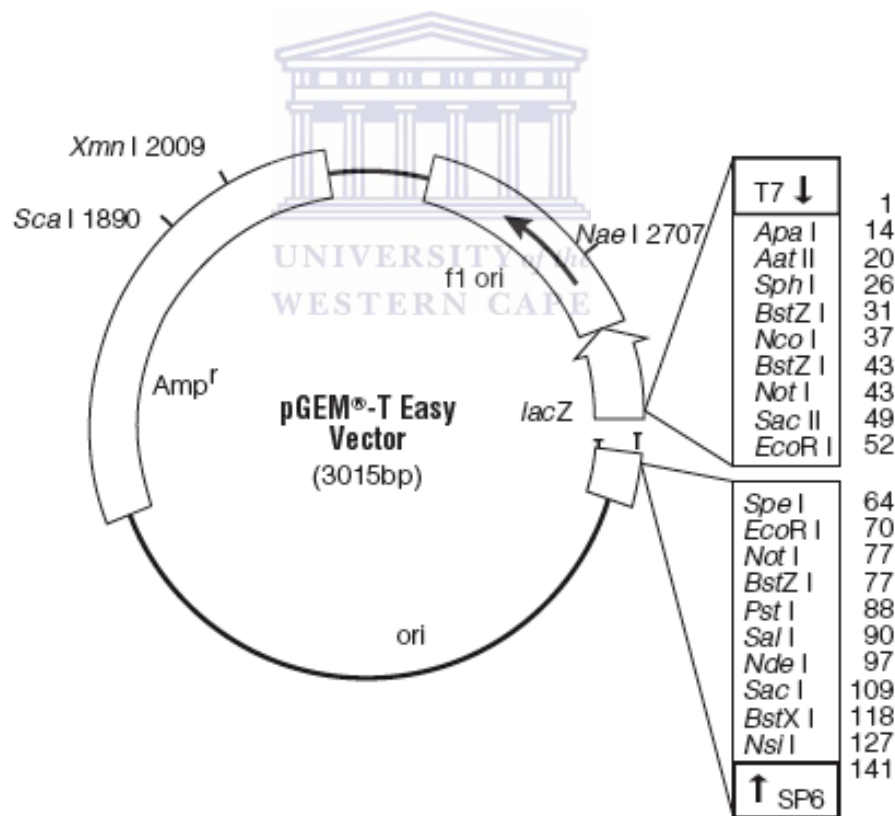
Figure 2.1. The pGEM®-T Easy Vector System (Promega) for direct cloning of PCR fragments.

2.10.2 pGEX-6P-2

The Glutathione S-Transferase (GST) gene fusion system (GE Healthcare) is a 4900 bp protein expression system, which can be used for the expression, purification and detection of recombinant fusion proteins produced in *E. coli*. (Smith and Johnson, 1988). The GST domain acts as an affinity tag that allows for the purification of the fusion protein by affinity chromatography using glutathione agarose. A number of GST fusion vectors have been developed. One such vector is pGEX-6P-2 (Figure 2.2).
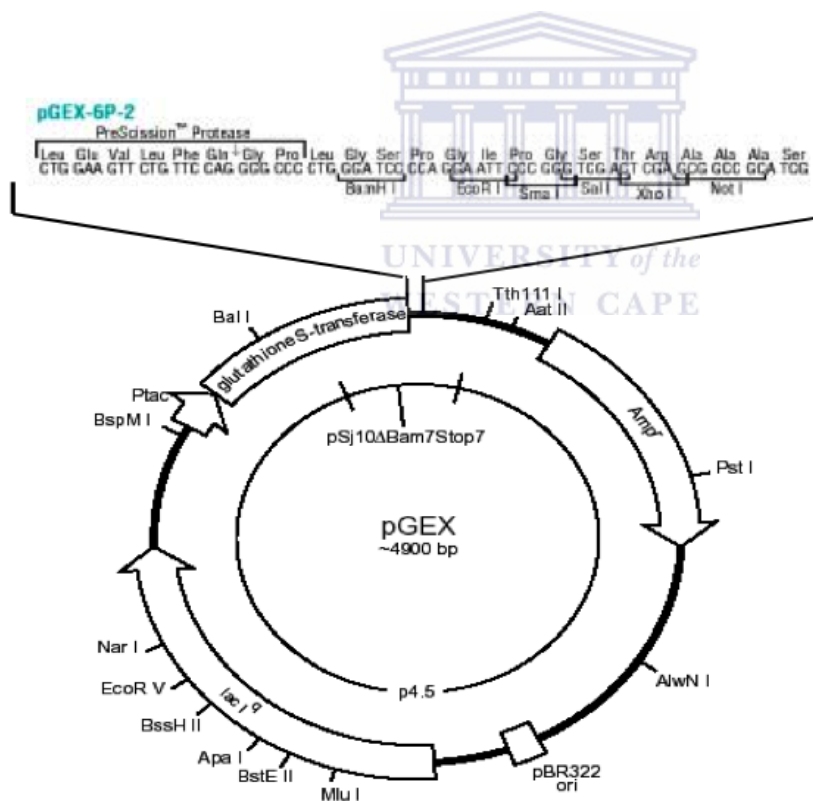
Figure 2.2. Circular map of the pGEX-6P-2 system.

2.10.3 pcDNA 3.1D/V5-His-TOPO®

pcDNA 3. 1D/V5-His-TOPO® Expression Kit (Invitrogen) is a 5514 bp vector system for
stable and transient expression in mammalian hosts, facilitated by the human
cytomelagovirus (CMV) promoter. Neomycin allows for antibiotic selection in mammalian
cells. The vector has the V5 epitope as well as a polyhistidine tag to aid in confirmation of
protein expression by Western blot analysis.
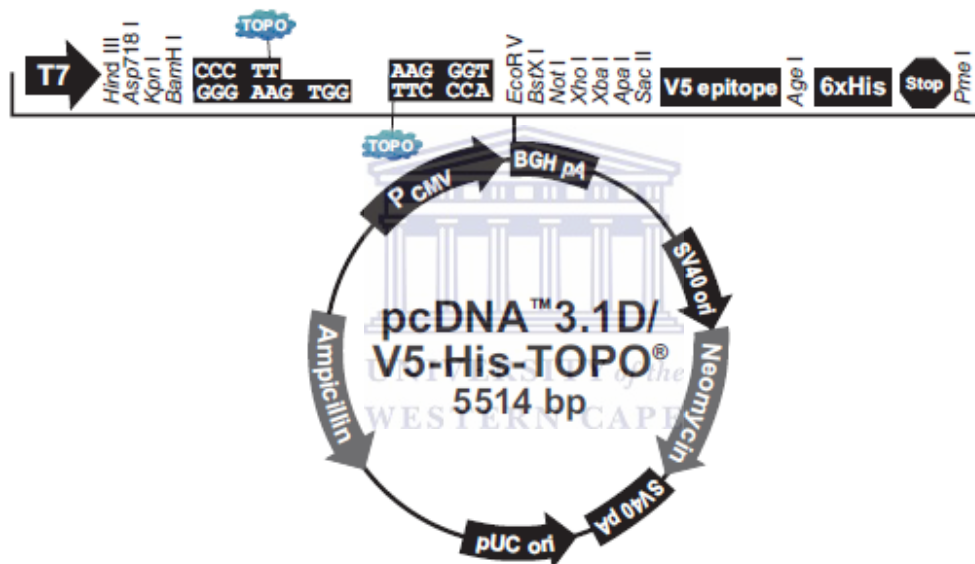
Figure 2.3. Circular map and Restriction sites of pcDNA3.1D/V5-His-TOPO®

2.10.4 pEGFP-N3

pEGFP-N3 (BD Biosciences) is used for fusion of proteins to the C-terminus of EGFP. The fluorescence of the native protein allows localization of the fusion protein inside a cell using fluorescence microscopy. It can be used to express EGFP within a cell and could also be used for stable tranfections within a cell line of interest. pEGFP-N3 is a 4700 bp vector system and encodes a GFP variant for the emission of greater fluorescence as well as higher levels of expression in mammalian cells. A circular map of the vector system can be seen below (Figure 2.4).
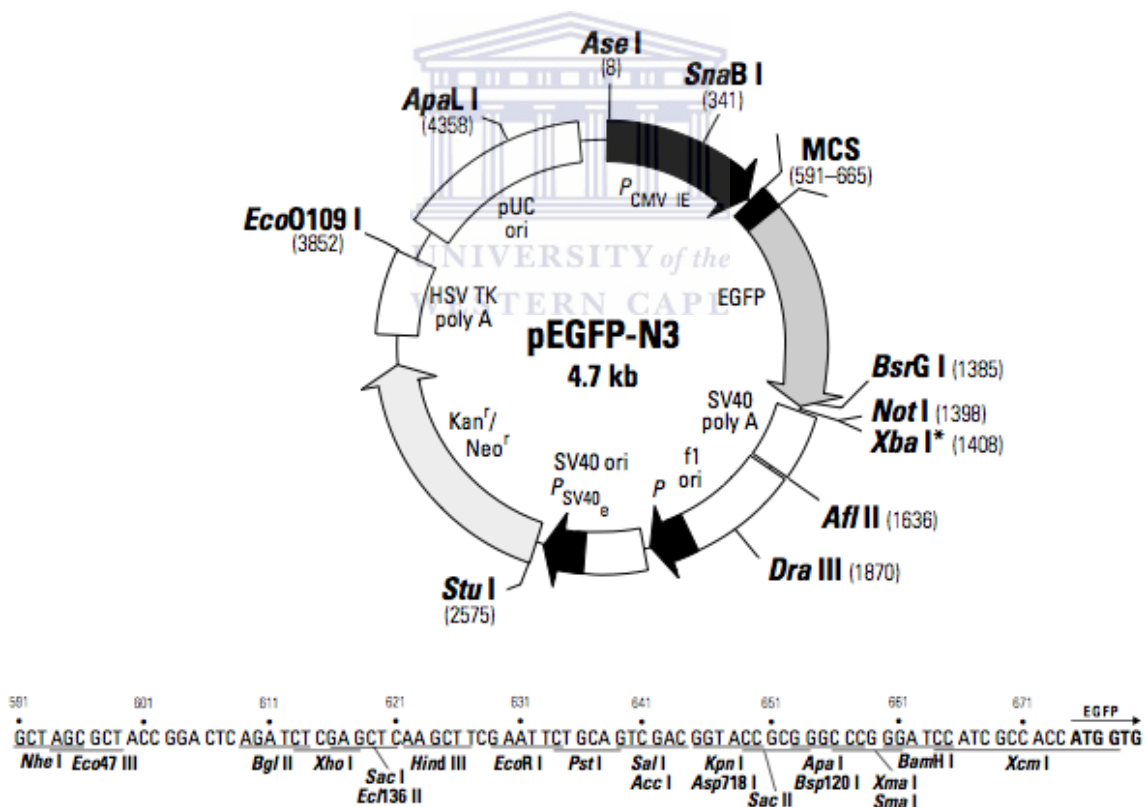
Figure 2.4. Circular and restriction map of pEFGP-N3.

2.10.5 pET21a

The pET-21a vector (Novagen) is a 5443 bp bacterial protein expression vector that is used for the expression of fusion proteins due to the presence of a C-terminal polyhistidine tag. It carries an N-terminal T7 Tag® sequence for cloning plus an optional C-terminal His Tag® sequence for fusion construct purification.

Figure 2.5. Circular and restriction map of pET21a.

2.11 Restriction enzyme digestion of DNA

Restriction enzymes were used according to manufacturer's instructions. In general, 1 µg of DNA was digested with 1 unit of enzyme in the appropriate buffer and at the appropriate temperature. Restriction enzymes were inactivated by either heating the reaction mixture at 70 °C or 85 °C for 10 minutes.

2.12 Ligation of DNA

Ligation reactions were set up according to the manufacturer's instructions. Reactions

were performed in 1X Ligase buffer (30 mM Tris-HCl, pH 7.8, 10 mM MgCl$_2$, 10 mM

DTT and 1 mM ATP) using T4 DNA ligase (Promega).

Table 2.3. Volumes for ligation reactions

Reaction component	Standard Reaction	Background Control
2x Rapid Ligation Buffer, T4 DNA ligase	5 µl	5 µl
pGEM®-T Easy Vector (50ng)	1 µl	1 µl
PCR product	X µl	-
T4 DNA Ligase (3 Weiss units/ µl	1 µl	1 µl
Nuclease-free water to a final volume of	**10 µl**	**10 µl**

The samples were mixed by vortexing and then incubated at room temperature for 3 hours.

After ligation, 100 µl of competent cells were added to the ligation mix and transformations

were done.

2.13 Bacterial cultures

2.13.1 Strains used

(1). *Escherichia coli* MC1061 (Casadaban and Cohen, 1980):

F−, *ara*D139, (*ara leu*) 7697, Δ*lac*x74, *gal*U−, *gal*K−, *hsm*+, *str*A.

(2). *Escherichia coli* BL21 Star™ pLysS (DE3) (Stratagene):

F− *omp T hsdSB (rB−mB−) gal dcm rne131* (DE3)

(3). *Escherichia coli* CodonPlus® competent cells (Stratagene) B F− ompT hsdS (rB− mB−)
dcm+ Tetr gal λ (DE3) endA Hte [argU proLCamr] [argU ileY leuW Strep/Specr]

(4). Rosetta™2 (DE3) pLysS (Novagen)

2.13.2 Cultures

MC1061 *E.coli* was used to produce plasmid DNA, while BL21 Star™ pLys (DE3) *E. coli*
was used to express recombinant fusion proteins. *E. coli* was grown in Luria broth and on
Luria agar plates with or without ampicillin. When required ampicillin or kanamycin was
added to Luria broth and Luria agar plates to a final concentration of 100 μg/ml.

All cultures were grown at 37 °C. Glycerol stocks were prepared directly from overnight
cultures, grown under selectable conditions, by dilution of the culture with an equal volume
of 80 % sterile glycerol. Stocks were stored as 500 μl aliquots at − 70 °C.

2.13.3 Preparation of competent cells for transformation

Cells were streaked out on a Luria agar plate and incubated at 37 ºC for 16 hours. A single colony was picked and used to inoculate 20 ml TYM broth, which was incubated at 37 ºC until the optical density at 550 nm (OD_{550}) reached 0.2. 100 ml of fresh TYM broth was added to the culture and the cells were further incubated at 37 ºC until the OD_{550} reached 0.2. 400 ml of fresh TYM broth was added and the cells incubated at 37 ºC until the OD_{550} reached 0.5. The cells were rapidly cooled by gently swirling of the flask in ice water and the culture was transferred to sterile 250 ml polypropylene tubes and centrifuged at 6000 x g at 4 ºC for 10 minutes in a Beckman centrifuge with a JA-14 rotor. The cell pellet was re-suspended in 250 ml ice-cold Tfb1 buffer and incubated on ice for 30 minutes, followed by centrifugation at 6000 x g at 4 ºC for 10 minutes. The pellet was gently re-suspended in 50 ml Tfb2 buffer. Re-suspended cells were dispensed in 2 ml aliquots and subsequently snap frozen in liquid nitrogen. Aliquots were stored at - 80 ºC until required.
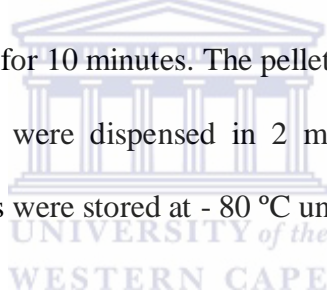
2.13.4 Transformation

High efficiency competent cells of 1 x 10^7 cfu/µg were used for transformations. To each ligation reaction that was prepared above, 100 µl of competent cells were added. These samples were then incubated for 30 minutes on ice. While these samples were incubated, 2 Luria agar plates containing either Ampicillin or Kanamycin (depending on which DNA vector was used) were prepared for each reaction. To the sample tubes, 900 µl Luria Broth without ampicillin was added and incubated at 37 °C for an hour. The plates were prepared in duplicate. 100 µl of each transformation was plated and then incubated overnight at 37 °C.

2.14 PCR

2.14.1 DNA Amplification by PCR

PCR reactions were performed in 1 X reaction buffer according to the manufacturer's instructions. ExSel *Taq* polymerase (Jain Biologicals), Pfu DNA polymerase [Inqaba Biotechnical Industries (Pty) Ltd] and DreamTaq™ Green Master Mix 2 X [Inqaba Biotechnical Industries (Pty) Ltd] was used according to manufacturer's instructions. The primers were present at 1 pmol and between 1 and 10 ng of cDNA template was used in each reaction. The $MgCl_2$ concentration was 1.5 mM. PCR reactions were cycled according the following parameters:

Initial denaturation at 95 °C for 2 minutes

Denaturation at 94 °C for 30 s

*Annealing for 45 s   x 40 cycles

Elongation at 72 °C for 30 s
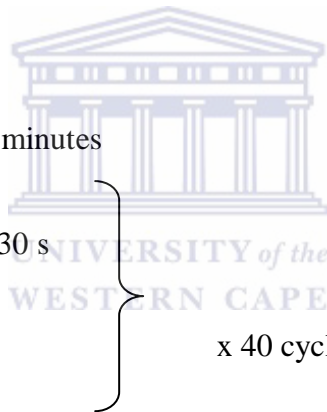
Final elongation at 72 °C for 7 minutes

Incubation at 4 °C

* Annealing temperature was dependent on primer sequence.

2.14.2 Colony PCR

The colonies that appeared on the plate were counted and some of the colonies were selected. The colonies were resuspended in 10 µl sterile deionised water (dH$_2$O) and these were stored at 4 °C. Colony PCR to identify positive clones was performed to screen for recombinant clones.

2.15 Protein Expression

2.15.1 Expression screening of transformants

Positive clones were selected and plasmid DNA was prepared from them. The plasmid DNA was then transformed in *E.coli* BL21 pLys S (DE3) competent cells and after overnight growth on Luria agar plates, a single colony was inoculated into 1 ml of appropriate media containing 0.3 % glucose, and 100 µg/ml ampicillin in a 1.5 ml tube. The samples were cultured at 37 °C for 4 hours. After incubation, the culture was split into two 0.5 ml samples. To the one sample (induced sample), 0.3 mM IPTG was added and both tubes were incubated at 37 °C. Cells were pelleted by centrifugation for 1 minute and the supernatant was discarded. The cells were then resuspended into 100 µl of PBS. A volume of 20 µl of the cell suspension and 20 µl of 2 X SDS sample buffer were thoroughly mixed and incubated at 95 °C for 5 minutes. The samples were then briefly vortexed and pelleted by centrifugation. Proteins were analysed by SDS-PAGE as described in section 2.4.

2.15.2. Large-scale expression of recombinant protein

Large-scale expression was performed by an inoculation of a single colony into 100 ml of Luria Broth (containing 100 μg/ml ampicillin) and incubating the culture at 37 °C overnight. Luria Broth (900 ml containing 100 μg/ml ampicillin) was added and incubated at 37 °C until the OD_{550} was between 0.4-0.6. IPTG was added to a final concentration of 0.5 mM. The sample was then incubated with shaking at 37 °C for 4 hours or 30 minutes, depending on the protein that was being expressed. Bacteria were recovered by centrifugation at 5000 x g for 10 minutes. The supernatant was discarded and the pellet could be stored at –20 °C until further use. The pellet was resuspended in 20-25 ml of Lysis buffer. Lysis was carried out by freezing at –70 °C for 5 min, and thawing at 37 °C for 5 min.

The freeze thaw process was done three or more times. The protein lysate was stored at 4 °C until purification. Immediate purification was preferable since degradation by proteases (proteolysis) could occur. A concentration of 0.02 % of sodium azide was included to inhibit bacterial growth.

2.15.3 Protein purification using BugBuster™ and Ni-NTA His Bind Resin

Native purification was performed according to manufacturer's instructions. In brief, the cell pellet was resuspended in BugBuster™ reagent containing Benzonase. The lysate was then centrifuged at 3 000 x g for 20 minutes. The Ni-NTA His Bind matrix was added to 1 X Ni-NTA Bind Buffer and the resin was allowed to settle by gravity. The supernatant containing the soluble protein was added to the His Bind resin and mixed on a shaker for 1 hour at 4 °C.

The lysate was loaded onto a column and the flow-through was collected and saved for analysis. The column was washed with 1 X Ni-NTA Wash Buffer and wash fractions were collected for analysis. Protein was eluted with 1 X Ni-NTA Elution Buffer and saved for analysis. Protein samples were stored at 4 °C and SDS-PAGE analysis was done. Columns containing His Resin were stored in 10 % ethanol.

2.15.4 Dialysis and storage of protein

Upon confirmation of purified protein, the eluted samples were pooled and dialysis was performed using a Slide-A-Lyzer Dialysis Cassette from Thermo Scientific, with a molecular weight cut off of 7 kDa. MES buffer was used to dialyse the imidazole out of the protein sample and the dialysed protein samples were lyophilised overnight using a Virtis model 10-020 bench lyophiliser and stored at – 80 °C.
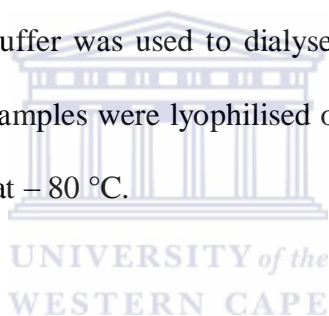
2.16 Cell culture

2.16.1 Cell thawing and seeding

Vials containing cells stored at -150 °C were removed and briefly placed in a 37 °C water bath, until just thawed. Cells from the vial were then transferred to a 15 ml tube containing 5 ml complete media (containing serum and antibiotics). Cells were then centrifuged for 2 minutes at 800 x g to pellet them, and the cell pellet was resuspended in 5 ml of complete media and transferred to a 25 cm^2 cell culture flask. Cells were incubated at 37 °C with 5 % CO_2.

2.16.2 Media replacement

For adherent cell lines, media was removed from the cells and discarded. Fresh complete media was added to cells before incubating at 37 °C with 5 % CO_2. For suspension cells, cells were transferred to a 15 ml tube and centrifuged at 90 x *g* for 2 minutes. The media was discarded and the cell pellet was resuspended in complete media and added to a culture flask before incubating at 37 °C with 5 % CO_2.

2.16.3 Cell count

The Countess™ automated cell counter from Invitrogen was used for accurate cell counts.

2.16.4 Subculturing of cells

The cell suspensions were subcultured when cultures reached confluency. Adherent cells were trypsinised by incubating the cells in 1 X trypsin and incubated for 2 minutes at 37 °C with 5 % CO_2.

The cells were then transferred to an appropriately sized sterile tube and centrifuged at 800 x *g* for 3 minutes to pellet cells. The cell pellets were then resuspended in complete media and subcultured into culture flasks.

2.16.5 Cryopreservation of cells

Once trypsinised, cell pellets were resuspended in complete media containing 10 % DMSO. Cell suspensions were transferred to cryo-vials at volumes of 1.5 ml per vial. These were then stored at -150 °C until further use.

2.16.6 Morphological analysis

Throughout the growth and treatment process, the morphology of cells was monitored with the use of a Nikon microscope at 20 X magnification. Images were captured using a Leica EC3 digital camera.

2.16.7 Transfection of mammalian cell line

A repulsive membrane acidolysis (RMA)-based transfection reagent, Metafectene™ Pro was used to transfect cells. This reagent works on the principle that a DNA-lipid complex forms and cationic liposomes come into contact with DNA. These complexes are then transported via endocytosis through the outer cell membrane. These newly-formed endosomes possess H+ pumps which allow the acidification of the endosome. An osmotic disruption is caused and the lipoplexes are released into the cytoplasm. These lipoplexes must then enter the nucleus in order to be incorporated into the cell and this is made possible by cell division.

The standard protocol was followed as per the manufacturer's instructions. CHO cells were seeded in a 6-well plate. Once 70 % cell confluency was achieved, solutions A and B were prepared. Solution A was made up of 1.0 μg of DNA for transfection in 50 μl of Hams F12 media. Solution B contained 6.0 μl of Metafectene™ Pro transfection reagent in 50 µl of Hams F-12. The two solutions were then combined and gently pipetted up and down. The mixture was then allowed to stand at room temperature for 15-20 minutes. After the incubation period, the mixture was added to the cells and mixed by gentle swirling. The cells were then incubated at 37 °C and 5 % CO_2 overnight. The transfection mixture was removed and complete media was added to the wells. The cells were then incubated at 37 °C and 5 % CO_2 until selection was performed.

2.17 Cytotoxicity assays

2.17.1 Measurement of apoptosis using APOPercentage[TM] apoptosis assay by flow cytometry

Upon reaching 80-90 % confluency in 24-well culture plates, cells were treated with various concentrations of functionalised gold nanoparticles for 24 hours. As a positive control, 14 μM camptothecin (a known inducer of apoptosis) was used to treat cells for 24 hours. For the purposes of a negative control, cells were left untreated for 24 hours. Media containing dead, floating cells was transferred to centrifuge tubes. Subsequent to trypsination at 37 °C with 5 % CO_2, cells were transferred to a 15 ml centrifuge tube and these were centrifuged at 800 x *g* for 3 minutes. A 1:160 dilution of APOPercentage[TM] dye was prepared and the cell pellet was resuspended in 200 µl of this dye.

The tubes were incubated at 37 °C with 5 % CO_2 for 30 minutes. After incubation, 1500 µl of 1 X PBS was added to each of the tubes and the tubes were centrifuged at 800 x g for 3 minutes. The cell pellet was resuspended in 200 µl of 1 X PBS and the cells were acquired and analysed on a FACScan™ (Becton Dickson) instrument, with a 488 nm Argon laser as light source. This was done within one hour of the assay. Cells were acquired by setting the forward scatter (FSC) and side scatter (SSC) on a log scale dot plot. A linear histogram dot plot was used to measure APOPercentage™ on the FL-3 channel, which was measured against relative cell number. A minimum of 10 000 cells per sample was acquired and analysed using CellQuest™ Pro software (Meyer *et al.*, 2008).

2.17.2 Measurement of cellular viability using 7-Aminoactinomycin D (7-AAD) nucleic acid dye

Upon reaching 80-90 % confluency in 24-well culture plates, cells were treated with various concentrations of functionalised gold nanoparticles for 24 hours. As a positive control, 14 µM camptothecin was used to treat cells for 24 hours. For the purposes of a negative control, cells were left untreated for 24 hours. Subsequent to incubation at 37 °C with 5 % CO_2, cells were transferred to a 15 ml centrifuge tube and centrifuged at 800 x g for 3 minutes. Cells were then resuspended in media containing 20 µg/ ml 7-AAD. Cells were then incubated at 4 °C in the dark for 20 minutes. Cells were acquired and analysed on a FACScan™ (Becton Dickson) instrument, with a 488 nm Argon laser as light source. Cells were acquired by setting the forward scatter (FSC) and side scatter (SSC) on a log scale dot plot. A linear histogram dot plot was used to measure 7-AAD uptake in FL-3, which was measured against relative cell number. A minimum of 10 000 cells per sample was acquired and analysed using CellQuest™ Pro software.

2.17.3 Measurement of cytotoxicity using the ApoTox-Glo™ Triplex Assay (Promega)

Upon reaching 80-90 % confluency in 96-well culture plates, cells were treated with various concentrations of functionalised gold nanoparticles for 24 hours. As a positive control, 0.2 µM camptothecin was used to treat cells for 24 hours. For the purposes of a negative control, cells were left untreated for 24 hours, so as to distinguish between normal and treated cells. After incubation at 37 °C with 5 % CO_2 for 24 hours, cells were treated with 20 µl of Viability/Cytotoxicity reagent, containing bis-AAF-R110 substrate, a fluorogenic cell-impermeant peptide substrate to measure dead-cell protease activity. Only cells that have lost membrane integrity are capable of producing a fluorescent signal. After orbital shaking to evenly distribute the reagent on cells, the plates were incubated for a further 30 minutes at 37 °C. After incubation, the fluorescent signal from treated cells was measured at an excitation wavelength of 485 nm and an emission wavelength of 520 nm, using the POLARstar Omega plate reader from BMG Labtech.
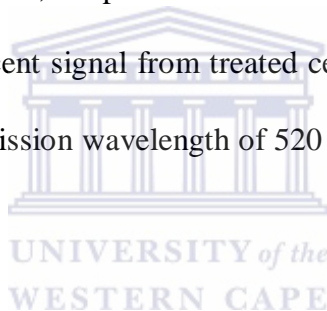
2.18 RNA Isolation from cells

RNA was isolated from cells using Trizol® Reagent from GibcoBRL according to manufacturer's instructions. In brief, Trizol® Reagent was added to cells and lysis was carried out by passing the cells in Trizol® Reagent through a pipette tip several times. The aqueous phase was separated from the phenol-chloroform phase by centrifugation at 12 000 x *g*. The aqueous phase was transferred to a fresh microcentrifuge tube and the RNA was precipitated by the addition of isopropyl alcohol. Samples were incubated at room termperature for 10 minutes and the RNA pellet was collected by centrifugation at 12 000 x *g* for 10 minutes at 4 °C. The supernatant was discarded and the RNA pellet was washed in 75% ethanol. The pellet was again collected by centrifugation at 7 000 x *g* at 4 °C.

The RNA pellet was allowed to air-dry at room temperature before redissolving the pellet in RNase-free water. RNA was stored at -20 °C until used.

2.19 cDNA synthesis from RNA

cDNA was synthesised according to manufacturer's instructions using the Improm-II® Reverse Transcription Kit from Promega. In brief, isolated RNA was combined with oligo $(dT)_{15}$ primers and incubated at 70 °C for 5 minutes. After chilling on ice for 5 minutes, reverse transcription mix was prepared, to which the RNA and oligos were added. Primers were annealed at 25 °C for 5 minutes, followed by first-strand cDNA synthesis at 42 °C for 60 minutes. The reverse transcriptase was heat-inactivated at 70 °C for 15 minutes and cDNA samples were stored at -20 °C until further use.

2.20 Western blot analysis

Protein samples were electrophoresed on PAGE gels as described in Section 2.4**.** The proteins were transferred onto a PVDF-P membrane (GE Healthcare) using a Mini Protean II system (Bio-Rad). Before transfer the membrane was pre-wet in methanol for a few seconds, washed in deionised water for 5 minutes and equilibrated in Transfer Buffer for 10 minutes. The SDS PAGE gels were also equilibrated in Transfer Buffer for 10 minutes. Transfer was performed at 4 °C, 100 V (constant voltage) for 1 hr in pre-cooled Transfer Buffer. After transfer the membranes were stained with Ponceau S (Sigma) to check for protein transfer. The membranes were incubated in TBS-MT for 1 hr.

The purified primary antibody was diluted (1:5 000 for His-probe, 1:500 for caspase-3 and 1:1000 for V5 epitope) in TBS-MT and the membranes were incubated in the primary antibody overnight. The membrane was washed three times for 10 minutes in TBS-MT.

The secondary antibody was diluted (1:20 000) in TBS-MT and the membranes were incubated in this antibody for 1 hour. The membrane was washed three times for 10 minutes in TBS-MT. This was followed by three more washes with TBS-T.

Detection was performed using the SuperSignal West Pico Chemiluminescent Substrate (Thermo Scientific), which was added to the membrane. The membrane was exposed to the film in the dark at 1 minute and 5 minute intervals and then developed, using developer and fixer from Agfa Healthcare, and processed using the Curix 60 Film Processor from Agfa.

2.21 Microscopy

Cell morphology was monitored using a Nikon light microscope at 40 X magnification.

Cells containing fluorescent constructs were visualised using the Zeiss Axioplan 2 Fluorescence Microscope. For this process, cells were cultured on coverslips and then fixed in 4 % paraformaldehyde. Coverslips were mounted on a microscope slide using either 1 X PBS or Mowiol mounting medium. Images were taken at 40 X magnification using an Axiocam HRM microscope camera.

2.22 Gold nanoparticle preparation and synthesis

Gold nanoparticles were synthesised by the citrate reduction method (Brust *et al*. 1994), by Dr Ndabenhle Sosibo at the Advanced Materials Division, Mintek SA. Various other gold nanoparticles were synthesised together with Mr Francois Taute in the Biotechnology Department at the University of the Western Cape.

Gold nanoparticle synthesis can be done using various methods. The methods that were employed to produce the particles used in this study were the citrate reduction method as well as the one-pot dual-ligand functionalisation of nanoparticles (Zheng and Huang, 2007). The citrate reduction method involved the addition of 17 mM trisodium citrate to 0.3 mM gold chloride to produce gold nanoparticles at around 14 nm in size. This synthesis, as well as the subsequent functionalisation with nitriloacetic acid (NTA), was carried out by Dr Ndabenhle Sosibo at the Advanced Materials Division, Mintek SA.
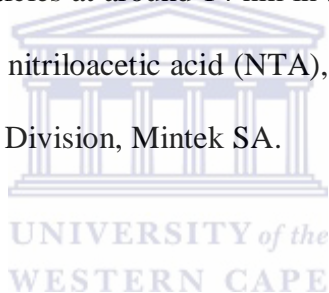
The one-pot method involved the addition of desired chemical functional groups, at pre-determined concentrations of 0.25 mM each, to a 1 mM gold chloride solution, and the dropwise reduction of this mixture by 1 mM sodium borohydride in a single reaction while stirring. The mixture was allowed to stir for an hour after which particles were collected by centrifugation at 3500 x *g*. The particles were then resuspended and dialysed in 0.3 M MES buffer (pH 6.5) using the Slide-A-Lyzer Dialysis cassette G2 with a 7 kDA cut off size from Thermo Scientific. The resultant particles can vary in size, depending on the concentration of individual reagents added to the mixture. To facilitate optimal cellular uptake of the nanoparticles, the synthesised particles were synthesised to yield 14 nm sized particles.

2.22.1 Nickel titration of NTA-functionalised gold nanoparticles for the conjugation of Histidine-tagged proteins

In order to conjugate His-tagged proteins to NTA- functionalised gold nanoparticles, a nickel titration was done to determine which concentration of nickel would result in the conjugation of the His-tagged proteins, and thus a shift in the surface plasmon resonance (SPR) band of the particles. This was done by adding the His-tagged proteins to NTA-functionalised nanoparticles, and titrating with various concentrations of nickel sulphate.

The concentration that yielded the most dramatic shift in the SPR band of the particles, while maintaining the integrity of the nanoparticles, was 0.5 mM nickel sulphate ($NiSO_4$).

2.23 Gold nanoparticle characterisation

Characterisation of gold nanoparticles is usually done by either UV-Vis spectroscopy or transmission electron microscopy (TEM) or both. For the purposes of the project, both methods were employed to characterise gold nanoparticles.

2.23.1 UV-Vis spectroscopy

UV-Vis spectroscopy was performed on nanoparticles using the POLARstar Omega plate reader from BMG Labtech. Spectra were collected in a range of 400-700 nm in 1 nm increments. Based on data by Haiss and colleagues in 2007, UV-Vis spectra data was used to extrapolate the size and concentration of synthesised gold nanoparticles using various extinction coefficients and the peak absorbance values of gold nanoparticles (Haiss et al., 2007).

2.23.2 Transmission electron microscopy (TEM)

High resolution transmission electron microscopy (HR-TEM) images were taken by Dr Subelia Botha using the HR-TEM instrument at the Physics Department of the University of the Western Cape. Transmission electron microscopy (TEM) of biological samples was performed by the National Health Laboratory Services (NHLS) at Tygerberg Hospital. The HR-TEM images served to verify the size and structure of nanoparticles, while the biological TEM demonstrated the size of nanoparticles as well as whether they were taken up by cells.

2.23.3 Energy-dispersive X-ray spectroscopy (EDX)

Energy-dispersive X-ray spectroscopy or EDX is an analytical technique used for the chemical characterisation of a sample based on the atomic structure of each element. These atomic structures result in the formation of unique peaks for each element on its X-ray spectrum. A high energy beam of charged electrons is used to excite the atoms in a sample, resulting in the formation of these unique peaks, allowing for the analysis of the elemental composition of a given sample. The HR-TEM data and EDX spectra were generated simultaneously by the same transmission electron microscope.

CHAPTER 3: CONSTRUCTION OF A "HIV-INFECTED" CELL MODEL SYSTEM

3.1 Introduction

3.2. Cloning of CD4 into pEGFP-N3

　　3.2.1 PCR amplification of CD4

　　3.2.2 Preparation of pEGFP-N3 for cloning

　　3.2.3 Ligation of CD4 into pEGFP-N3

　　3.2.4 Sequence analysis of pEGFP-N3-CD4

3.3 Cloning of HIV-1 protease into pcDNA™ 3.1D/V5-His-TOPO

　　3.3.1 PCR amplification of HIV-1 protease

　　3.3.2 Ligation of HIV-1 protease into pcDNA™ 3.1D/V5-His-TOPO

　　3.3.3 Sequence analysis of pcDNA™ 3.1D/V5-His-

　　TOPO-HIV-1 protease

3.4 Transfection of pEGFP-N3-CD4 and pcDNA™ 3.1D/V5-His-TOPO-HIV-1 protease into CHO cells

3.5 Evaluation of CD4 and HIV-1 protease expression in CHO cells

　　3.5.1 Sorting transfected CHO cells towards establishing a homogenous

　　population of transfected cells

3.6 Summary

CHAPTER 3: CONSTRUCTION OF A "HIV-INFECTED" CELL MODEL SYSTEM

3.1 Introduction

For the purposes of this study, the effect of a cell death inducing protein, caspase-3, on HIV-infected cells was to be investigated to determine whether HIV-infected cells could be specifically targeted and destroyed. Given the nature of cells containing infectious material and the harm that it potentially poses, it is common practice in scientific disease research to generate a non-infectious, cell model system, which mimics the conditions of the disease under investigation. In this study, CHO cells were genetically engineered to mimic HIV infection by inducing expression of CD4 and HIV-1 protease.

In order to make it possible for mammalian CHO cells to express the proteins mentioned previously, the individual genes were amplified, cloned into mammalian expression vectors (pEGFP-N3 and pcDNA™ 3.1D/V5-His-TOPO), as described in section 2.10 Chapter 2 and transfected into CHO cells as described in section 2.16.7. Many methods for DNA transfection exist, but in this study, a polycationic transfection reagent based on liposome technology was used to introduce plasmid DNA into mammalian cells. Transfected cells were placed under selection pressure, resulting in the stable expression of CD4 and HIV-1 protease. Since both pEGFP-N3 and pcDNA™ 3.1D/V5-His-TOPO use the same antibiotic (G418) for the selection of stably transfected cells, cells were co-transfected with pEGFP-N3-CD4 and pcDNA™ 3.1D/V5-His-TOPO-HIV-1 protease at a concentration ratio 1:10, as demonstrated by Figure 3.1.
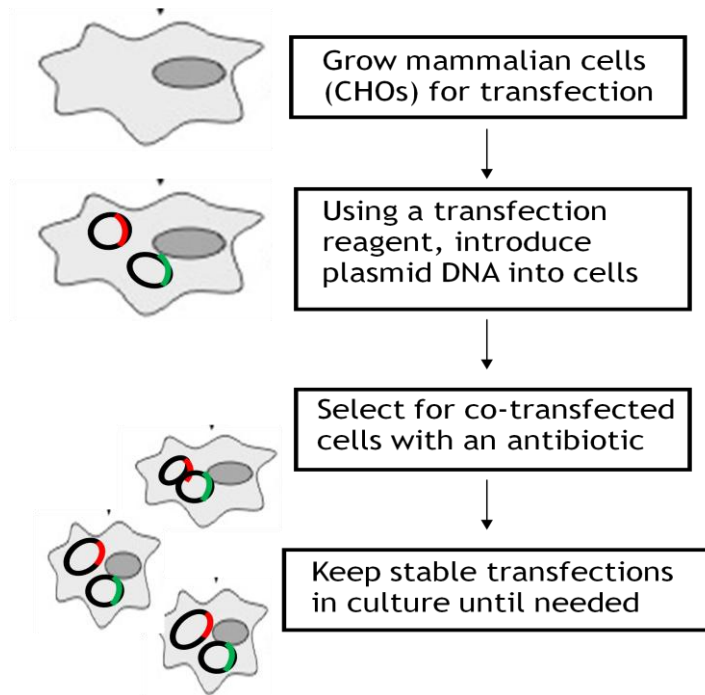
Figure 3.1 Schematic representation of mammalian cells co-transfected with CD4 and HIV-1 protease.
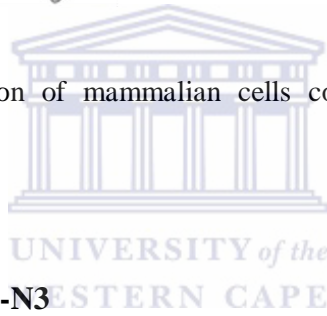
3.2 Cloning of CD4 into pEGFP-N3

CD4 was PCR amplified from immortalised human T lymphocytes called Jurkat T cells. Since pEGFP-N3 allows for the expression of GFP tagged fusion proteins, cells expressing CD4-GFP can be visualised under a fluorescence microscope. Consequently, these cells can also be sorted by flow cytometry.

3.2.1 PCR amplification of CD4

The human CD4 DNA sequence was PCR amplified from cDNA generated from Jurkat T cells. The CD4 Forward Primer and CD4 reverse primer A (listed in Table 2.2) was used to amplify CD4 as described in section 2.14.
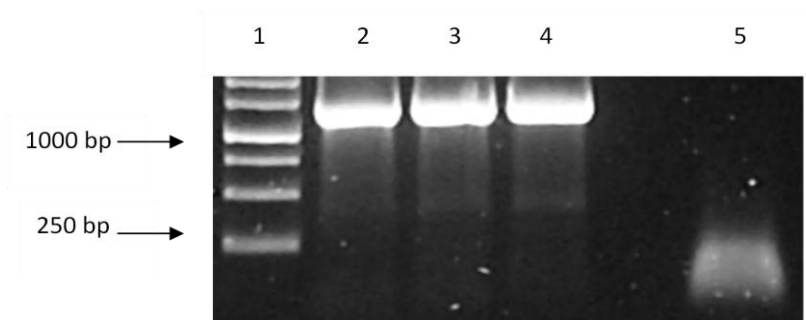
Figure 3.2 1% Agarose gel electrophoresis of PCR product of CD4. Lane 1 indicates a molecular weight marker. Lanes 2-4 indicate PCR amplified CD4. Lane 5 indicates the negative control for the PCR containing nuclease-free water.
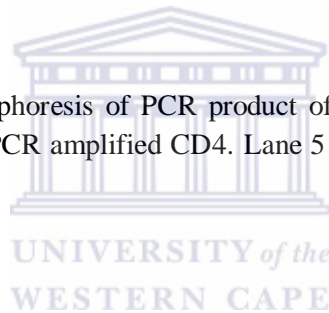
After amplification by PCR (seen in Figure 3.2) the samples were electrophoresed on an agarose gel, as described in section 2.3. Upon detection of DNA (section 2.3.3) a band corresponding to the expected size for the CD4 gene could be observed at ~1.2 kb. Suspected CD4 PCR products were excised and purified from a 1 % agarose gel, as described in section 2.3.4. The purified DNA was used as an insert to clone into the pEGFP-N3 plasmid vector. *Eco*RI and *Xma*I restriction sites were engineered into the CD4 Forward Primer and CD4 reverse primer A, respectively. After gel purification, the purified PCR product was digested with *Eco*RI and *Xma*I restriction enzymes as described in section 2.11.

3.2.2 Preparation of pEGFP-N3 for cloning

Large-scale preparation of pEGFP-N3 plasmid DNA was performed by CsCl/EtBr fractionation, as described in section 2.7. As indicated in Figure 3.3, the plasmid DNA was cut with *Eco*RI and *Xma*I restriction enzymes, as described in section 2.11 and purified from an agarose gel (section 2.3.4) to prepare the plasmid vector for ligation of the CD4 insert.
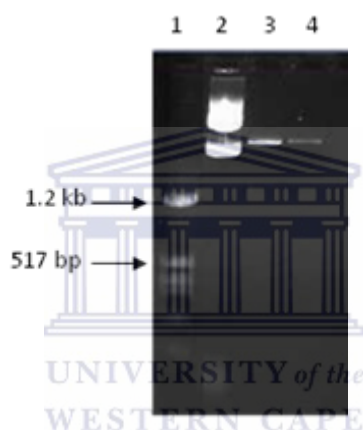
Figure 3.3 1% Agarose gel electrophoresis of restriction enzyme digested pEGFP-N3 plasmid DNA. Lane 1 indicates a molecular weight marker. Lane 2 indicates undigested pEGFP-N3 plasmid DNA. Lane 3 indicates pEGFP-N3 cut with *Eco*RI and Lane 4 indicates pEGFP-N3 cut with *Xma*I.

As seen in Figure 3.3, circular pEGFP-N3 plasmid DNA was digested with restriction enzymes to produce linearised DNA with the overhangs needed for ligation of *Eco*RI and *Xma*I digested the CD4 PCR product.

3.2.3 Ligation of CD4 into pEGFP-N3

Once the CD4 PCR product and pEGFP-N3 plasmid were both digested with restriction enzymes and purified, a ligation reaction was performed to ligate the sticky ends of CD4 insert into the mammalian expression vector, pEGFP-N3, as described in section 2.12. Ligation reactions were used to transform into *E.coli* MC1061 cells, as described in section 2.13.4. The resulting clones were screened by colony PCR (as described in section 2.14.2) for the presence of pEGFP-N3-CD4. Figure 3.4 shows the results of the colony PCR on 6 clones. Distinct bands can be observed at the expected size for the CD4 gene (~1.2 kb). A number of non-specific products of higher molecular weight can also be observed.

Plasmid DNA was prepared from 3 of these clones, as described in section 2.6, and samples were sent to Inqaba Biotechnical Industries (Pty) Ltd for sequence analysis.
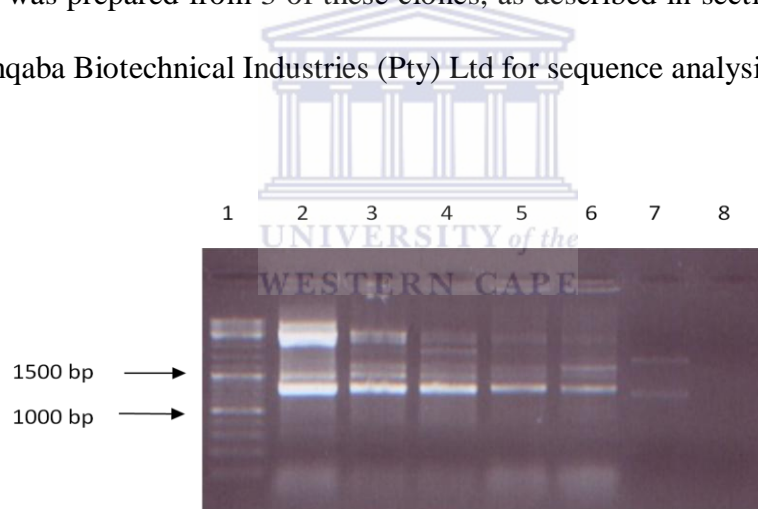
Figure 3.4 1% Agarose gel of colony PCR screen for CD4 cloned into pEGFP-N3. Lane 1 indicates molecular weight marker. Lanes 2-7 indicate colonies 1-6 for CD4 cloned into pEGFP-N3. Lane 8 indicates the negative control for the PCR containing nuclease-free water.

3.2.4 Sequence analysis of pEGFP-N3-CD4

Plasmid DNA from 3 positive clones (colony 3, 4 and 5) (see section 3.2.3) was sent to Inqaba Biotechnical Industries (Pty) Ltd for sequence analysis. The Basic Local Alignment Search Tool (BLAST®) from the National Centre for Biotechnology Information (NCBI) was used to perform an amino acid sequence alignment of human CD4 sequence (accession number, NM_000616) with pEGFP-N3-CD4. Upon analysis of the data, there was a 99 % amino acid sequence match between human CD4 from the database and pEGFP-N3-CD4 clone 5, as demonstrated by Figure 3.5.

This clone demonstrated the highest sequence similarity to human CD4 and was selected for mammalian transfection of pEGFP-N3-CD4 into CHO cells.

```
CD4          IVVLAFQKASSIVYKKEGEQVEFSFPLAFTVEKLTGSGELWWQAERASSSKSWITFDLKN
199-258      ||||||||||||||||||||||||||||||||||||||||||||||||||||||||||||
EGFP-N3-CD4  IVVLAFQKASSIVYKKEGEQVEFSFPLAFTVEKLTGSGELWWQAERASSSKSWITFDLKN
1-60


CD4          KEVSVKRVTQDPKLQMGKKLPLHLTLPQALPQYAGSGNLTLALEAKTGKLHQEVNLVVMR
259-318      |||||||||||||||||||||||||||||||||||||||| |||||||||||||||||||
EGFP-N3-CD4  KEVSVKRVTQDPKLQMGKKLPLHLTLPQALPQYAGSGNLTLTLEAKTGKLHQEVNLVVMR
61-120


CD4          ATQLQKNLTCEVWGPTSPKLMLSLKLENKEAKVSKREKAVWVLNPEAGMWQCLLSDSGQV
319-378      ||||||||||||||||||||||||||||||||||||||||||||||||||||||||||||
EGFP-N3-CD4  ATQLQKNLTCEVWGPTSPKLMLSLKLENKEAKVSKREKAVWVLNPEAGMWQCLLSDSGQV
121-180


CD4          LLESNIKVLPTWSTPV
379-394      ||||||||||||||||
EGFP-N3-CD4  LLESNIKVLPTWSTPV
181-196
```

Figure 3.5 Amino acid sequence alignment of the Homo Sapiens CD4 (NM_000616) and pEGFP-N3-CD4 clone 5.

3.3 Cloning of HIV-1 protease into pcDNA™ 3.1D/V5-His-TOPO

The pBAD-TOPO-HIV-1 protease plasmid was obtained from Ms Zarinah Sonday at the Institute for Infectious Diseases and Molecular Medicine (IIDMM) at the University of Cape Town. Two primers, HIV-1 protease TOPO Forward and Reverse, were designed to PCR amplify and clone HIV-1 protease from the aforementioned vector into pcDNA™3.1D/V5-His-TOPO (Invitrogen™) (see Table 2.2).

3.3.1 PCR amplification of HIV-1 protease

HIV-1 protease was PCR amplified from pBAD-TOPO-HIV-1 protease using primers that would facilitate the directional cloning of HIV-1 protease into pcDNA™3.1D/V5-His-TOPO mammalian expression vector. PCR amplification was performed as described in section 2.14.
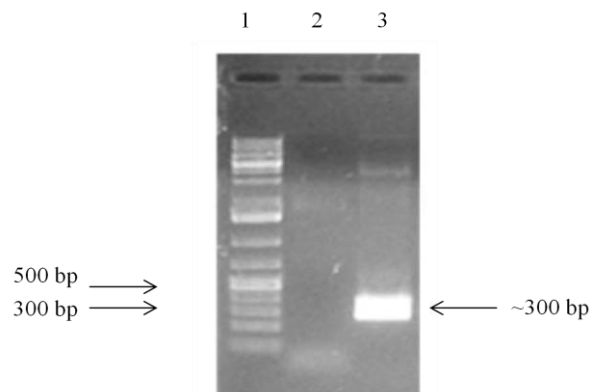
Figure 3.6. 1% Agarose gel electrophoresis of HIV-1 protease PCR. Lane 1 indicates the molecular weight marker. Lane 2 indicates the negative control of the PCR containing nuclease-free water. Lane 3 indicates PCR amplified HIV-1 protease.

A 300 bp product was generated, as indicated in Figure 3.6, corresponding to the expected size of HIV-1 protease. The PCR product was isolated from the agarose gel, purified (as described in section 2.3.4) and used as an insert to clone into the pcDNA™3.1D/V5-His-TOPO expression vector.

3.3.2 Ligation of HIV-1 protease into pcDNA™ 3.1D/V5-His-TOPO

The gel purified DNA was ligated into pcDNA™ 3.1 1D/V5-His-TOPO, as described in section 2.12. The cloning was performed using the Directional TOPO® Expression Kit (Invitrogen™). The ligated DNA was transformed into *E.coli* cells, as described in section 2.13.4. After plating transformations on agar plates containing the appropriate antibiotic, the resulting colonies were selected and screened for the presence of HIV-1 protease by colony PCR (as described in section 2.14.2), as indicated by Figure 3.7.
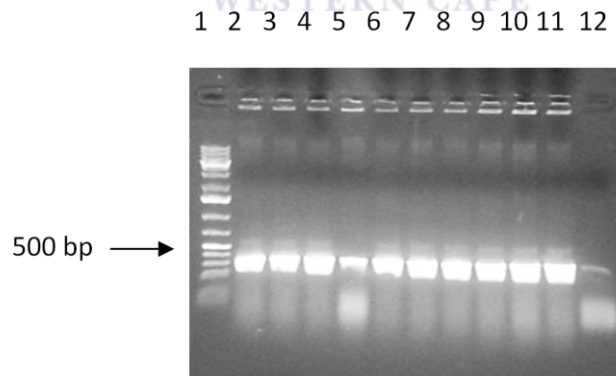
Figure 3.7 1% Agarose gel of colony PCR products to screen for HIV-1 protease cloned into pcDNA™ 3.1 1D/V5-His-TOPO. Lane 1 indicates a molecular weight marker. Lanes 2-11 indicate colonies 1-10 for HIV-1 protease cloned into pcDNA™ 3.1 1D/V5-His-TOPO. Lane 12 indicates the negative control for the PCR containing nuclease-free water.

As demonstrated by Figure 3.7, a PCR product which corresponds to the expected size of 300 bp for HIV-1 protease was generated. A 300 bp band is also visible in the negative control, possibly indicating seeping from lane 11 into the negative control lane, but the intensity of the band is much lower in comparison to the experimental samples that were screened. Five of the clones were selected, plasmid DNA was prepared (as described in section 2.6) and samples were sent to Inqaba Biotechnical Industries (Pty) Ltd to be sequenced.

3.3.3 Sequence analysis of pcDNA™ 3.1D/V5-His-TOPO-HIV-1 protease

Plasmid DNA from 5 positive clones (colony 1, 2, 3, 4 and 5) (see section 3.2.3) was sent to Inqaba Biotechnical Industries (Pty) Ltd for sequence analysis. The Basic Local Alignment Search Tool (BLAST®) from the National Centre for Biotechnology Information (NCBI) was used to perform an amino acid sequence alignment of HIV-1 protease in the sequence database with pcDNA™ 3.1D/V5-His-TOPO-HIV-1 protease. Upon analysis of the data, there was a 100 % amino acid sequence match between HIV-1 protease from the database and pcDNA™ 3.1D/V5-His-TOPO-HIV-1 protease clone 5, as demonstrated by Figure 3.8. This clone demonstrated the highest sequence similarity to HIV-1 protease and was selected for mammalian transfection of pcDNA™ 3.1D/V5-His-TOPO-HIV-1 protease into CHO cells.

```
Synthetic    MPQITLWQRPLVSIKVGGQIKEALLDTGADDTVLEEINLPGKWKPKMIGGIGGFIKVRQY
1-60         ||||||||||||||||||||||||||||||||||||||||||||||||||||||||||||
Clone 5      MPQITLWQRPLVSIKVGGQIKEALLDTGADDTVLEEINLPGKWKPKMIGGIGGFIKVRQY
1-60

Synthetic    DQILIEICGKKAIGTVLVGPTPVNIIGRNMLTQLGCTL
61-98        ||||||||||||||||||||||||||||||||||||||
Clone 5      DQILIEICGKKAIGTVLVGPTPVNIIGRNMLTQLGCTL
61-98
```

Figure 3.8 Amino acid sequence alignment of a synthetic HIV-1 protease, labelled "Synthetic" with pcDNA™ 3.1D/V5-His-TOPO-HIV-1 protease clone 5, labelled "Clone 5".

3.4 Transfection of pEGFP-N3-CD4 and pcDNA™ 3.1D/V5-His-TOPO-HIV-1 protease into CHO cells

Plasmid DNA was prepared for pEGFP-N3-CD4 and pcDNA™ 3.1D/V5-His-TOPO-HIV-1 protease, as described in section 2.6. CHO cells were cultured in 6-well plates and co-transfected with the plasmids, as described in section 2.16.7. Transfection was achieved using Metafectene™ Pro transfection reagent from Biontex. To produce stable transfectants, selection pressure was applied. Since both vectors make use of neomycin as a selectable marker, G-418 solution from Roche was used to select positive transfectants at a concentration of 800µg/ml. Figure 3.9 A) shows that un-transfected cells are killed by G-418 treatment, while Figure 3.9 B) shows co-transfected with pEGFP-N3-CD4 and pcDNA™ 3.1D/V5-His-TOPO-HIV-1 protease plasmid DNA are resistant to G418.
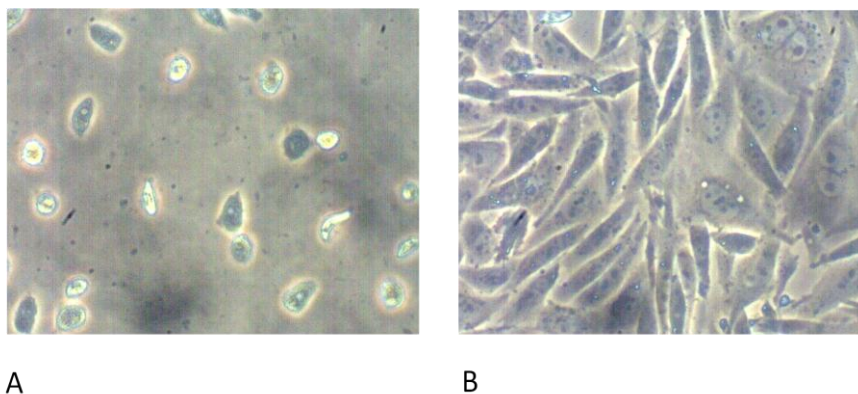
Figure 3.9 Light microscopy images of CHO cells co-transfected with pEGFP-N3-CD4 and pcDNA™ 3.1D/V5-His-TOPO-HIV-1 protease. A) Untransfected CHO cells 7 days after selection. B) CHO cells co-transfected with pEGFP-N3-CD4 and pcDNA™ 3.1D/V5-His-TOPO-HIV-1 protease 7 days after selection. Images were captured at a 20X magnification.

3.5 Evaluation of pEGFP-N3-CD4 expression in CHO cells

After CHO cells were successfully transfected with GFP-N3-CD4 and pcDNA™ 3.1D/V5-His-TOPO-HIV-1 protease, cells were cultured on cover slips. The cells were prepared for microscopy by fixing the coverslips in 4 % paraformaldehyde, as described in section 2.21. After fixation, cover slips were mounted onto microscope slides, using Fluoroshield™ with DAPI (4',6-diamidino-2-phenylindole). DAPI is a fluorescent stain that binds to AT regions of DNA sequences and used in fluorescence microscopy to stain cell nuclei. Since CD4 will be expressed as a fusion protein with GFP, and the sequence data shows no mutations or stop codons between GFP and CD4, the presence of GFP can be used as an indication of the presence of CD4. Moreover, since the concentration of the pcDNA™ 3.1D/V5-His-TOPO-HIV-1 protease was 10 times greater than that of pEGFP-N3-CD4, the presence of pEGFP-N3-CD4 would indicate that both plasmids were successfully transfected. CHO cells co-transfected with pEGFP-N3-CD4 and pcDNA™ 3.1D/V5-His-TOPO-HIV-1 protease were visualised using the Zeiss Axioplan 2 Fluorescence Microscope. Images were taken using the Axiocam HRM microscope camera.
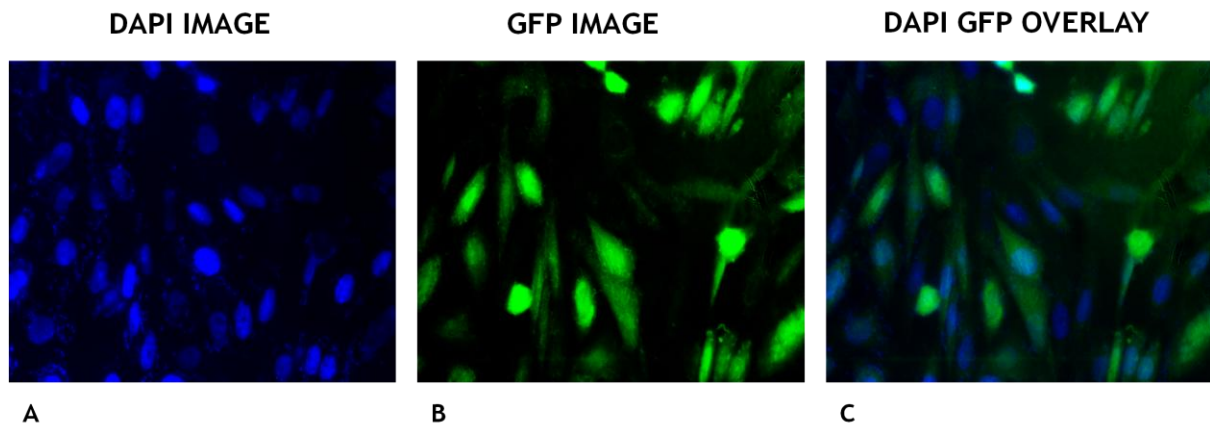
Figure 3.10 Fluorescence microscopy images of CHO cells co-transfected with pEGFP-N3-CD4 and pcDNA™ 3.1D/V5-His-TOPO-HIV-1 protease. A) Transfected CHO cells captured using the blue fluorescence filter of the microscope. B) Transfected CHO cells captured using the green fluorescence filter of the microscope. C) An overlay of images A) and B).

Figure 3.10 A) shows that 100% of the cells stain blue with DAPI, while Figure 3.10 B) shows that ~70 % of the cells are positively expressing GFP. The fluorescence of DAPI staining is localised to the nucleus while the fluorescence of GFP is dispersed all over the cell. In order to achieve a homogenous cell population where all the cells express GFP, the cells were sorted by Fluorescence Activated Cell Sorting (FACS).

3.5.1 Sorting transfected CHO cells towards establishing a homogenous population of transfected cells

FACS was performed on CHO cells co-transfected with pEGFP-N3-CD4 and pcDNA™ 3.1D/V5-His-TOPO-HIV-1 protease. This process was used to generate a homogenous population of cells co-transfected with pEGFP-N3-CD4 and pcDNA™ 3.1D/V5-His-TOPO-HIV-1 protease. Cells co-transfected with pEGFP-N3-CD4 and pcDNA™ 3.1D/V5-His-TOPO-HIV-1 protease will fluoresce green. Sterile cell sorting was performed using the BD FACSVantage SE flow cytometer. All cell-sorting experiments were performed by Mr Ronnie Dreyer at the Department of Immunology at the University of Cape Town. The mixed (transfected and un-transfected) population of CHO cells was trypsinised, as described in section 2.16.4, and then placed in the flow cytometer for sorting transfected cells from un-transfected cells. GFP-expressing cells were detected in the FL1 channel of the flow cytometer. This sorting process ensured that a pure population of transfected CHO cells was obtained. As a negative control un-transfected CHO cells was used as a reference sample to distinguish between transfected (green fluorescing) and un-transfected (non-fluorescing) cells.

The histograms in Figure 3.11 show the relative fluorescence of the cells. Figure 3.11-A shows a single peak for un-transfected, non-fluorescing control cells between 10^0 and 10^1 on the x-axis, which is in the M1 region of the histogram. Figure 3.11-B shows two distinct peaks. One peak between 10^0 and 10^1, and a second between 10^1 and 10^3. The cells in the second peak (also indicated in the M2 region of the histogram) make up ~90% of the total cell population, fluorescing green and respresenting the co-transfected cells. The cells were subjected to FACS to sort out the green fluorescing cell. Figure 3.11-C shows fluorescence in these cells after cell sorting was performed.

Figure 3.11-C shows that close to 99% of the cells are in the second peak. These cells were transferred to cell culture flasks and cultured as usual, according to standard cell culture protocols.
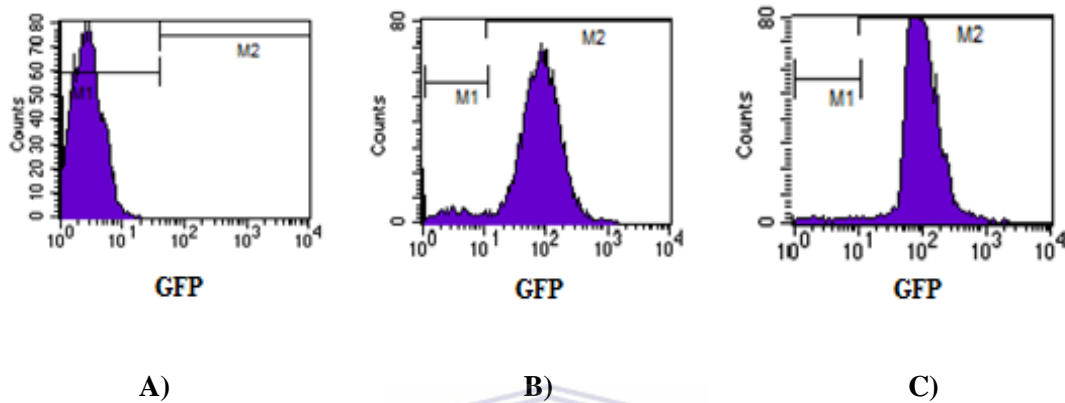
Figure 3.11 Fluorescent activated cell sorting of CHO cells co-transfected with pEGFP-N3-CD4 and pcDNA™ 3.1D/V5-His-TOPO-HIV-1 protease. A) GFP fluorescence in un-tranfected CHO cells B) GFP fluorescence in tranfected CHO cells before sorting by flow cytometry C) GFP fluorescence in tranfected CHO cells after sorting flow cytometry.
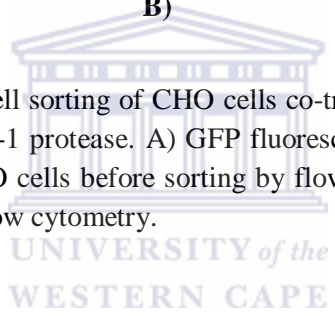
3.6 Summary

CD4 and HIV-1 protease PCR products were successfully cloned into mammalian expression vectors, as confirmed by DNA sequence data. The sequenced constructs, pEGFP-N3-CD4 and pcDNA™ 3.1D/V5-His-TOPO-HIV-1 protease, were then co-transfected into CHO cells to generate a cell line expressing both CD4 as well as HIV-1 protease. The presence of CD4 in these cells was confirmed by fluorescence microscopy as well as flow cytometry. In view of the above-mentioned data, a cell line representing HIV infected cells was successfully generated by gene engineering. These "HIV-infected cells" were used to target a HIV-1 protease-cleavable mutant caspase-3 nanostructure, with the expectancy that the targeted nanostructure would induce programmed cell death in the "HIV-infected cells".

CHAPTER 4. GENERATION OF MUTANT CASPASE-3 IN A BACTERIAL EXPRESSION SYSTEM FOR TARGETING "HIV-INFECTED" CELLS

4.1 Introduction

4.2 Design and synthesis of mutant caspase-3

4.3 Expression and purification of mutant caspase-3

4.4 Summary

CHAPTER 4. GENERATION OF MUTANT CASPASE-3 IN A BACTERIAL EXPRESSION SYSTEM FOR TARGETING TO "HIV-INFECTED" CELLS

4.1 Introduction

Apoptosis, or programmed cell death, is a biological process that is characterised by the controlled destruction of cells, accompanied by distinct morphological changes that occur in these cells. Caspase-3 is an executioner caspase that cleaves cellular proteins, giving rise to the morphological changes characteristic of apoptosis (Wyllie 2010). Vocero-Akbani and colleagues demonstrated that a mutant form of caspase-3 that was activated by HIV-1 protease is able to kill HIV-infected cells through the activation of apoptosis (Vocero-Akbani *et al*., 1999).

The aim of this study, is to achieve more specific, targeted destruction of HIV-infected cells. In the presence of an HIV-infected cell expressing HIV-1 protease, the mutant caspase-3 is activated, resulting in controlled, programmed cell death also known as apoptosis. A mutant caspase-3 was designed by introducing cleavage sites A (SQVSQNY-PIVQNLQ) and D (CTERQAN-FLGKIWP) for HIV-1 protease into the sequence of wildtype caspase-3.

4.2 Design and synthesis of mutant caspase-3

The DNA synthesis for mutant caspase-3 was based on the DNA sequence of caspase-3. The sequence was designed to contain an N-terminal polyhistidine tag, followed by the mutant caspase-3 containing the HIV-1 protease sites, A and D. Figure 4.1 A) shows the N-terminal polyhistidine tag followed by HIV-1 protease cleavage site D. This is flanked by the p17 subunit of caspase-3. Thereafter the second cleavage site for HIV-1 protease, A, is shown and is flanked by the p12 subunit of caspase-3. A simplified version of the synthesised contruct is demonstrated by Figure 4.1 B).

Figure 4.1 A) Mutant caspase-3 amino acid sequence for cloning into pET21b bacterial expression vector.

102
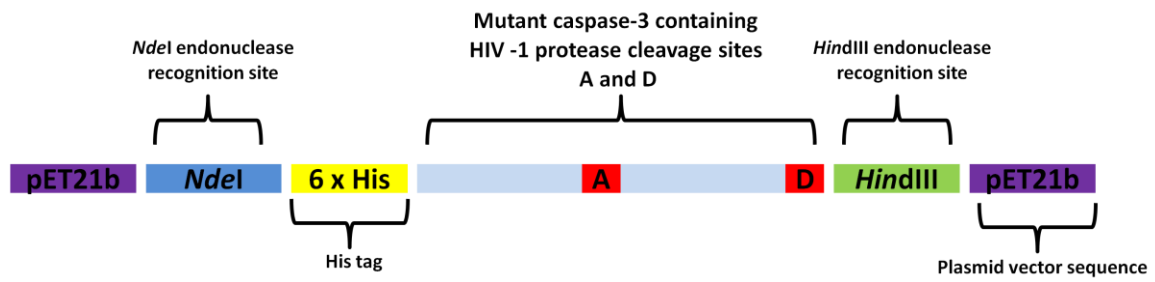
B) Animated version of mutant caspase-3 design for cloning into pET21b bacterial expression vector.

The DNA sequence information was sent to GenScript for optimised gene synthesis and subcloning into the pET21b bacterial expression vector, thereby generating pET21b-mutant caspase-3.

4.3 Expression and purification of mutant caspase-3

To determine expression of mutant caspase-3, the construct obtained from GenScript, as described in section 4.2, was transformed into *E.coli* BL21 codon plus™ cells, as described in section 2.13.4. Cells were plated on luria agar containing 100 µg/ ml ampicillin. After incubating plates at 37° C overnight, 4 colonies were selected and these were screened for expression of mutant caspase-3 by inducing cultures with IPTG, as described in section 2.14.1. Figure 4.2 shows the expression levels of mutant caspase-3 in *E.coli*.
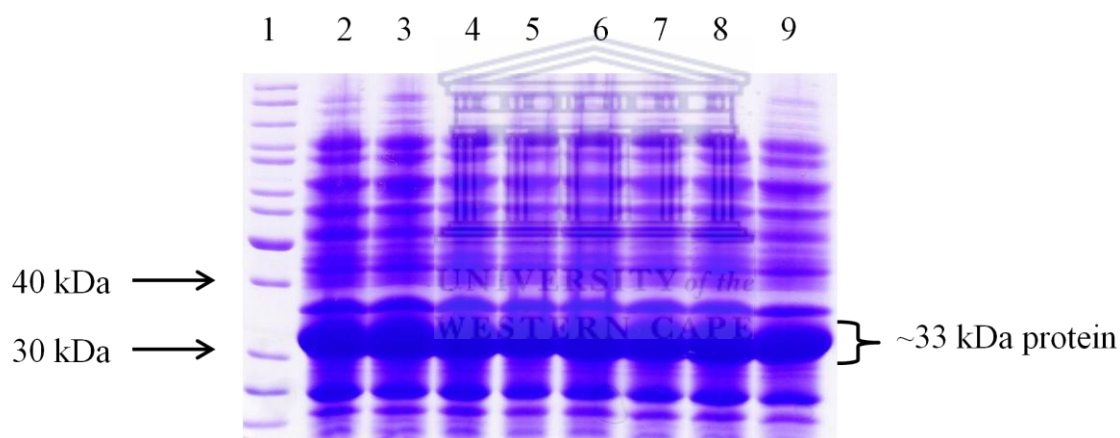
Figure 4.2 12% SDS-PAGE gel demonstrating expression of mutant caspase-3 in *E.coli*. *E.coli* BL21 codon plus™ colonies transformed with pET21b-mutant caspase-3 were screened to determine expression of the His-tagged fusion protein. Lane 1 indicates a molecular weight marker. Lanes 2, 4, 6 and 8 indicate uninduced protein samples, containing no IPTG. Lanes 3, 5, 7 and 9 indicate protein samples induced with 1 mM IPTG. A band corresponding to ~33 kDa relative to the protein marker is highly expressed.

As can be seen from Figure 4.2, no demonstrable difference could be seen between clones 1-4. Notably, the construct was equally well expressed in the uninduced samples as a result of leaky or unintended expression. Clone 4 was randomly selected and, a large-scale culture of pET21b-mutant caspase-3 was prepared and induced with IPTG, as described in section 2.14.2.

The cell lysate was then purified on a nickel sepharose column, as described in section 2.14.3. Fractions and elutes were collected by gravity for analysis by SDS-PAGE, as demonstrated by Figure 4.3.
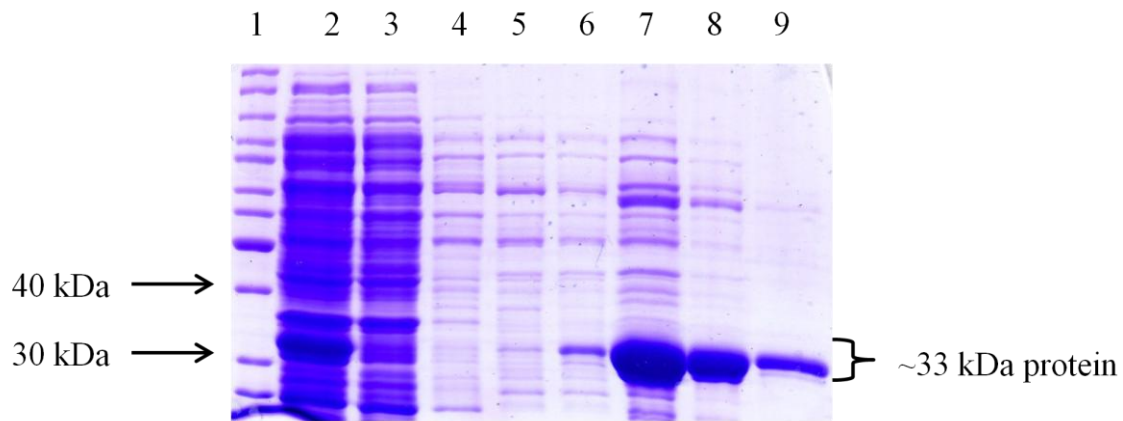
Figure 4.3 12% SDS-PAGE gel demonstrating nickel affinity purification of His-tagged mutant caspase-3 from *E.coli*. Lane 1 indicates a molecular weight marker. Lane 2 indicates the bacterial lysate subsequent to induction, while lane 3 indicates the flow-through after the lysate was passed over the nickel affinity column. Lanes 4-6 indicate the wash fractions containing 40 mM imidazole. Lanes 7-9 indicate purified protein fractions after elution with 250 mM imidazole.

As indicated by Figure 4.3, a ~33 kDa protein was eluted from the nickel affinity column, corresponding to the expected size of the mutant caspase-3 protein. The eluted protein from lanes 7-9 were pooled and stored at -20° C. To confirm that the 33 kDA protein was indeed mutant caspase-3, purified samples were loaded on an SDS-PAGE gel and Western blot analysis was done using a caspase-3 antibody.
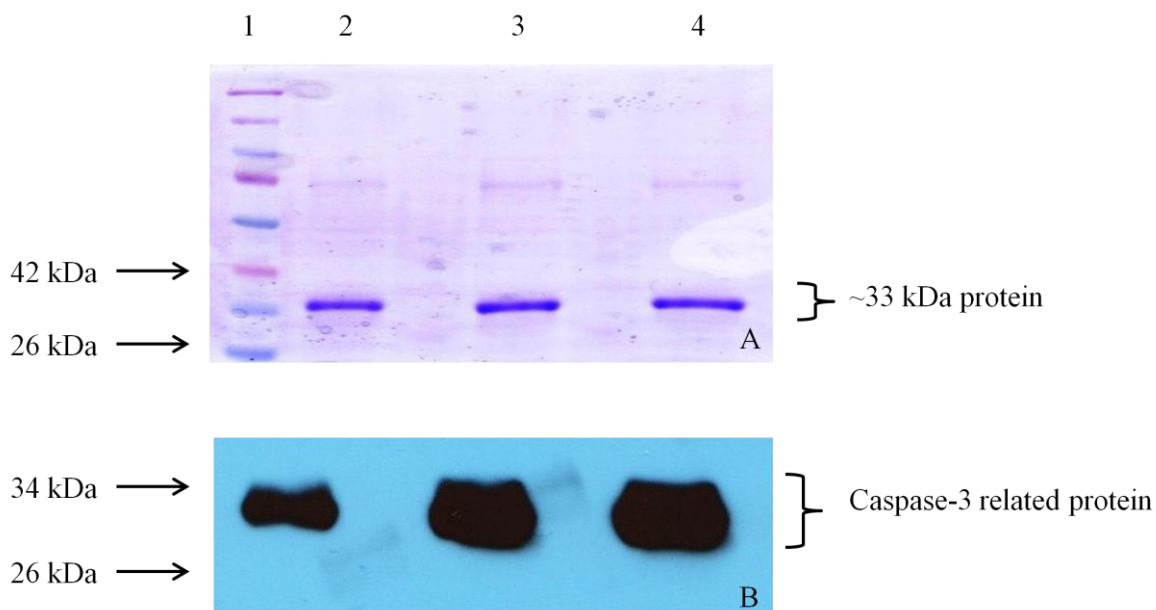
Figure 4.4 A) 12% SDS-PAGE gel of purified mutant caspase-3. Lane 1 indicates a molecular weight marker. Lanes 2-4 indicate purified samples of the 33 kDa protein. **B)** Western blot analysis of purified mutant caspase-3, probed with a caspase-3-specific antibody . Lanes 1-3 indicate the purified protein samples shown in A, probed with caspase-3 antibody.
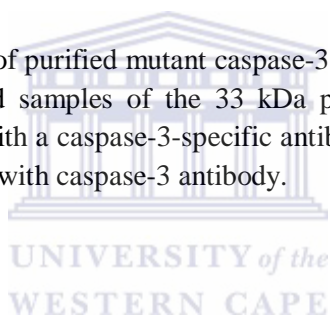
Figure 4.4 A) shows the eluted 33 kDa protein electrophoresed on an SDS-PAGE gel, as described in section 2.4. Figure 4.4 B) is a Western blot that was performed on the eluted samples. The Western blot confirmed that the 33 kDa protein was indeed a caspase-related protein, and was likely to therefore be the mutant caspase-3. Once expression and purification of mutant caspase-3 was confirmed by Western blot, as demonstrated by Figure 4.4, purified protein was dialysed in MES buffer using a Slide-A-Lyzer Dialysis Cassette from Thermo Scientific, with a molecular weight cut off of 7 kDa. The protein was lyophilised and stored at -80° C, as described in section 2.15.4.

4.4 Summary

The aim of the study was to generate a mutant form of the apoptosis-inducing protein, caspase-3, that is cleavable only by HIV-1 protease. Mutant caspase-3 was designed and synthesised, and the histidine-tagged construct was successfully expressed and purified. The results demonstrated here show the successful generation of a mutant form of caspase-3, to be used as a pro-apoptotic agent for the induction of apoptosis in "HIV-infected" cells. The generation of a cell line representing HIV infection was previously demonstrated (Chapter 3) and serves as the target for the death-inducing agent, mutant caspase-3. The expected outcome, therefore, is that the HIV-1 protease believed to be expressed by the cell line will result in the mutant caspase-3 becoming active, thereby eliciting apoptosis in those cells.

UNIVERSITY of the
WESTERN CAPE

CHAPTER 5. DESTRUCTION OF "HIV-INFECTED" CELLS USING CD4-TARGETING Ni-NTA MUTANT CASPASE-3 GOLD NANOPARTICLES

5.1 Introduction

5.2 Toxicity testing of gold nanoparticles prior to functionalisation with a CD4-targeting peptide and mutant caspase-3

5.3 Synthesis and characterisation of gold nanoparticles

5.4 Cell viability and apoptosis induction of "HIV-infected" cells treated with NTA-gold nanoparticles functionalised with a CD4-targeting peptide and mutant caspase-3

5.6 Summary

CHAPTER 5. DESTRUCTION OF "HIV-INFECTED" CELLS USING CD4-TARGETING Ni-NTA MUTANT CASPASE-3 GOLD NANOPARTICLES

5.1 Introduction

Gold nanoparticles possess a wide variety of applications in the field of biotechnology. These applications include disease detection, cellular imaging as well as sensor technology. Due to their inert nature and small size, gold nanoparticles have also been investigated for the purposes of targeted drug delivery in cellular systems. Gold nanoparticles have been shown to be particularly less toxic than other nanostructures and have therefore been identified as one of the nanostructures of choice in the field of drug delivery (Sperling *et al.*, 2008). Another useful characteristic of gold nanoparticles is that these particles can be conjugated to biomolecules (Mishra *et al.*, 2009). It is this ability to conjugate gold nanoparticles to biomolecules that prompted its use for the targeted delivery of the mutant caspase-3 that was generated, as described in Chapter 4.

As described in Chapter 3, a mammalian cell line was generated that express HIV-1 protease as well as the CD4 receptor in an attempt to generate a model cell line that represents a HIV-infected cell. To deliver mutant caspase-3 to these cells for the induction of apoptosis, gold nanoparticles would need to be targeted to them in some way. To this end, gold nanoparticles were synthesised and dual-functionalised with a CD4-targeting peptide as well as mutant caspase-3.

In this study the gold nanoparticles were used to deliver mutant caspase-3 to cells. To demonstrate that the nanoparticles themselves are not toxic the toxcity of these particles were invesitigated. Mammalian cells were exposed to the nanoparticles and the toxicity of the particles were evaluated using 7-AAD staining and the APOPercentage™ assay .

5.2 Toxicity screening of gold nanoparticles prior to functionalisation with CD4-targeting peptide and mutant caspase-3
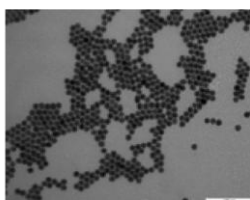
A

Figure 5.1. TEM images of gold nanoparticles conjugated with 50 % NTA NPs.

Gold nanoparticles were synthesised and conjugated with nitriloacetic acid (NTA), as described in section 2.22. The TEM image in Figure 5.1 shows the sizes of synthesised and functionalised nanoparticles before cellular treatment. Once characterised by TEM, these particles were used to treat Jurkat T cells for 24 hours to determine the cytotoxic effect of these functionalised nanoparticles. As described in section 2.17.2, CHO cells were grown to ~80 % visual confluency and treated with 2.5×10^{11} nanoparticles per well in a 24-well culture plate. Camptothecin was used as a positive control at a concentration of 0.2 μM (a concentration known to induce apoptotic cell death in CHO cells), while untreated cells served as the negative control. After incubating for 24 hours, cells were exposed to 20 μg/ml of 7-AAD staining solution.

Viable and non-viable cells can be distinguished with 7-AAD, since this dye binds to double-stranded DNA. The dye is not cell permeable and can therefore only stain the DNA in cells with damaged membranes. Non-viable cells were detected and counted by flow cytometry in the FL-3 channel.
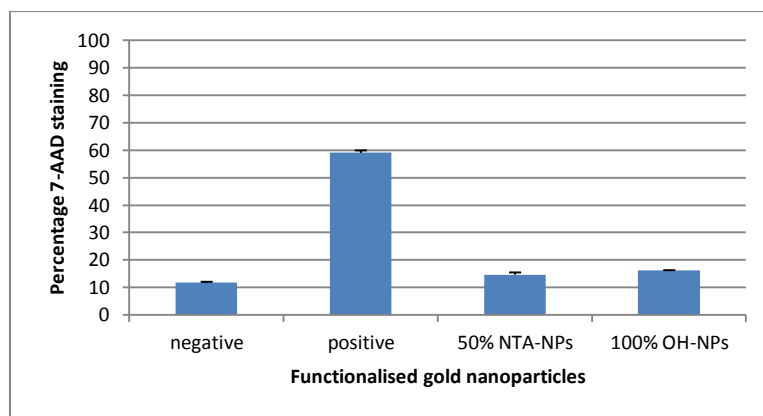
Figure 5.2. Percentage of 7-AAD staining measured in CHO cells treated with functionalised gold nanoparticles. 50% NTA NPs represent nanoparticles functionalised with a 50 % ratio of nitriloacetic acid (NTA). 100 % OH NPs represent nanoparticles functionalised with 100 % hydroxyl functional group. Cells were treated with 2.5 X 10^{11} nanoparticles. 0.2µM camptothecin served as a positive control, while untreated CHO cells served as the negative control.

As demonstrated by the graph in Figure 5.2, approximately 12 % of the untreated cells were non-viable. In the positive control (cells treated with camptothecin) nearly 60 % of the cells were non-viable. To further test that these gold nanoparticles, once functionalised with NTA, did not induce a cytotoxic response, CHO cells were treated with NTA-functionalised gold nanoparticles at various concentrations and apoptosis was measured by the APOPercentage™ assay, as described in section 2.17.3. Since CHO cells were used to generate the mammalian cell line representing HIV-infection, it was necessary to evaluate the toxicity of the NTA functionalised particles on these cells as well. CHO cells were grown to near visual confluency and treated in triplicate with three different concentrations of gold nanoparticles functionalised with NTA. From the data, represented by Figure 5.3, the negative control, containing untreated cells, showed less than15 % of the cells were positive for apoptosis. As for the positive control (cells treated with 0.2 µM camptothecin), more than 90 % of the cells were positive for apoptosis. Even at the maximum concentration of 0.5 nM, the NTA-functionalised nanoparticles did not induce significant levels of apoptosis (less than 10 % apoptosis was observed).

111
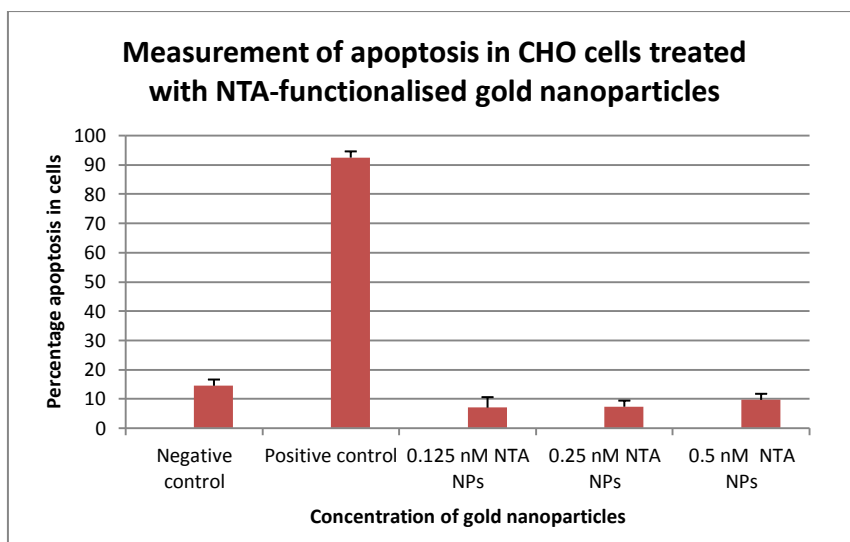
Figure 5.3. Measurement of percentage apoptosis in CHO cells treated with increasing concentrations of NTA-functionalised gold nanoparticles.

This demonstrates that at these concentrations, the particles did not result in cytotoxicity. Based on this data, and the fact that histidine-tagged proteins could be conjugated to NTA-functionalised nanoparticles with greater ease and stability than other chemical interactions, these particles were selected for the assembly of a CD4-targeting, mutant caspase-3 gold nanoparticle.

5.3 Characterisation of NTA-functionalised gold nanoparticles

As mentioned in section 2.22, gold nanoparticles were synthesised by both citrate reduction as well as the one-pot dual-ligand functionalisation of gold nanoparticles.
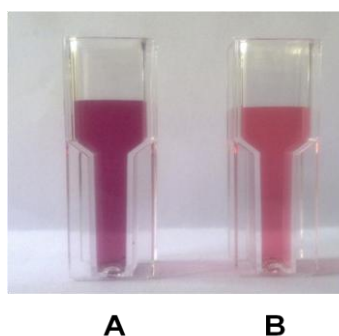
Figure 5.4. Gold nanoparticles synthesised by the one-pot method (A) and the citrate method (B).

As demonstrated by Figure 5.4 A and B, gold nanoparticles can vary in colour intensity, depending on the concentration of gold present in the sample. Citrate reduced nanoparticles were synthesised and then functionalised with NTA by Dr Sosibo Ndabenhle (Mintek), whereas with the one-pot method nanoparticles were functionalised with NTA during the synthesis process in a single step. Figure 5.5 demonstrates UV-Vis spectra of citrate reduced nanoparticles, as well as NTA-functionalised gold nanoparticles synthesised by the one-pot method. As the spectra suggest, the characteristic surface plasmon resonance (SPR) of unfunctionalised gold nanoparticles peaks at ~520 nm, while gold nanoparticles functionalised with NTA demonstrated a SPR maximum at ~530 nm. This clear shift in the SPR of the nanoparticles is only seen when nanoparticles are conjugated with a functional group.
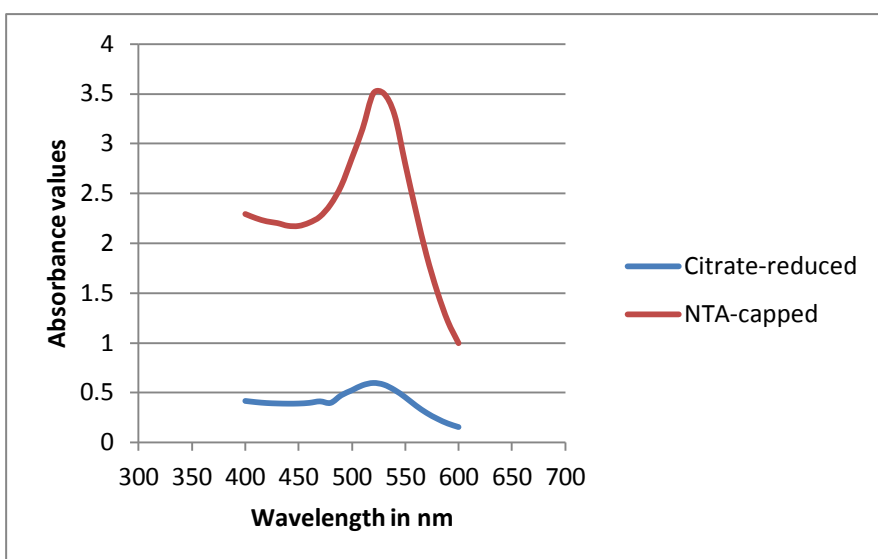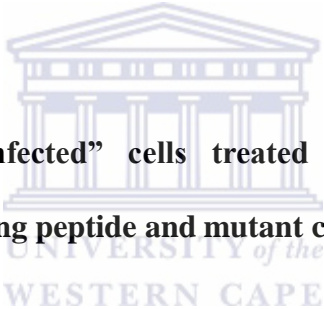
Figure 5.5. UV-Vis spectra of gold nanoparticles before and after functionalisation with NTA.
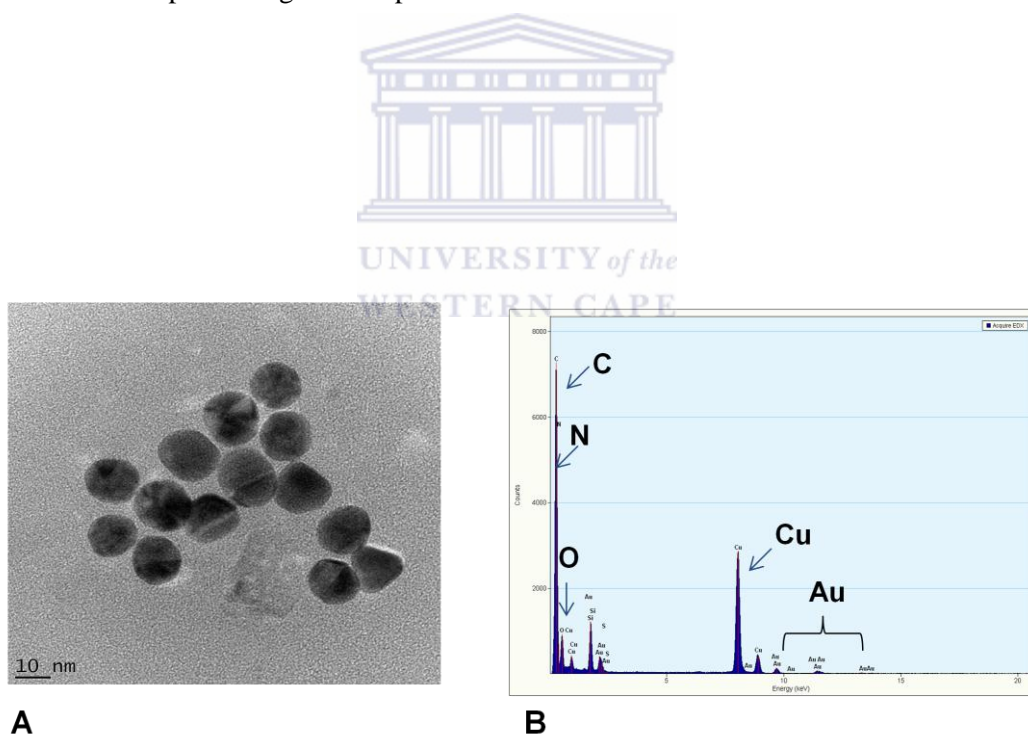
Figure 5.6. Characterising NTA-functionalised gold nanoparticles synthesised by the one-pot dual-ligand functionalisation method. **A** shows the HR-TEM analysis and **B** shows the EDX analysis.

The HR-TEM image of the gold nanoparticles functionalised with NTA (Figure 5.6 A) shows spherical particles with a diameter of 15-20nm. The particles appear relatively uniform in size and shape. The EDX data (Figure 5.6 B) shows the elemental composition of the nanoparticles. Various peaks are seen, each representative of the elements present in the sample. The nitrogen from the NTA is detected, as indicated by the N symbol. The gold from the gold nanoparticles is also detected, indicated by the Au symbol. The Cu indicates copper from the sample grid used to prepare the particles for TEM. The elemental composition depicted in Figure 5.6 B) further confirmed that NTA was indeed conjugated to the gold nanoparticles. These NTA-functionalised gold nanoparticles were stored at 4 °C until needed for further functionalisation.

5.4 Cell viability of "HIV-infected" cells treated with NTA-gold nanoparticles functionalised with CD4-targeting peptide and mutant caspase-3

The NTA-functionalised nanoparticles synthesised as described in section 2.22, by the one-pot dual-ligand functionalisation method, were used as the base particles for conjugation of a His-tagged CD4-targeting peptide and a His-tagged mutant caspase-3. The His-tagged CD4-targeting peptide was purchased from Thermo Scientific, while the His-tagged mutant caspase-3 was expressed and purified, as described in Chapter 4. The immobilisation of His-tagged proteins onto NTA-functionalised gold nanoparticles was performed as described by Abad and colleagues. In this study, they conjugated His-tagged proteins onto NTA-functionalised gold nanoparticles by 1-ethyl-3-[3´-(dimethylamino)propyl]carbodiimide (EDC)/ N-hydroxysuccinimide (NHS) chemistry (Abad *et al.*, 2005).

In this study, however, NTA was conjugated to gold nanoparticles in a single step during the synthesis process. His-tagged proteins were then added to NTA-functionalised gold

115

nanoparticles at a concentration ratio of 50:50 by adding $NiSO_4$ to the reaction, as described in section 2.22.1. Three dilutions of $NiSO_4$ were tested for conjugation in order to determine which concentration of $NiSO_4$ would generate the best shift in SPR from baseline, and therefore indicate a more stable conjugation reaction between the NTA-functionalised nanoparticles and the 2 histidine-tagged proteins. As demonstrated by Figure 5.7, the greatest shift in the SPR of the particles resulted when a concentration of 0.5 mM $NiSO_4$ was added to the reaction, indicated by the red curve. When compared to the control, which contained only NTA-functionalised gold nanoparticles, the addition of 0.5 mM $NiSO_4$ to particles containing the histidine-tagged proteins indicated a distinct shift in the SPR maxima of the particles, indicating the stable conjugation of protein onto the surface of Au-NTA particles.
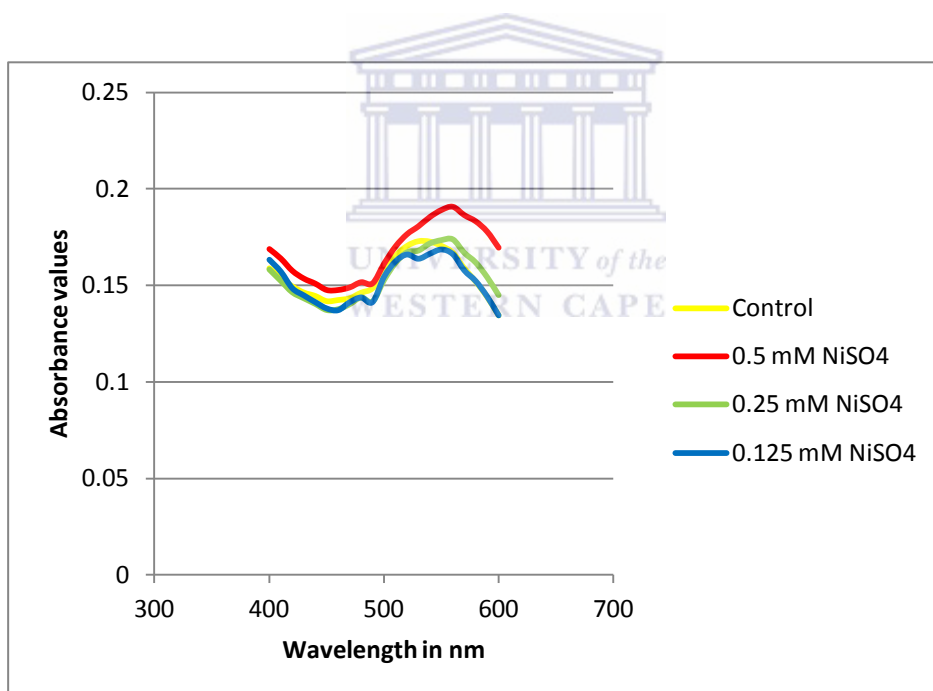
Figure 5.7. UV-Vis spectra of NTA-gold nanoparticles functionalised with CD4-targeting peptide and mutant caspase-3.

After determination of a concentration of $NiSO_4$ that would result in successful conjugation of histidine-tagged proteins onto Au-NTA nanoparticles, the dual-ligand conjugated gold

nanoparticles could be tested on cells. The "HIV-infected" cell model (described in Chapter 3) was used to test the targeted delivery of these particles to these cells.

As described in section 2.17.3, CHO cells representing HIV-infection were grown in 96-well plates until near visual confluency, and treated with increasing concentrations of functionalised gold nanoparticles for 24 hours. After treatment, 20 µl of viability/cytotoxicity reagent was added to cells and the plate was mixed briefly by orbital shaking.

The reagent was incubated at 37 °C for 30 minutes before measuring fluorescence. The two substrates present in the reagent, namely the GF-AFC substrate and the bis-AAF-R110 substrate, when cleaved, produce a fluorescent signal for viability and cytotoxicity respectively. The substrates each have their own excitation and emission wavelengths, making it possible to distinguish between a fluorescence signal for viability and for cytotoxicity. According to the protocol, cytotoxicity was measured at the excitation wavelength of 485 nm and an emission wavelength of 520 nm. Figure 5.8 demonstrates fluorescence (at the above-mentioned wavelengths) detected in cells treated with various concentrations of functionalised gold nanoparticles. The lowest concentration of particles, at 125 pM has a low level of fluorescence, indicating decreased cytotoxicity in these cells. As the concentration of nanoparticles increases, there appears to be an increase in the amount of fluorescence detected, indicating increased cytotoxicity. The 500 pM concentration of particles seemed to produce a fluorescence signal of half the cytotoxicity of the most cytotoxic concentration of particles. This concentration was therefore selected as the concentration that would be toxic in half the population of cells over the 24 hour period (LC_{50}).
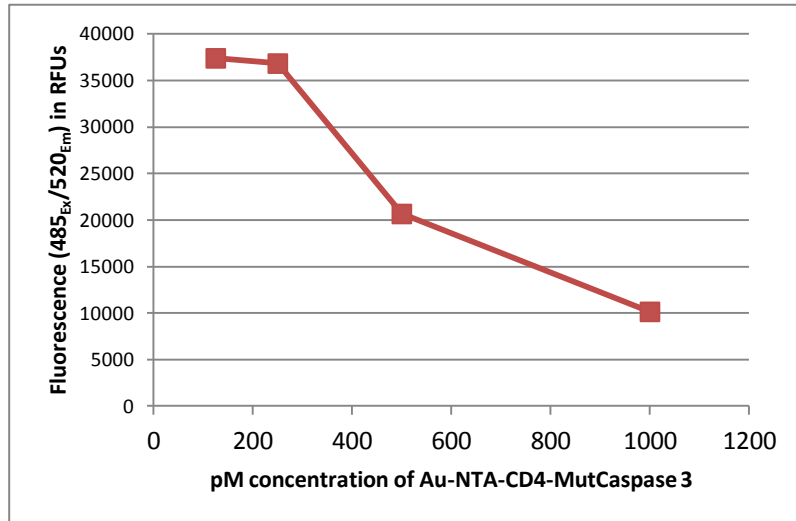
Figure 5.8. Viability of CHO cells representing HIV-infection after 24 hour treatment with increasing concentrations of NTA-CD4-targeting peptide-mutant caspase-3 functionalised gold nanoparticles.

Once the LC_{50} was determined to be 500 pM, as indicated by Figure 5.8, cells representing HIV infection were treated with this concentration of NTA-CD4-targeting peptide-Mutant caspase-3 gold nanoparticles for a period of 6 hours. Transfected cells expressing both CD4 and HIV-1 protease were seeded at a cell number of 1×10^5 cells per ml in a 6-well plate. As a negative control, one well, well A, containing only cells, was left untreated. The positive control, well B, contained cells treated with 50 % ethanol to demonstrate apoptosis-mediated cell death. Well C contained cells plus 500 pM NTA-gold nanoparticles. Well D contained cells plus 500 pM NTA-gold nanoparticles functionalised with CD4-targeting peptide. Well E contained cells plus 500 pM NTA-gold nanoparticles functionalised with mutant caspase-3. Finally, well F contained 500 pM NTA-CD4-targeting peptide-mutant caspase-3 gold nanoparticles. As a control experiment, untransfected CHO cells were also seeded at 1×10^5 cells per ml in a 6-well plate and treated identical to the transfected CHO cells, as described earlier. This experiment was done to determine whether the initiation of apoptosis would be specific to cells expressing HIV-1 protease.

118

5.5 Apoptosis induction in "HIV-infected" cells treated with NTA-gold nanoparticles functionalised with CD4-targeting peptide and mutant caspase-3

Since the CD4-targeting peptide-Mutant caspase-3 gold nanoparticles are expected to induce apoptosis in the "HIV-infected" cells, the cells were treated with the nanoparticles and apoptosis was assessed by the APOPercentage™ assay, as described in section 2.17.3. Cells were grown to near visual confluency and treated with CD4-targeting peptide-Mutant caspase-3 gold nanoparticles. From the APOPercentage™ data, represented by Figure 5.9, the negative control (untreated cells), showed that about 3 % of the cells were positive for apoptosis. The positive control (cells treated with 50 % ethanol), showed that more than 98 % of the cells were positive for apoptosis. Cells expressing both CD4 and HIV-1 protease demonstrated a less than significant percentage of apoptotic cells in cells treated with NTA-nanoparticles only and cells treated with NTA-CD4-targeting peptide nanoparticles. In cells treated with NTA-nanoparticles functionalised with mutant caspase-3, only 12 % of cells had undergone apoptosis. When treated with NTA-CD4-targeting peptide-mutant caspase-3 nanoparticles, only 15 % of cells had undergone apoptosis. Since this assay requires greater than 15 % for cells to be considered significantly apoptotic, these results do not conclude that the cells undergo increased levels of apoptosis.
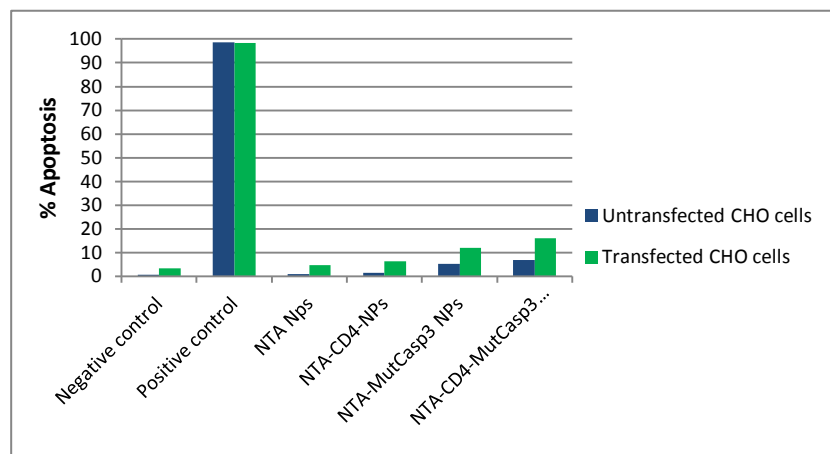
Figure 5.9. Measurement of apoptosis in "HIV-infected" cells treated with NTA-functionalised gold nanoparticles functionalised with CD4-targeting peptide and mutant caspase-3.

5.6 Morphological analysis of "HIV-infected" cells treated with NTA-CD4-targeting peptide-mutant caspase-3 gold nanoparticles

To determine whether any morphological changes occurred in cells after 6 hours of treatment, light microscope images were taken at 20 X magnification using a Leica EC3 digital camera. Figure 5.10 demonstrates the morphological changes that took place in transfected cells treated with various NTA-nanoparticles after 6 hours.
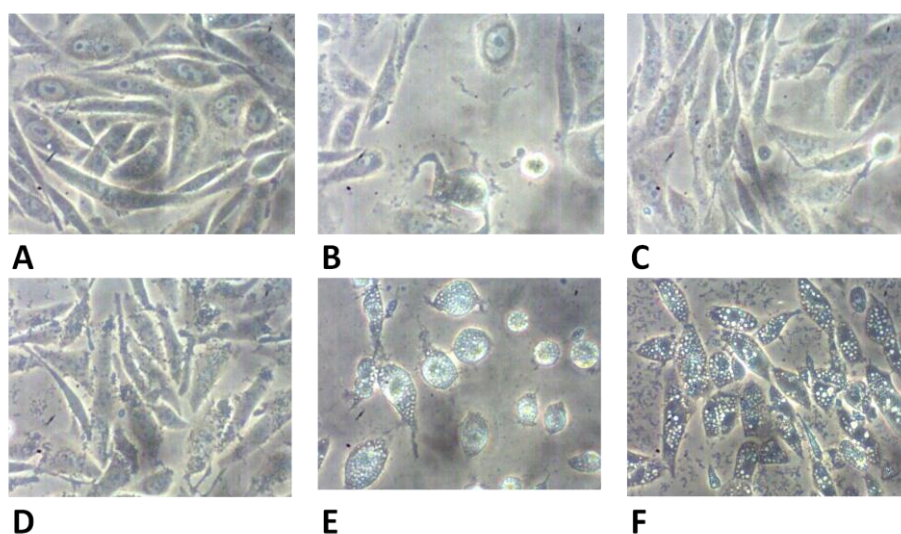
Figure 5.10. Light microscope images of CHO cells transfected with NTA-CD4-targeting peptide-mutant caspase-3 nanoparticles. A) Untreated transfected cells. B) Transfected cells treated with 50 % ethanol (positive control). C) Transfected cells treated with NTA-nanoparticles only. D) Transfected cells treated with NTA-CD4 targeting peptide nanoparticles. E) Transfected cells treated with NTA-mutant caspase-3 nanoparticles. F) Transfected cells treated with NTA-CD4-targeting peptide-mutant caspase-3 nanoparticles. Images were captured at 20 x magnification.

After 6 hours of treatment, untreated cells, Figure 5.10 A) remained unchanged, the positive control B) (cells treated with ethanol) changed morphology by rounding up and lifting from the well. Cells treated with NTA-nanoparticles, indicated by Figure 5.10 C) did not demonstrate any distinct morphological changes. Cells treated with NTA-CD4-targeting peptide nanoparticles (D) were also relatively unaffected, although the cells appeared more sindle shaped the cells did not detach from the plate. Cells treated with NTA-mutant caspase-3, however, showed cells starting to round up and the formation of a number of vesicles within cells, as seen in Figure 5.10 E). Cells treated with NTA-CD4-targeting peptide-mutant caspase-3 nanoparticles demonstrated an even greater incidence of vesicle formation after 6 hours of treatment, as indicated by Figure 5.10 F). Both NTA-mutant caspase-3 and NTA-CD4-targeting peptide-mutant caspase-3 particles caused cell detachment.

5.7 Summary

To determine which gold nanoparticles would cause the least amount of toxicity in cells before being conjugated to our death-inducing protein, nanoparticles with various functionalities were tested on cells. The NTA-functionalised gold nanoparticles demonstrated the lowest levels of apoptosis, and were therefore selected as the base particles for the conjugation of our CD4-targeting peptide as well as our death-inducing mutant caspase-3. The NTA group also made it possible to functionalise our proteins to the nanoparticle by means of nickel titration. The optimal concentration of nickel was determined to be 0.5 mM and was used to conjugate CD4-targeting peptide as well as mutant caspase-3 to form NTA-CD4-targeting peptide-mutant caspase-3 gold nanoparticles. These particles were used to treat cells expressing CD4 and HIV-1 protease, thereby representing HIV-infection, and apoptosis was measured. The APOPercentage™ assay revealed insignificant levels of apoptosis in cells transfected with CD4 and HIV-1 protease, when treated with NTA-CD4-targeting peptide-mutant caspase-3 nanoparticles. Morphological data, however, revealed that after 6 hours of treatment with NTA-CD4-targeting peptide-mutant caspase-3 nanoparticles, cells no longer resembled their untreated counterparts and increased levels of vacuole formation within cells was seen. From the morphological data, it is clear that after 6 hours of treatment, cells are being affected by the NTA-CD4-targeting peptide-mutant caspase-3 nanoparticles. An extension of this 6 hour experiment would most likely reveal a great deal more as to whether apoptosis is the mechanism of cell death occurring here.

CHAPTER 6. DISCUSSION AND CONCLUSION

6.1 Introduction

Vocero-Akbani and colleagues previously demonstrated that a mutant form of caspase-3 that was only cleavable by HIV-1 protease can be used to induce apoptosis in HIV infected cells (Vocero-Akbani *et al.*, 1999). The study by Vocero-Akbani made use of protein transduction to deliver the mutant form of caspase-3 to the HIV infected cells. Consequently, the strategy employed by Vocero-Akbani lacks specifity. The aim of this project was to use the same strategy, but to specifically target the delivery of the mutant caspase-3 to HIV infected cells using gold nanoparticles. These nanoparticles can potentially be used to treat HIV infection, since the induction of apoptosis in HIV infected cells can reduce viral load in HIV patients. To achieve this, a model cell line that resemble an HIV infected cell was generated using CHO cells. The CHO cells were mutagenised so that these cells express both CD4 (on the cell surface) as well as HIV-1 protease (in the cytosol). Gold nanoparticles conjugated with a CD4 targeting peptide and mutant caspase-3 were synthesised. The targeting peptide will specifically deliver the nanoparticles to bind to CD4 expressing cells and the mutant caspase-3 will activate apoptosis in cells containing HIV-1 protease. Upon cleavage of the mutant caspase-3 by HIV-1 protease, caspase-3 becomes active, thereby resulting in the initiation of apoptosis or programmed cell death in of HIV-infected cells.

6.2 Cloning and stable expression of pEGFP-N3-CD4 and HIV-1 protease-pcDNA™ 3.1D/V5-His-TOPO in CHO cells

In order to generate a cell line expressing both CD4 and HIV-1 protease, CD4 was first PCR amplified and run on an agarose gel. The size of the PCR product corresponded to ~ 1.2 kb, the expected size for the CD4 gene. The PCR product, as well as the expression vector, pEGFP-N3, were digested with the appropriate restriction enzymes before cloning the PCR product into the vector.

Colony PCR was done to identify clones into which the cloned PCR product was cloned. Three of the positive clones, clone 3, 4 and 5 were randomly selected to confirm that CD4 was indeed cloned into pEGFP-N3. Translation of the nucleic sequence data by *in silico* translation using the ExPASy tool revealed a 99 % amino acid similarity between human CD4 and the PCR product that was cloned into pEGP-N3. The single mismatched amino acid in the compared sequences was determined to be negligible since it does not affect the function of the protein, as determined by the ExPASy protein function analysis tool.

In a similar way, HIV-1 protease was PCR amplified, digested and cloned into pcDNA™ 3.1D/V5-His-TOPO. Colony PCR was done to to identify clones into which the cloned PCR product was cloned. In Figure 3.7, a faint band, of diminished intensity when compared to the other bands on the gel, can be seen in lane 12, the negative control. The presence of this band suggests that there may have been overflow from the PCR product in lane 11, resulting in a faint, similarly-sized band where no DNA should have been present. Due to the intensity of the other bands on the gel, the faint band was considered to be negligible. Five of the clones were randomly selected and sent for sequencing. Analysis of the sequence data revealed a 100 % match between HIV-1 protease and the PCR product cloned into pcDNA™ 3.1D/V5-His-TOPO.

6.3 Transfection and evaluation of expression of CD4-pEGFP-N3 and HIV-1 protease-pcDNA™ 3.1D/V5-His-TOPO in CHO cells

Both pEGFP-N3 and pcDNA™ 3.1D/V5-His-TOPO use neomycin resistance as a selectable marker to select for transfected cells. Consequently pcDNA™ 3.1D/V5-His-TOPO-HIV-1 protease was transfected at ten times the concentration of pEGFP-N3-CD4. After 7 days of selection with G-418 none of the control cells (untransfected cells) were viable. Cells co-transfected with pcDNA™ 3.1D/V5-His-TOPO-HIV-1 protease and pEGFP-N3-CD4, however, were still viable and proliferating in the presence of G-418 after 7 days.

The transfection of cells with pEGFP-N3-CD4 will result in the expression of CD4 as a fusion protein with GFP. Since GFP is a fluorescent protein, fluorescence microscopy was used to confirm the expression of CD4-GFP. The results demonstrated that approximately 70 % of transfected cells were positive for CD4-GFP expression. This indicated that only 70 % of the cell population had been successfully transfected with the pEGFP-N3-CD4 construct. To generate a homogenous population of these transfected cells, live cell sorting was performed using a Fluorescent Activated Cell Sorter. Once sorted, more than 99 % of the cell population was detected in the FL1 channel of the cytometer, indicating the expression of GFP. This therefore confirmed that the sorted cell population was a relatively pure population of CD4-pEGFP-N3 expressing cells.

Since the concentration of pcDNA™ 3.1D/V5-His-TOPO-HIV-1 protease plasmid was ten times higher than the concentration of pEGFP-N3-CD4, it can be assumed that pcDNA™ 3.1D/V5-His-TOPO-HIV-1 protease was also successfully transfected. A model cell line , CHO-HIV-1 protease-CD4, expressing both HIV-1 protease as well as CD4 was therefore successfully generated, and can be used to test nanoparticles as pro-apoptotic agents.

6.4 Recombinant expression and purification of mutant caspase-3 for conjugation to NTA-functionalised gold nanoparticles

In the study by Vocero-Akbani and colleagues in 1999, they were able to demonstrate the activation of apoptosis of HIV-infected cells by using site-directed mutagenesis to generate a mutant form of caspase-3. This mutant caspase-3 contained the activation sites for HIV-1 protease that allowed the cleavage of the caspase by the HIV-1 protease, resulting in apoptotic cell death of HIV-infected cells.

Based on the aforementioned study, we attempted to design mutant caspase-3 that could be activated in the presence of HIV-1 protease expressed in mammalian cells representing HIV-infection, as described in Chapter 3.

In order to achieve this, an NTA-functionalised gold nanoparticle bi-conjugated to a His-tagged CD4-targeting peptide and a His-tagged mutant caspase-3 protein was generated. A DNA sequence for the recombinant expression of mutant caspase-3 in pET21b expression vector was designed based on the study by Vocero-Akbani and colleagues. The sequence was submitted to GenScript for synthesis. BL21 codon plus™ *E.coli* cells were transformed with this construct. An expression screen revealed the expression of a ~33 kDa protein, which is the expected size for the mutant caspase-3.

As noted in section 4.3, the construct was expressed equally well in both the uninduced and induced samples. This is most likely attributed to leaky expression, a phenomenon caused by the presence of small amounts of lactose present in culture media during the bacterial expression of proteins (Studier, F. W., 2005).

After screening for the mutant form of caspase-3, the process was scaled up for the expression and purification of the protein. To confirm that the eluted protein sample was indeed mutant caspase-3, a Western blot using a caspase-3 antibody was done. The signal from the Western blot confirmed that the eluted protein was a caspase-3 related protein, and most likely mutant caspase-3.

NTA-functionalised gold nanoparticles were used as base particles for the generation of a gold nanoparticle containing both a CD4-targeting peptide, as well as a mutant caspase-3. This particle, Au-NTA-CD4-Mutcasp3, was assembled by adding His-tagged CD4 targeting peptide and His-tagged mutant caspase-3 to NTA-functionalised gold nanoparticles and incubating at room temperature overnight. To ascertain that the particle was indeed functionalised, TEM and EDX were performed to respectively determine the size and composition of nanoparticles.

6.5 Detection of cytotoxicity and apoptosis using the ApoTox-Glo™ Triplex Assay on CHO-HIV-1 protease-CD4 cells treated with Au-NTA-CD4-MutCasp3

Due to their inert nature, as well as the ability to attach various biomolecules to them, gold nanoparticles were used as vehicles for the targeted delivery of a death-inducing protein, mutant caspase-3. Nanoparticles were targeted to cells expressing CD4 and HIV-1 protease by conjugating the particles to a CD4-targeting peptide. In order to facilitate conjugation, and based on the low levels of cytotoxicity produced in cells, NTA-functionalised nanoparticles were selected.

6.5.1 Cytotoxicity in CHO-HIV-1 protease-CD4 cells 24 hours after treatment with Au-NTA-CD4-MutCasp3

Cytotoxicity of CHO-HIV-1 protease-CD4 cells treated for 24 hours with Au-NTA-CD4-MutCasp3 was determined using the ApoTox-Glo™ Triplex Assay cytotoxicity reagent. From this data, as described in Figure 5.8 of Chapter 5, it can be deduced that as the nanoparticle concentration increases, the level of cytotoxicity decreases. Based on this data, the LC_{50} of the functionalised nanoparticles was determined to be approximately 500 pM, the concentration at which half the cell population was no longer viable. This concentration of NTA-gold nanoparticles was used to perform a 50:50 ratio of His-tagged CD4 targeting peptide to His-tagged mutant caspase-3 functionalisation of NTA-gold nanoparticles.

6.5.2 Apoptosis in CHO-HIV-1 protease-CD4 cells 6 hours after treatment with

Au-NTA-CD4-MutCasp3

Apoptosis was measured by the APOPercentage^{TM} assay in CHO-HIV-1 protease-CD4 cells 6 hours after treatment with Au-NTA-CD4-MutCasp3. The APOPercentage^{TM} data, indicated in Figure 5.9, suggests that after 6 hours of treatment with Au-NTA-CD4-MutCasp3, only 15 % of cells underwent apoptosis. In order for the assay to show significant levels of apoptosis, 15 % or greater levels of apoptosis must be seen. This could therefore not be considered a significant resultThe experiment was, however, limited since the duration of treatment was only 6 hours. In order to more accurately determine the mechanism of cell death, as well as whether there is a marked increase in apoptosis, apoptosis would need to be measured at additional time points.

The percentage of apoptosis in cells treated only with NTA-mutant caspase-3 nanoparticles was ~ 12 %, which is not much lower than cells treated with the fully functionalised nanoparticle. Even though the number of cells that undergo apoptosis when treated with NTA-mutant caspase-3 nanoparticles and Au-NTA-CD4-MutCasp3 is ~ 12 % and 16 % respectively, this gap could widen with an increase in treatment duration to demonstrate that the death-inducing nanoparticles are, indeed, targeted to CHO-HIV-1 protease-CD4 cells expressing CD4 and HIV-1 protease. When one compares the apoptosis data for transfected cells treated with Au-NTA-CD4-MutCasp3 to that of untransfected cells treated with the same, it was also determined that a low level of apoptosis, ~ 7 %, is detected. This was an unexpected result, but could very possibly be attributed to the occurrence of auto-cleavage of the mutant caspase-3.

Auto-cleavage is a common occurrence where proteins are cleaved in the absence of an activation enzyme. The phenomenon usually occurs as a result of changes in pH and

temperature. In order to minimise the occurrence of auto-cleavage in future, various salt concentrations and temperatures could be tested to determine which conditions would be optimal.

6.5.3 Morphological analysis of CHO-HIV-1 protease-CD4 cells 6 hours after treatment with Au-NTA-CD4-MutCasp3

Before apoptosis was measured in cells, as described section 6.4.2, light microscopy was performed to identify morphological changes that had taken place 6 hours after treatment, as displayed in Figure 5.10. When visualised under a light microscope, the negative control, containing untreated cells only, displayed the usual morphology of CHO cells. The positive control, containing a known inducer of apoptosis, displayed rounding up and lifting of cells from the culture surface, indicating cell death. CHO-HIV-1 protease-CD4 cells treated with NTA-nanoparticles only did not display any noticeable morphological changes, as was the case with cells treated with NTA-CD4 nanoparticles.

Cells that were treated with Au-NTA-CD4-MutCasp3 nanoparticles did, however, demonstrate distinctive morphological changes. After 6 hours of treatment, these cells demonstrated high levels of vacuole formation, seen in nearly the entire cell population. The same phenomenon occurred in cells treated with NTA-CD4-targeting peptide-mutant caspase-3. This marked increase in vacuole formation is reminiscent of a process termed autophagy, a catabolic process during which a membrane develops around cell contents, forming vacuoles. These vacuoles are then transported to lysosomes, where they undergo degradation.

Although apoptosis has been classified as the primary form of programmed cell death, recent years have seen the advent of autophagic death as a secondary type of cell death, based largely on morphological changes (Debnath *et al.*, 2005).

Based on the morphological data alone, as displayed in Figure 5.10, it would appear that after 6 hours of treatment, these cells do undergo autophagy. Although autophagy is considered to be a mechanism that protects cells from proteotoxic and oxidative stress, it has also been linked to apoptosis itself. Cells have been known to alternate between apoptosis and autophagy, suggesting that autophagy may be a supporting mechanism of cell death and that both processes could very well share the same pathways in response to cellular stress (Maiuri *et al.*, 2007).

6.6 Conclusion

The results of this study show that NTA-gold nanoparticles functionalised with a CD4-targeting peptide as well as a death-inducing mutant caspase-3 results in cell death after 6 hours of treatment. The APOPercentage™ data suggests that these cells start to undergo apoptosis after 6 hours. Additionally, the morphological data demonstrates the formation of a large number of vacuoles by these cells, suggesting the occurrence of autophagy. This preliminary data suggests that gold nanoparticles could potentially serve as effective drug delivery tools and that the mutant caspase-3, coupled to these particles, results in death in cells representing HIV-infection, irrespective of the mechanism of death. Future investigation will focus on the improvement of specificity of mutant caspase-3 for cells expressing HIV-1 protease by limiting the occurrence of auto-cleavage. Longer duration of treatment could also shed light on the extent of cell death that takes place in "HIV-infected" cells.

Cellular uptake studies will also be done to determine the concentration of particles within cells, as well as whether uptake is greater in those cells expressing CD4. Once the therapeutic agent has proven to be successful *in vitro*, an animal model of HIV will be treated with functionalised gold nanoparticles to determine whether they induce apoptosis in an *in vivo* setting, and thereby reduce viral load towards the eradication of HIV-infected cells.

REFERENCES

ABAD, J.M., MERTENS, S.F.L., PITA, M., FERNÁNDEZ, V.M. & SCHIFFRIN, D.J. (2005) Functionalization of Thioctic Acid-Capped Gold Nanoparticles for Specific Immobilization of Histidine-Tagged Proteins. *J Am Chem Soc*, 127, 5689-5694.

ADAMSON, C. S. & FREED, E. O. (2008) Recent progress in antiretrovirals--lessons from resistance. *Drug Discov Today,* 13, 424-32.

ALIVISATOS, A. P., GU, W. & LARABELL, C. (2005) Quantum dots as cellular probes. *Annu Rev Biomed Eng,* 7, 55-76.

BAWA, R., MELETHIL, S., SIMMONS, W.J. & HARRIS, D. (2008) Nanopharmaceuticals: patenting issues and FDA regulatory challenges. *The SciTech Lawyer*, 5, 10-15.

BENDER, A.R., VON BRIESEN, H., KREUTER, J., DUNCAN, I.B. & RÜBSAMEN-WAIGMANN, H. (1996) Efficiency of nanoparticles as a carrier system for antiviral agents in human immunodeficiency virus-infected human monocytes/macrophages *in vitro*. *Antimicrob Agents Chemother*, 40, 1467-1471.

BERGER, E. A., MURPHY, P. M. & FARBER, J. M. (1999) Chemokine receptors as HIV-1 coreceptors: roles in viral entry, tropism, and disease. *Annu Rev Immunol,* 17, 657-700.

BOATRIGHT, K. M. & SALVESEN, G. S. (2003) Mechanisms of caspase activation. *Curr Opin Cell Biol,* 15, 725-31.

BOWMAN, M., BALLARD, T.E., ACKERSON, C.J., FELDHEIM, D.L., MARGOLIS, D.M. & MELANDER, C. (2008) Inhibition of HIV fusion with multivalent gold nanoparticles. *J Am Chem Soc*, 130, 6896-6897.

BRIK, A. & WONG, C.H. (2003) HIV-1 protease: mechanism and drug discovery. *Org Biomol Chem,* 1, 5-14.

BRINKMAN, K., SMEITINK, J. A., ROMIJN, J. A. & REISS, P. (1999) Mitochondrial toxicity induced by nucleoside-analogue reverse-transcriptase inhibitors is a key factor in the pathogenesis of antiretroviral-therapy-related lipodystrophy. *Lancet,* 354, 1112-5.

BRIZ, V., POVEDA, E. & SORIANO, V. (2006) HIV entry inhibitors: mechanisms of action and resistance pathways. *J Antimicrob Chemother,* 57, 619-27.

BRODER, S. (2010) The development of antiretroviral therapy and its impact on the HIV-1/AIDS pandemic. *Antiviral Research*, 85, 1-18.

BRUST, M., WALKER, M., BETHELL, D., SCHIFFRIN, D.J. & WHYMAN, R. (1994) Synthesis of thiol-derivatised gold nanoparticles in a two-phase liquid–liquid system. *J Chem Soc Chem Commun*, 7, 801-802.

BUSHMAN, F. D. & CRAIGIE, R. (1991) Activities of human immunodeficiency virus (HIV) integration protein *in vitro*: specific cleavage and integration of HIV DNA. *Proc Natl Acad Sci USA,* 88, 1339-43.

CARR, A. & COOPER, D. A. (2000) Adverse effects of antiretroviral therapy. *Lancet,* 356, 1423-30.

CASADABAN, M.J., CHOU, J. & COHEN, S.N. (1980) *In vitro* gene fusions that join an enzymatically active beta-galactosidase segment to amino-terminal fragments of exogenous proteins: Escherichia coli plasmid vectors for the detection and cloning of translational initiation signals. *Journal of Bacteriology*, 143, 971-980.

CHAN, W. C., MAXWELL, D. J., GAO, X., BAILEY, R. E., HAN, M. & NIE, S. (2002) Luminescent quantum dots for multiplexed biological detection and imaging. *Curr Opin Biotechnol,* 13, 40-6.

CHEN, M. & WANG, J. (2002) Initiator caspases in apoptosis signaling pathways. *Apoptosis,* 7, 313-9.

CHOI, C.H., ALABI, C.A., WEBSTER, P. & DAVIS, M.E. (2010) Mechanism of active targeting in solid tumors with transferrin-containing gold nanoparticles. *Proc Nat Acad Sci* USA, 107, 1235-1240.

CHOWDHURY, I., THARAKAN, B. & BHAT, G. K. (2008) Caspases - an update. *Comp Biochem Physiol B Biochem Mol Biol,* 151, 10-27.

CLONINGER, M. J. (2002) Biological applications of dendrimers. *Curr Opin Chem Biol,* 6, 742-8.

COHEN, G.M. (1997) Caspases: the executioners of apoptosis. *Biochem J*, 326, 1-16.

COSTIN, J. M. (2007) Cytopathic mechanisms of HIV-1. *Virol J,* 4, 100.

DANIEL, M.C. & ASTRUC., D. (2004) Gold nanoparticles: assembly, supramolecular chemistry, quantum-size-related properties, and applications toward biology, catalysis, and nanotechnology. *Chem Rev*, 104, 293-346.

DAS NEVES, J., AMIJI, M.M., BAHIA, M.F. & SARMENTO, B. (2010) Nanotechnology-based systems for the treatment and prevention of HIV/AIDS. *Advanced Drug Delivery Reviews,* 62, 458-477.

DE, M., GHOSH, P.S. & ROTELLO, V. (2008) Applications of nanoparticles in biology. *Advanced Materials*, 20, 4225-4241.

DEBNATH, J., BAEHRECKE, E.H. & KROEMER, G. (2005) Does autophagy contribute to cell death? *Autophagy*, 1, 66-74.

DE LA ROSA, R., HARRIS, M., UYEDA, L., GOODISON, K., KEOWN, P. & MONTANER, J. S. (2004) Life-threatening reaction after first ever dose of abacavir in an HIV-1-infected patient. *Aids,* 18, 578-9.

DERFUS, A.M., CHAN, W.C.W. & BHATIA, S.N. (2004) Probing the cytotoxicity of semiconductor quantum dots. *Nano Letters*, 4,11-18.

DORR, P., WESTBY, M., DOBBS, S., GRIFFIN, P., IRVINE, B., MACARTNEY, M., MORI, J., RICKETT, G., SMITH-BURCHNELL, C., NAPIER, C., WEBSTER, R., ARMOUR, D., PRICE, D., STAMMEN, B., WOOD, A. & PERROS, M. (2005) Maraviroc (UK-427, 857), a potent, orally bioavailable, and selective small-molecule inhibitor of chemokine receptor CCR5 with broad-spectrum anti-human immunodeficiency virus type 1 activity. *Antimicrob Agents Chemother*, 49, 4721-4732.

DOUEK, D. C., BRENCHLEY, J. M., BETTS, M. R., AMBROZAK, D. R., HILL, B. J., OKAMOTO, Y., CASAZZA, J. P., KURUPPU, J., KUNSTMAN, K., WOLINSKY, S., GROSSMAN, Z., DYBUL, M., OXENIUS, A., PRICE, D. A., CONNORS, M. & KOUP, R. A. (2002) HIV preferentially infects HIV-specific CD4+ T cells. *Nature,* 417, 95-8.

EARNSHAW, W. C., MARTINS, L. M. & KAUFMANN, S. H. (1999) Mammalian caspases: structure, activation, substrates, and functions during apoptosis. *Annu Rev Biochem,* 68, 383-424.

EDO-MATAS, D., VAN DORT, K.A., SETIAWAN, L.C., SCHUITEMAKER, H. & KOOTSTRA, N.A. (2011) Comparison of *in vivo* and *in vitro* evolution of CCR5 to CXCR4 coreceptor use of primary human immunodeficiency virus type 1 variants. *Virology*, 412, 269-277.

EDWARDS, P.P. & THOMAS, J.M. (2007) Gold in a metallic divided state- from Faraday to present-day nanoscience. *Angewandte Chemie International Edition*, 46, 5480-5486.

EIGLER, D.M. & SCHWEIZER, E.K. (1990) Positioning single atoms with a scanning tunnelling microscope. *Nature*, 344, 524-526.

EKIMOV, A.I. & ONUSHCHENKO, A.A. (1982) Quantum size effect in the optical spectra of semiconductor microcrystals. *Semiconductors*, 16, 1215-1219.

EL-SAYED, I.H., HUANG, X. & EL-SAYED, M.A. (2005) Surface Plasmon Resonance Scattering and Absorption of anti-EGFR Antibody Conjugated Gold Nanoparticles in Cancer Diagnostics: Applications in Oral Cancer. *Nano Letters*, 5, 829-834.

ELECHIGUERRA, J.L., BURT, J.L., MORONES, J.R., CAMACHO-BRAGADO, A., GAO, X., LARA, H.H. & YACAMAN, M.J. (2005) Interaction of silver nanoparticles with HIV-1. *Journal of Nanobiotechnology*, 3, 6.

ELMORE, S. (2007) Apoptosis: a review of programmed cell death. *Toxicol Pathol*, 35, 495-516.

FAUCI, A. S. (2003) HIV and AIDS: 20 years of science. *Nat Med*, 9, 839-43.

FERRARI, M. (2005) Cancer nanotechnology: opportunities and challenges. *Nat Rev Cancer*, 5, 161-71.

FEYNMAN, R.P. (1992) There's plenty of room at the bottom. *J Microelectromech Syst*, 1, 60-66.

FLEXNER, C. (1998) HIV-protease inhibitors. *N Engl J Med,* 338, 1281-92.

GALLO, R. C. & MONTAGNIER, L. (2003) The discovery of HIV as the cause of AIDS. *N Engl J Med,* 349, 2283-5.

GAO, X., CHUNG, L. W. & NIE, S. (2007) Quantum dots for *in vivo* molecular and cellular imaging. *Methods Mol Biol,* 374, 135-45.

GHOSH, P., HAN, G., DE, M., KIM, C. K. & ROTELLO, V. M. (2008) Gold nanoparticles in delivery applications. *Adv Drug Deliv Rev,* 60, 1307-15.

GHOSH, A.K., KULKAMI, S., ANDERSEN, D.D., HONG, L., BALDRIDGE, A., WANG, Y.F., CHUMANEVICH, A.A., KOVALEVSKY, A.Y., TOJO, Y., AMANO, M., KOH, Y., TANG, J.WEBER, I.T. & MITSUYA, H. (2009) Design, Synthesis, Protein-Ligand X-ray Structure, and Biological Evaluation of a Series of Novel Macrocyclic Human Immunodeficiency Virus-1 Protease Inhibitors to Combat Drug Resistance. *J Med Chem.*, 52, 7689-7705.

GILLIES, E. R. & FRECHET, J. M. (2005) Dendrimers and dendritic polymers in drug delivery. *Drug Discov Today,* 10, 35-43.

GIRARD, M.P., OSMANOV, S., ASSOSOU, O.M. & KIENY, M. (2011) Human immunodeficiency virus (HIV) immunopathogenesis and vaccine development: a review. *Vaccine*, 29, 6191-6218.

GODNICK, K. (2007) Profitability versus the Public Interest: Is International Patent Law Hindering Third World Countries Access to HIV/AIDS Medications. *Rich J L & Pub Int*, 86, 2006-2007.

HAISS, W., THANH, N.T.K., AVEYARD, J. & FERNIG, D.G. (2007) Determination of Size and Concentration of Gold Nanoparticles from UV-Vis Spectra. *Anal Chem*, 79, 4215-4221.

HASELTINE, W. A. (1991) Molecular biology of the human immunodeficiency virus type 1. *Faseb J,* 5, 2349-60.

HERNANDEZ, L. D., HOFFMAN, L. R., WOLFSBERG, T. G. & WHITE, J. M. (1996) Virus-cell and cell-cell fusion. *Annu Rev Cell Dev Biol,* 12, 627-61.

HOFFMANN, C. (2007) The epidemiology of HIV coreceptor tropism. *Eur J Med Res*, 12, 385-390.

HOOD, E. (2004) Nanotechnology: looking as we leap. *Environ Health Perspect,* 112, A740-9.

HUO, Q. A. W., J.G. (2007) Monofunctional gold nanoparticles: synthesis and applications. *Journal of Nanoparticle Research*, 9, 1013-1025.

JAISWAL, J. K., MATTOUSSI, H., MAURO, J. M. & SIMON, S. M. (2003) Long-term multiple color imaging of live cells using quantum dot bioconjugates. *Nat Biotechnol,* 21, 47-51.

JAISWAL, J. K. & SIMON, S. M. (2004) Potentials and pitfalls of fluorescent quantum dots for biological imaging. *Trends Cell Biol,* 14, 497-504.

KAHN, J. O. & WALKER, B. D. (1998) Acute human immunodeficiency virus type 1 infection. *N Engl J Med,* 339, 33-9.

KAM, P. C. & FERCH, N. I. (2000) Apoptosis: mechanisms and clinical implications. *Anaesthesia,* 55, 1081-93.

KANDUC, D., MITTELMAN, A., SERPICO, R., SINIGAGLIA, E., SINHA, A. A., NATALE, C., SANTACROCE, R., DI CORCIA, M. G., LUCCHESE, A., DINI, L., PANI, P., SANTACROCE, S., SIMONE, S., BUCCI, R. & FARBER, E. (2002) Cell death: apoptosis versus necrosis (review). *Int J Oncol,* 21, 165-70.

KANG, H.J., LEE,Y., JEONG, Y.J., PARK, K., JANG, M., PARK, S.G., BAE, K., KIM, M.

& CHUNG, S.J. (2008) Large-scale preparation of active caspase-3 in *E. coli* by designing its thrombin-activatable precursors. *BMC Biotechnol*, 8, 92.

KERR, J.F., WYLLIE, A.H. & CURRIE, A.R. (1972) Apoptosis: a basic biological phenomenon with wide-ranging implications in tissue kinetics. *Br J Cancer*, 26, 239-257.

KLAJNERT, B. & BRYSZEWSKA, M. (2001) Dendrimers: properties and applications. *Acta Biochim Pol,* 48, 199-208.

KOHL, N.E., EMINI, E.A., SCHLEIF, W.A., DAVIS, L.J., HEIMBACH, J.C., DIXON, RA, SCOLNICK, E.M. AND SIGAL, I.S. (1988) Active human immunodeficiency virus protease is required for viral infectivity. *Proc Natl Acad Sci*, 85, 4686-4690.

KUBIK, T., BOGUNIA-KUBIK, K. & SUGISAKA, M. (2005) Nanotechnology on duty in medical applications. *Curr Pharm Biotechnol,* 6, 17-33.

KUMAR, S. (2007) Caspase function in programmed cell death. *Cell Death Differ,* 14, 32-43.

LEVY, J.A. (2006) HIV pathogenesis: knowledge gained after two decades of research. *Advances in dental research*, 19, 10-16.

MAIURI, M.C., ZALCKVAR, E., KIMCHI, A. & KROEMER, G. (2007) Self-eating and self-killing: crosstalk between autophagy and apoptosis. *Nature Reviews Molecular Biology*, 8, 741-752.

MAMALIS, A.G. (2007) Recent advances in nanotechnology. *Journal of Materials Processing Technology*, 181, 52-58.

MATTHEWS, G. V., BOWER, M., MANDALIA, S., POWLES, T., NELSON, M. R. & GAZZARD, B. G. (2000) Changes in acquired immunodeficiency syndrome-related lymphoma since the introduction of highly active antiretroviral therapy. *Blood,* 96, 2730-4.

MATUTE-BELLO, G. & MARTIN, T. R. (2003) Science review: apoptosis in acute lung injury. *Crit Care,* 7, 355-8.

MAYNARD, A. D. (2007) Nanotechnology: the next big thing, or much ado about nothing? *Ann Occup Hyg,* 51, 1-12.

MEDINTZ, I.L., UYEDA, H.T., GOLDMAN, E.R. & MATTOUSSI, H. (2005) Quantum dot bioconjugates for imaging, labelling and sensing. *Nature Materials*, 4, 435-446.

MENENDEZ-ARIAS, L. & TOZSER, J. (2008) HIV-1 protease inhibitors: effects on HIV-2 replication and resistance. *Trends Pharmacol Sci,* 29, 42-9.

MEYER, M., ESSACK, M., KANYANDA, S. & REES, J (1998) A low-cost flow cytometric assay for the detection and quantification of apoptosis using an anionic halogenated fluorescein dye. *Biotechniques*, 45, 317-320.

MISHRA, B., PATEL, B. B. & TIWARI, S. (2009) Colloidal nanocarriers: a review on formulation technology, types and applications toward targeted drug delivery. *Nanomedicine*.

MOGHIMI, S. M., HUNTER, A. C. & MURRAY, J. C. (2001) Long-circulating and target-specific nanoparticles: theory to practice. *Pharmacol Rev,* 53, 283-318.

MUKHERJEE, P., BHATTACHARYA, R., WANG, P., WANG, L., BASU, S., NAGI, J.A., ATALA, A., MUKHOPADHYAY,D. & SOKER, S. (2005) Antiangiogenic properties of gold nanoparticles. *Clin Can Res*, 11, 3530-3534.

NAVENOT, J. M., WANG, Z. X., TRENT, J. O., MURRAY, J. L., HU, Q. X., DELEEUW, L., MOORE, P. S., CHANG, Y. & PEIPER, S. C. (2001) Molecular anatomy of CCR5 engagement by physiologic and viral chemokines and HIV-1 envelope glycoproteins: differences in primary structural requirements for RANTES, MIP-1 alpha, and vMIP-II Binding. *J Mol Biol*, 313, 1181-93.

NICHOLSON, D. W. (1999) Caspase structure, proteolytic substrates, and function during apoptotic cell death. *Cell Death Differ,* 6, 1028-42.

NIE, S., XING, Y., KIM, G.J. AND SIMONS, J.W. (2007) Nanotechnology applications in cancer. *Annu Rev Biomed Eng*, 7, 257-288.

NIJHUIS, M., VAN MAARSEVEEN, N.M. & BOUCHER, C.A.B. (2007) HIV protease resistance and viral fitness. *Curr Opin HIV/AIDS*, 2, 108-115.

NUNEZ, G., BENEDICT, M. A., HU, Y. & INOHARA, N. (1998) Caspases: the proteases of the apoptotic pathway. *Oncogene*, 17, 3237-45.

PANTALEO, G., GRAZIOSI, C., DEMAREST, J.M., BUTINI, L., MONTRONI, M., FOX, C.H., ORENSTEIN, J.M., KOTLER, D.P. & FAUCI, A.S. (1993) HIV infection is active and progressive in lymphoid tissue during the clinically latent stage of disease. *Nature*, 362, 355-358.

PARK, H. H., JAMISON, A. C. & LEE, T. R. (2007) Rise of the nanomachine: the evolution of a revolution in medicine. *Nanomed,* 2, 425-39.

POLAVARAPU, L. & XU, Q. (2009) A simple method for large scale synthesis of highly monodisperse gold nanoparticles at room temperature and their electron relaxation properties. *Nanotechnology*, 20, 1-7.

PORTER, A.G. & JÄNICKE, R.U. (1999) Emerging roles of caspase-3 in apoptosis. *Cell Death and Differention*, 6, 99-104.

RICHMAN, D. D. (2001) HIV chemotherapy. *Nature,* 410, 995-1001.

ROCO, M. C. (2003) Nanotechnology: convergence with modern biology and medicine. *Curr Opin Biotechnol,* 14, 337-46.

SALAMANCA-BUENTELLO, F., PERSAD, D. L., COURT, E. B., MARTIN, D. K., DAAR, A. S. & SINGER, P. A. (2005) Nanotechnology and the developing world. *PLoS Med,* 2, e97.

SAMAD, A., SULTANA, Y. & AQIL, M. (2007) Liposomal drug delivery systems: an update review. *Curr Drug Deliv,* 4, 297-305.

SANTINI, M. T., RAINALDI, G. & INDOVINA, P. L. (2000) Apoptosis, cell adhesion and the extracellular matrix in the three-dimensional growth of multicellular tumor spheroids. *Crit Rev Oncol Hematol,* 36, 75-87.

SASHIN, D., SPANBOCK, J. & KLING, D.H. (1939) *The Journal of Bone and Joint Surgery*, 21, 723-734.

SHAH, L.K. & AMIJI, M.M. (2006) Intracellular delivery of saquinavir in biodegradable polymeric nanoparticles for HIV/AIDS. *Pharm Res*, 23, 2638-2345.

SHERMAN, M. P. & GREENE, W. C. (2002) Slipping through the door: HIV entry into the nucleus. *Microbes Infect,* 4, 67-73.

SHIOHARA, A., HOSHINO, A., HANAKI, K., SUZUKI, K. & YAMAMOTO, K. (2004)On the cytotoxicity caused by quantum dots. *Microbiol Immunol*, 48, 669-675.

SHUKLA, R., BANSAL, V., CHAUDHARY, M., BASU, A., BHONDE, R. R. & SASTRY, M. (2005) Biocompatibility of gold nanoparticles and their endocytotic fate inside the cellular compartment: a microscopic overview. *Langmuir*, 21, 10644-54.

SHVEDOVA, A.A., MAYNARD, A.D., BARON, P.A., FOLEY, M., KISIN, E.R. & CASTRANOVA, V. (2004) Exposure to Carbon Nanotube Material: Aerosol Release During the Handling of Unrefined Single-Walled Carbon Nanotube Material. *Journal of Toxicology and Environmental Health*, 67, 87-107.

SIMON, V., HO, D. D. & ABDOOL KARIM, Q. (2006) HIV/AIDS epidemiology, pathogenesis, prevention, and treatment. *Lancet,* 368, 489-504.

SLEPUSKHIN, V.A., SALEM, I.I., DAZIN, P. & DÜSGÜNES, N. (1996). Targeting of liposomes to HIV-1-infected cells by peptides derived from the CD4 receptor. *Biochem Biophys Res Commun*, 227, 827-833.

SMITH, D.B. & JOHNSON, K.S. (1988) Single-step purification of polypeptides expressed in Escherichia coli as fusions with glutathione S-transferase. *Gene*, 67, 31-40.

SOFOU, S. & SGOUROS, G. (2008) Antibody-targeted liposomes in cancer therapy and imaging. *Expert Opin Drug Deliv,* 5, 189-204.

SOLOMAN, R. & GABIZON, A. A. (2008) Clinical pharmacology of liposomal anthracyclines: focus on pegylated liposomal Doxorubicin. *Clin Lymphoma Myeloma,* 8, 21-32.

SPERLING, R. A., RIVERA GIL, P., ZHANG, F., ZANELLA, M. & PARAK, W. J. (2008) Biological applications of gold nanoparticles. *Chem Soc Rev,* 37, 1896-908.

SQUIRES, K. E. (2001) An introduction to nucleoside and nucleotide analogues. *Antivir Ther,* 6 Suppl 3, 1-14.

STORM, G. & CROMMELIN, D.J.A (1998) Liposomes: quo vadis? *PSTT*, 1, 19-31.

STUDIER, F.W. (2005) Protein production by auto-induction in high-density shaking cultures. *Protein Expression and Purification*, 41, 207-234.

TEMESGEN, Z., WARNKE, D. & KASTEN, M. J. (2006) Current status of antiretroviral therapy. *Expert Opin Pharmacother,* 7, 1541-54.

THE HIV GENOME, available at: http://www.yale.edu/bio243/HIV/genome.html

TOMALIA, D. A., REYNA, L. A. & SVENSON, S. (2007) Dendrimers as multi-purpose nanodevices for oncology drug delivery and diagnostic imaging. *Biochem Soc Trans,* 35, 61-7.

TORCHILIN, V. P. & LUKYANOV, A. N. (2003) Peptide and protein drug delivery to and into tumors: challenges and solutions. *Drug Discov Today,* 8, 259-66.

TRKOLA, A. (2004) HIV-host interactions: vital to the virus and key to its inhibition. *Curr Opin Microbiol,* 7, 555-9.

TSHIKHUDO, T. R., WANG, Z. AND BRUST, M. (2004) Biocompatible gold nanoparticles. *Materials Science and Technology*, 20, 980-984.

TSIBRIS, A. M. & KURITZKES, D. R. (2007) Chemokine antagonists as therapeutics: focus on HIV-1. *Annu Rev Med,* 58, 445-59.

TURKEVICH, J., STEVENSON, P.C. & HILLIER, J. (1951) A study of the nucleation and growth processes in the synthesis of colloidal gold. *Discussions of the Faraday Society*, 11, 55-75.

UN Joint Programme on HIV/AIDS, Global Report: UNAIDS Report on the Global AIDS Epidemic: 2010, December 2010, ISBN 978-92-9173-871-7, available at: http://www.unhcr.org/refworld/docid/4cfca9c62.html

VANDEGRAAFF, N. & ENGELMAN, A. (2007) Molecular mechanisms of HIV integration and therapeutic intervention. *Expert Rev Mol Med,* 9, 1-19.

VOCERO-AKBANI, A. M., HEYDEN, N. V., LISSY, N. A., RATNER, L. & DOWDY, S. F. (1999) Killing HIV-infected cells by transduction with an HIV protease-activated caspase-3 protein. *Nat Med,* 5, 29-33.

WILCOXON, J.P., WILLIAMSON, R.L. & BAUGHMAN, R. (1993) Optical properties of gold colloids formed in inverse micelles. *J Chem Phys*, 98, 9933-9950.

WYLLIE, A.H. (2010) "Where, O Death, Is Thy Sting?" A Brief Review of Apoptosis Biology. *Molecular Neurobiology*, 42, 4-9.

YIH, T. C. & AL-FANDI, M. (2006) Engineered nanoparticles as precise drug delivery systems. *J Cell Biochem,* 97, 1184-90.

YIYUN, C. & TONGWEN, X. (2005) Dendrimers as potential drug carriers. Part I. Solubilization of non-steroidal anti-inflammatory drugs in the presence of polyamidoamine dendrimers. *Eur J Med Chem*, 40, 1188-92.

YU, W.W., CHANG, E., DREZEK, R & COLVIN, V.L. (2006) Water-soluble quantum dots for biomedical applications. *Biochemical and Biophysical Research Communications*, 348, 781-786.

ZADOR, Z., LACZA, Z., BENYO, Z., HARKANY, T. & HORTOBAGYI, T. (2003) Apoptosis in focal brain ischemia. *Ideggyogy Sz,* 56, 216-28.

ZHENG, M. & HUANG, X. (2007) Biofunctionalization of Gold Nanoparticles. *Nanotechnologies for the Life Sciences*, Wiley-VCH, 99-124.

ZORKO, M. & LANGEL, Ü. (2005) Cell-penetrating peptides: mechanism and kinetics of cargo delivery. *Advanced Drug Delivery Reviews*, 4, 529-545.